

THÈSE EN COTUTELLE PRÉSENTÉE
POUR OBTENIR LE GRADE DE

DOCTEUR DE

L'UNIVERSITÉ DE BORDEAUX

ÉCOLE DOCTORALE DES SCIENCES PHYSIQUES ET DE L'INGÉNIEUR DE
L'UNIVERSITÉ DE BORDEAUX

ET DE

L'UNIVERSITÉ DU QUÉBEC À CHICOUTIMI

DÉPARTEMENT DES SCIENCES APPLIQUÉES DE
L'UNIVERSITÉ DU QUÉBEC À CHICOUTIMI

Par Minh-Van THAI

**ÉVALUATION DU COMPORTEMENT EN VIBRATION ET
OPTIMISATION DE LA CONCEPTION DES PLANCHERS
COMPOSITE EN BOIS LAMELLÉ COLLÉ CROISÉ-BÉTON**

Sous la direction de Sylvain MENARD
et de Sidi Mohammed ELACHACHI
Encadrée par Philippe GALIMARD

Soutenue le 2 décembre 2021

Membres du Jury

M. Pierre BLANCHET	PR Université Laval	Président du jury
M. Abdel Hamid BOUCHAIR	PR Université Clermont Auvergne	Membre externe / Rapporteur
M. Daniel MARCEAU	PR Université du Québec à Chicoutimi	Membre externe / Rapporteur
Mme. Francesca LANATA	MCF Ecole Supérieure du Bois	Membre externe / Examinatrice
M. Nicolas SAUVAT	MCF Université de Limoges	Membre externe / Examineur
M. Sylvain MENARD	PR Université du Québec à Chicoutimi	Directeur de recherche
M. Sidi Mohammed ELACHACHI	PR Université de Bordeaux, I2M	Directeur de thèse
M. Philippe GALIMARD	MCF Université de Bordeaux, I2M	Encadrant / Examineur

ABSTRACT

This research project aims to evaluate the vibration behavior and optimize the design of cross-laminated timber-concrete composite floors. These floor structures are a composite made of a cross-laminated timber panel and a concrete layer. They are connected by a notch carved into the cross-laminated timber and reinforced by two vertical screws. This connection is an innovative solution and still needs further regulation by a technical notice. Nonetheless, it remains economically accessible, requires only simple machining, and limits on-site intervention. The composite floor will have a large span necessary, particularly in Quebec and France, to construct multi-story timber buildings whose market is in total development. Such floor systems will satisfy the demand for low or no carbon footprint floor solutions for reducing the static height while complying with the normative constraints of which the most demanding is the vibration.

First, the behavior of a single composite notch connector was studied. The chosen connector, screw reinforced notched, has been tested in static shear. Furthermore, a finite element model has been proposed to describe the static stiffness and the shear strength of the connector of different configurations.

Then, three long-span (9 meters) cross-laminated timber-concrete beams with different connector densities were subjected to vibration and static bending tests. Analytical expressions proposed by Eurocode 5 and a simplified finite element model gave reasonable estimates of the measured natural frequencies. However, the module calibration of the cross-laminated timber panels due to the impact of the notches was necessary.

Finally, multi-objective optimization of cross-laminated timber-concrete floors was carried out. Its objectives were to minimize the weight, the static height of the floor, and the total cost while complying with the constraints of the serviceability limit state (deflection and vibration) and the ultimate limit state (bending and shearing). A Pareto front of optimized solutions was obtained. The configuration tested is a conventional engineering solution that does not appear on this Pareto front. The optimization tool is, therefore, potentially relevant and can help engineers define their designs.

Keywords: Cross laminated timber-concrete composite, notched connector, vibrational behavior, optimization multi-objective, cross-laminated timber, floor systems, composite beam, NSGA-II.

RÉSUMÉ

Ce projet de recherche vise l'évaluation du comportement en vibration et l'optimisation de la conception des planchers composite en bois lamellé collé croisé-béton. La connexion est réalisée par entaille dans le CLT renforcée par deux vis. Cette connexion n'est pas sous avis technique. Néanmoins, elle reste donc accessible économiquement, ne nécessite qu'un usinage simple et limite l'intervention sur site. Elle vise à réaliser des planchers de grandes portées nécessaires, particulièrement au Québec et en France, pour la réalisation de bâtiments multiétages en bois dont le marché est en plein développement et en demande de solutions planchers peu ou pas carbonées, de hauteur statique réduite satisfaisant aux contraintes normatives dont la plus exigeante est la vibration.

D'abord, le comportement d'un connecteur composite individuel a été étudié. Le connecteur à l'entaille renforcée par vis a été testé en cisaillement statique. Un modèle par des éléments finis a été proposé permettant de décrire la rigidité statique et la résistance en cisaillement du connecteur de différente configuration.

Ensuite, trois poutres en bois lamellé collé croisé-béton de longue portée (9 mètres) avec différentes densités de connecteurs, ont été soumises à des essais de vibration et de flexion statique. Des expressions analytiques, dont une est proposée par la norme Eurocode 5, ainsi qu'un modèle simplifié par éléments finis ont donné de bonnes estimations des fréquences naturelles mesurées. Pourtant, une calibration des modules des panneaux en bois lamellé collé croisé due à l'impact des entailles a été nécessaire.

Enfin, une optimisation multi-objectif des planchers en bois lamellé collé croisé-béton a été effectuée. Elle a pris comme objectifs à minimiser le poids, la hauteur statique du plancher et le coût total en restant soumis aux contraintes de l'état limite de service (flèche et vibration) et de l'état limite ultime (flexion et cisaillement). Un front de Pareto des solutions optimisées a été obtenu. La configuration testée est une solution d'ingénierie conventionnelle qui ne figure pas sur ce front de Pareto. L'outil d'optimisation se révèle donc potentiellement pertinent susceptible d'aider les ingénieurs à définir leurs conceptions.

Mot-clés : Composite bois lamellé collé croisé-béton, connecteur à l'entaille, comportement en vibration, optimisation multi-objectif, bois lamellé collé croisé, système de plancher, poutre composite, NSGA-II.

RÉSUMÉ ÉTENDU

CONTEXTE SCIENTIFIQUE ET INDUSTRIEL

Les composites bois-béton (timber-concrete composite - TCC) sont utilisés pour leurs multiples avantages : bilan carbone avantageux, énergie grise réduite, bonne résistance et rigidité, performances des planchers bois améliorées en termes de sécurité incendie, de sismique, de l'acoustique, du confort thermique, facilité et rapidité de mise en œuvre, capacité de préfabrication et de déconstruction.

Récemment, les panneaux de bois lamellé-collé croisé (cross-laminated timber - CLT) - un produit d'ingénierie du bois innovant - a été associé à du béton pour former un composite CLT-béton (CLT-concrete composite - CCC) destiné à la construction de planchers. Ce système hybride bénéficie, d'une part, des avantages mentionnés ci-haut des structures TCC traditionnelles, et d'autre part, d'une faible hauteur statique (épaisseur) par rapport aux TCC. Ainsi, pour une même hauteur totale d'un bâtiment TCC de 10 étages, le bâtiment à plancher CCC gagnera un étage de plus. Les structures CCC, qui emploient l'interaction composite entre le CLT et le béton, sont aussi des solutions pour des planchers de longue portée (plus de 8 m). Cependant, elles nécessitent une meilleure compréhension des interactions entre les composants du composite dans la contribution aux performances en vibration.

La structure TCC comprend trois composants principaux : le bois, la dalle de béton et la connexion mécanique qui peut être discrète ou continue dans le cas du collage. Les connecteurs mécaniques discrets ont fait l'objet de nombreuses études, plusieurs solutions propriétaires sont aujourd'hui proposées [1]–[3]. De même, ces connecteurs peuvent être appliqués aux structures CCC sous réserve de certaines modifications mineures dues à l'épaisseur limitée du CLT. Effectivement, parmi les solutions de connecteurs proposées [4]–[6], le connecteur à entaille est considéré comme une solution équilibrée sur le plan de la fonction à assurer et du coût.

Les dalles bois-béton utilisant les panneaux en bois massif CLT avec le système de connecteur composite ont démontré leur intérêt lors de leur utilisation dans la construction du bâtiment à moyenne ou grande hauteur. Cependant, le CCC n'est pas encore une technique de construction très courante dans le marché de la construction. La pratique adoptée par exemple au Québec est de construire les dalles CLT avec une chape en béton et un film acoustique sans connecteurs permettant la collaboration mécanique entre les deux matériaux. En France, l'utilisation des planchers CCC dans la construction est encore en développement. Le coût de construction élevé ainsi que l'impact des choix

de béton-bois-connecteur, tous sous avis technique, dans la conception reste un frein au développement.

PROBLÉMATIQUE

Les planchers mixtes en béton CLT nécessitent des systèmes de connecteurs robustes, économiques, faciles à poser et éco-responsable. La performance du connecteur en cisaillement est donc importante à bien identifier pour la modélisation du comportement du plancher CCC. Le connecteur doit être économique contrairement à tous les systèmes propriétaires existants.

A l'instar des planchers légers à grande portée, la conception des planchers CCC est généralement limitée par le critère de vibration [7]. La compréhension du comportement dynamique de ces planchers est nécessaire pour l'établissement d'un critère de performance en vibration. Les connecteurs de type entaille impliquent un enlèvement de matière bois qui peut être significatif et impacter le panneau CLT.

Malgré les intérêts structuraux et environnementaux de ce type de structure, son développement est subrogé à la minimisation d'objectifs économiques et de hauteur statique. En effet ces deux critères s'avèrent actuellement rédhibitoires sans une volonté affirmée de la maîtrise d'ouvrage. La conception de la dalle CCC passe par plusieurs variables fonctionnelles. Il est donc nécessaire de pouvoir disposer d'un ensemble de solutions optimisées pour un ensemble d'objectifs prédéfinis. Le choix de la solution finale est alors défini par une analyse multicritère non effectuée dans cette étude car totalement dépendante de l'environnement du projet.

OBJECTIVES DE LA THÈSE

L'un des principaux objectifs du projet de recherche est d'évaluer le comportement vibratoire des structures de plancher CCC. Cette évaluation vise particulièrement les structures de plancher de longue portée car leur conception est généralement régie par les performances vibratoires. Cette étude expérimentale et numérique est divisée en deux étapes : les connecteurs CLT-béton et les poutres mixtes de grande portée (9m). Dans la première étape, la solution d'un connecteur par entaille est retenue pour son faible coût et son absence de propriété puis évaluée mécaniquement. L'évaluation expérimentale renseigne un modèle numérique pour prédire les performances du connecteur en configuration variable. La seconde étape concerne le comportement vibratoire des poutres mixtes CLT-béton. Les paramètres à analyser sont le système d'assemblage, la rigidité en flexion effective de la section et la portée des poutres. Les critères de conception définis dans l'Eurocode 5 [8] et la CSA-O86 [9] pour le plancher en bois léger seront validés à l'aide des résultats expérimentaux.

Le deuxième objectif est d'optimiser la conception du plancher CCC afin de pouvoir proposer les meilleures solutions compétitives par rapport à d'autres systèmes constructifs. Les informations obtenues à partir des phases d'évaluation seront injectées dans l'optimisation multiobjective pour montrer les conceptions optimisées des planchers CCC. Les fonctions objectives sont la masse, l'épaisseur et le coût total de la construction du plancher. Les conceptions optimisées sont aussi soumises aux fonctions contraintes structurales de l'état limite de service et ultime.

DÉMARCHE ADOPTÉE

Une revue de littérature a été effectuée pour consolider les informations sur le comportement des structures composites bois-béton, ainsi sur les méthodes de contrôle ou de mesure de la vibration des planchers légers. Les essais expérimentaux sur la performance du connecteur composite individuel et de la poutre composite en bois lamellé collé croisé-béton ont été abordés dans cette revue.

Le projet de recherche s'est divisé en deux parties : l'évaluation et optimisation. L'évaluation est effectuée aux échelles du connecteur et de la poutre CCC. Les travaux expérimentaux de cette phase de recherche sont des tests expérimentaux sur les connecteurs individuels de type entaille puis sur des poutres composites utilisant ce même type de connecteur. Le connecteur composite à entaille renforcé par deux vis a été étudié et employé pour les poutres composites de longue portée.

La performance mécanique des connecteurs à entaille renforcée par vis ainsi que l'influence des variables géométriques à la rigidité et la résistance du connecteur ont été étudiées. Un modèle des éléments finis pour déterminer la rigidité et la résistance du connecteur à l'entaille a été développé et validé par les résultats expérimentaux.

L'évaluation a été effectuée sur les poutres composites en bois lamellé collé croisé-béton à long-portée utilisant des connecteurs à l'entaille. Les tests expérimentaux statique et dynamique sur trois poutres composites ont été effectués et analysés. Une calibration de la rigidité des panneaux en bois lamellé collé croisé montre l'influence des entailles sur la rigidité des panneaux et donc sur les fréquences propres et la flèche de la poutre.

Enfin, l'optimisation multiobjective portant sur la conception des planchers en bois lamellé collé croisé-béton a été effectuée. En utilisant les résultats de la phase d'évaluation précédente et l'algorithme génétique NSGA-II (Non-dominated Sorting Genetic Algorithm-II), les conceptions optimisées de la dalle CCC ont été obtenues dans le sens du front Pareto. Les fonctions objectives sont la masse, l'épaisseur et le coût. Les fonctions contraintes structurelles ont été adoptées : contraintes de services, d'ultime, de vibration et d'incendie.

RÉSULTATS MARQUANTS

- La rigidité et la résistance du connecteur à entaille dépend fortement de la profondeur de l'entaille. La résistance maximale au cisaillement augmente quand la profondeur de l'entaille augmente. La rigidité de l'entaille la plus profonde n'est pas la plus élevée.
- Les autres variables géométriques telles que l'épaisseur du béton, longueur de vis et longueur du talon n'influencent pas la performance du connecteur, c.-à-d., la rigidité et la résistance au cisaillement
- Les poutres CCC utilisant un connecteur à entaille atteignent un niveau de connexion important. Pourtant, un nombre important de l'entaille sur la surface des poutres CLT mènerait à une réduction de la rigidité et résistance de la poutre composite CCC.
- Une bonne corrélation a été trouvée entre les expressions analytiques et les résultats expérimentaux de la fréquence fondamentale des poutres CCC.
- L'optimisation multi-objectifs des planchers CCC est une approche très pertinente lors des phases préliminaires de conception.
- Les informations relatives aux coûts de béton et CLT sont cruciales pour la compétitivité des conceptions du plancher CCC.

ACKNOWLEDGMENT

This thesis work commenced at the University of Quebec at Chicoutimi in January 2018, continued by a laborious experimental phase at the laboratory of the pavilion G.H.Kruger of Laval University, and finished at the I2M laboratory of the University of Bordeaux in July 2021. This project enabled me to go to many places, meet great people, and granted me priceless experiences despite many difficulties and obstacles.

First, I would like to thank my supervisors, Dr. Sylvain Ménard and Dr. Sidi Mohammed Elachachi, for offering me a chance to work on this research project in Canada and France, for your relentless encouragement and helpful support. My sincere gratitude goes to my co-supervisor, Dr. Philippe Galimard, for the precious discussions and guidance.

I am grateful to Dr. Pierre Blanchet, director of CIRCERB, for allowing me to work at the laboratory of the pavilion G.H.Kruger. Furthermore, I want to thank Pierre Gagné, Guylaine Bélanger, CIRCERB, UQAC, and MRQ personnel for making the administrative procedures smoothly. Thanks to the technicians, Jean, Félix, Benoit, and Daniel. Despite the bulky dimension of the beams and the pandemic hardship, you helped my experiments at the laboratory completed successfully.

I am also grateful for the support of the industrial partners and sponsors: Sylvain Gagnon, Samuel Cuerrier-Auclair, Anes Omeranovic at FPInnovations for allowing me to use the experimental equipment, giving me lots of valuable advice, Williams Munoz at Nordic Structures for sharing me many unique industrial perspectives, Jean-Philippe Letarte at My-Ti-Con for sponsoring the screws for my shear tests.

During my thesis, I have been to three universities, and I am grateful to have my colleagues alongside during our arduous but fantastic journeys, Cheng, Axel, Etienne, Mohammad at Chicoutimi, Thành at Quebec City, Renaud, Cédric at Bordeaux. Thanks to many friends, Hằng, Đức Anh, Trung Anh, Nguyệt, Phi, Lâm for making my stay at their places so delightful. Thành and Tú, thank you for being my family during those unforgettable five months in Québec City.

I am filled with gratitude for my family in Vietnam for their perpetual love and unconditioned support. Cảm ơn Cha, Mẹ và chị Hai vì tất cả những cố gắng và hi sinh để con có được như ngày hôm nay.

My thanks to Mai Lien for her patience, understanding, and love. Yêu em.

THÁI Minh-Văn

CONTENT

ABSTRACT	ii
RÉSUMÉ	iv
RÉSUMÉ ÉTENDU	vi
ACKNOWLEDGMENT	x
CONTENT	xii
PUBLICATIONS	xiv
LIST OF TABLES	xvi
LIST OF FIGURES	xvii
LIST OF ABBREVIATIONS AND ACRONYMS	xix
INTRODUCTION	1
1. LITERATURE REVIEW: VIBRATION OF CROSS-LAMINATED TIMBER – CONCRETE COMPOSITE FLOORS	5
1.1. TIMBER-CONCRETE COMPOSITE.....	5
1.1.1. Composite action.....	6
1.1.2. Effective bending stiffness of the composite section.....	7
1.1.3. Constituent materials.....	8
1.1.4. Shear connector.....	11
1.2. VIBRATION OF TIMBER FLOORS.....	20
1.2.1. Vibration theory.....	20
1.2.2. Parameters of vibration.....	21
1.2.3. Human perception toward floor vibration.....	22
1.2.4. Design criterions.....	23
1.3. EXPERIMENTAL METHOD.....	25
1.3.1. Experimental studies on CCC structures in literature.....	25
1.3.2. Shear tests on connectors.....	26
1.3.3. Vibration tests on beams.....	28
1.4. CONCLUSION.....	30
2. PERFORMANCE OF NOTCH CONNECTOR FOR CLT-CONCRETE COMPOSITE FLOORS	31
2.1. INTRODUCTION.....	33
2.2. SPECIMEN GEOMETRY AND MATERIAL.....	34
2.2.1. Materials properties.....	34
2.2.2. Test specimens.....	36
2.2.3. Test setups.....	38
2.3. EXPERIMENTAL RESULTS AND DISCUSSION.....	40
2.3.1. Overview.....	40
2.3.2. Influence of heel length.....	43
2.3.3. Influence of notch depth.....	43
2.3.4. Influence of concrete thickness and screw length.....	45
2.3.5. Influence of loading sequence.....	46
2.3.6. Influence of moisture content of timber.....	46
2.3.7. Failure types.....	46
2.4. FINITE ELEMENTS MODEL VALIDATION.....	49
2.4.1. Materials.....	50
2.4.2. Models.....	52
2.4.3. Results.....	53

2.5. CONCLUSION	55
3. VIBRATIONAL BEHAVIOR OF CLT-CONCRETE COMPOSITE BEAMS USING NOTCHED CONNECTORS.....	59
3.1. INTRODUCTION.....	61
3.2. MATERIALS AND METHODS	63
3.2.1. Materials properties.....	63
3.2.2. Specimens.....	63
3.2.3. Supports	64
3.2.4. Test procedure	65
3.3. ANALYTICAL AND NUMERICAL MODELING	67
3.3.1. Bending stiffness of bare CLT panels	67
3.3.2. Bending stiffness of CCC beams	69
3.3.3. Finite elements model of CCC beams	71
3.4. RESULTS.....	73
3.4.1. Static deflection tests of CLT and CCC beams.....	73
3.4.2. Vibration tests of CCC and CLT beams	73
3.4.3. Bending stiffness of bare CLT panels	74
3.5. ANALYSIS AND DISCUSSION.....	75
3.5.1. Bending stiffness of bare CLT panels	75
3.5.2. Vibration characteristics of CCC beams	77
3.5.3. Comparison to other studies on the CCC beams	79
3.6. CONCLUSION	83
4. OPTIMIZATION MULTI-OBJECTIVE OF CLT-CONCRETE COMPOSITE FLOORS USING NSGA-II.....	85
4.1. INTRODUCTION.....	87
4.1.1. Structural multi-objective optimization	87
4.1.2. Multi-objective optimization algorithm	88
4.2. CLT-CONCRETE FLOOR DESIGN.....	89
4.2.1. CLT-concrete composite floor and the reference design	89
4.2.2. Notch connector influence.....	91
4.2.3. Design constraints.....	91
4.2.4. Optimization variables.....	92
4.3. OPTIMIZATION PROBLEMS.....	94
4.3.1. Objectives functions	94
4.3.2. Constraints functions.....	95
4.4. OPTIMIZATION ALGORITHM	98
4.5. ANALYSIS AND DISCUSSION.....	99
4.5.1. Pareto front of the optimal solutions and the reference solution.....	99
4.5.2. Parametric study	102
4.6. CONCLUSION	104
CONCLUSION AND PERSPECTIVES.....	107
REFERENCES.....	111
ANNEX.....	123

PUBLICATIONS

Peer-reviewed journal articles

Thai, Minh Van, Sylvain Ménard, Sidi Mohammed Elachachi, et Philippe Galimard. "Performance of notched connectors for CLT-concrete composite floors." *Buildings* 10, no. 7 (July 2020): 122. [10.3390/buildings10070122](https://doi.org/10.3390/buildings10070122)

Thai, Minh Van, Sidi Mohammed Elachachi, Sylvain Ménard, et Philippe Galimard. "Vibrational behavior of CLT-Concrete composite beams using notched connectors." *Engineering Structures*, vol. 249, 2021, [10.1016/j.engstruct.2021.113309](https://doi.org/10.1016/j.engstruct.2021.113309)

Thai, Minh Van, Philippe Galimard ; Sidi Mohammed Elachachi, et Sylvain Ménard. "Multi-objective optimization of CLT-concrete composite floor using NSGA-II." *Accepted for publication on Journal of Building Engineering*, 2022

Conference articles and presentations

Thai, Minh Van, Sidi Mohammed Elachachi, Sylvain Ménard, et Philippe Galimard. "Sensitivity analysis of CLT-concrete composite floor vibrations." *11èmes Journées de Fiabilité Des Matériaux et Structures 2020 (JFMS 2020)*. Clermont-Ferrand, 2020 (presentation accepted but conference canceled due to sanitary conditions).

Thai, Minh Van, Sidi Mohammed Elachachi, Sylvain Ménard, et Philippe Galimard. "Simplified finite element model for natural frequencies estimation of CLT-concrete composite beams using notched connectors." *9èmes journées du Groupe de Recherche (GDR) 3544 « Sciences du bois »*. Grenoble, France, 18 November 2020.

Thai, Minh Van, Philippe Galimard, Sidi Mohammed Elachachi, and Sylvain Ménard. "Multiobjective optimization of CLT-concrete composite floor using NSGA-II algorithm." *39èmes Rencontres Universitaires De Génie Civil (RUGC)*. Online. *Academic Journal of Civil Engineering (AJCE)*, from 26 to 28 May 2021.

Thai, Minh Van, Sylvain Ménard, Sidi Mohammed Elachachi, et Philippe Galimard. "Mechanical performance of CLT-concrete notched connector by push-out tests." *World Conference in Timber Engineering 2021 (WCTE 2021)*. Santiago, Chile, from 9 to 12 August; 2021.

Scientific vulgarization

Thai, Minh Van, Sylvain Ménard, Sidi Mohammed Elachachi, et Philippe Galimard. "Performance of notched connector for CLT-concrete composite floors." Scientific vulgarization for *Réseau des Matériaux Renouvelables Québec (MRQ)*. Québec, 2020. <https://www.reseaumrq.com/post/minh-van-thai-connecteur-performant-planchers-bois-beton>.

LIST OF TABLES

Table 1.1. Summary of criteria for the vibrational design of timber floors.....	25
Table 2.1. Properties of CLT and concrete.	35
Table 2.2. Parameters of test series, in mm.	37
Table 2.3. Summary of tested series	41
Table 2.4. Summary of the timber parameters of the FEM model.....	51
Table 3.1. Properties of CLT and concrete.	63
Table 3.2. Calculation of effective bending stiffness by two analytical methods	68
Table 3.3. Results of static deflection tests (MNm ² /m)	73
Table 3.4. Natural frequencies and damping	73
Table 3.5. <i>E_{leff}</i> of bare CLT beams based on analytic expressions.....	74
Table 3.6. <i>E_{leff}</i> of bare CLT beams based on vibration test results	75
Table 3.7. Comparison between experimentally calibrated and analytic CLT stiffness.....	77
Table 3.8. Natural frequencies comparison between experiments and models	82
Table 3.9. Comparison experimental-model results of CCC beam vibration studies	82
Table 4.1. Load combination, load duration factor, and bending stiffness of SLS and ULS constraints	92
Table 4.2. Creep coefficient for effective bending stiffness	92
Table 4.3. Optimization variables	93
Table 4.4. Optimization objectives	94
Table 4.5. Price and density of floor components	94
Table 4.6. Variables of some solutions	100
Table 4.7. Cost contribution	101

LIST OF FIGURES

Figure 1.1. CLT panels with preinstalled HBV connectors, at the UMass Olver Design Building, University of Massachusetts, Amherst, USA. Image courtesy of Alex Schreyer.	5
Figure 1.2. Relationship between the effective bending stiffness of the composite beam and the slip modulus on a logarithmic scale, per Van der Linden [24].	6
Figure 1.5. Comparison of different types of typical TCC connectors by Dias [25].	12
Figure 1.6. Load-slip curves of SFS screws (A) and regular screws (B) by Steinberg <i>et al.</i> [49]	14
Figure 1.7. Specimens with STS at 30° and pairs of STS at 45° with insulation layer, by Gerber [59]......	14
Figure 1.8. Lag screws connectors, by Deam <i>et al.</i> [58]......	15
Figure 1.9. Screw, bolt, and SFS screw, by Mai <i>et al.</i> [4]	15
Figure 1.10. HBV installation, by Gerber [59]	16
Figure 1.11. Round notch (or plug) connector, by Deam <i>et al.</i> [58]......	17
Figure 1.12. Three geometry form of notch connectors, by Yeoh [60]	18
Figure 1.13. Notch with dowel connectors and image of Hilti dowel, by Gutkowski <i>et al.</i> [62] ..	19
Figure 1.14. Notched connector geometry, by C. Auclair <i>et al.</i> [63]	19
Figure 1.15. A simple two-degree-of-freedom system model.	20
Figure 1.16. K_u and K_{ser} , by Lukaszewska [96]	26
Figure 1.17. Configuration symmetric for shear connector tests, adapted by C. Auclair [43].	27
Figure 1.18. Configuration non-symmetric for shear connector tests, (a) Boccadoro [55], (b) Lamothe [52]	28
Figure 2.1. Specimen with preinstalled polyethylene film (a), vertical attachment part with a threaded screw, counter-sunk washer and plastic sleeve installed (b), reinforcing steel mat of the specimens (c).	36
Figure 2.2. Diagram of a typical specimen, with indicated (a) heel length, (b) notch depth, (c) screw length, (d) concrete thickness.	37
Figure 2.3. Adaptor for the asymmetrical CLT-concrete specimen (left). Actual image of adaptor (right).	39
Figure 2.4. Theoretical loading procedure from EN 26891 [95] (a) and stiffness K1 (red) and K2 (green) determination of specimen A2 (blue) on raw data representation (b).	40
Figure 2.5. Load-displacement curves of specimens that have (a) 400 mm, (b) 350 mm, (c) 300 mm heel length, curves in red indicate 20 mm notch depth specimens, 25 mm in green, and 35 mm in blue.	42
Figure 2.6. Stiffness K1 (a), K2 (b), and maximum load F_{max} (c) of different notch depths.	43
Figure 2.7. Stiffness K1 (a), K2 (b), and maximum load F_{max} (c) of different heel lengths.	44
Figure 2.8. Stiffness K1 (a), K2 (b), and maximum load F_{max} (c) per notch depth of different heel lengths.	45
Figure 2.9. Stiffness K1 (a), K2 (b), and maximum load F_{max} (c) in terms of screw length and concrete thickness.....	45
Figure 2.10. Screw uninstallation	45
Figure 2.11. Correlation between stiffness K1 and moisture content of timber of different series. 20 mm notch depth specimens are represented by the red points, 25 mm in green, and 35 mm in blue.	46
Figure 2.12. Load-slip curves of different failure types.	47
Figure 2.13. Typical different failure types.	48
Figure 2.14. Number of specimens with different failure types.	49
Figure 2.15. Mesh definition of timber and concrete part and boundary conditions.	52
Figure 2.16. FEM envelop of stiffness K1 and K2 per depth of multiple heel length.	53

Figure 2.17. FEM envelop of maximum load F_{max} per notch depth.	54
Figure 2.18. Load-displacement curves comparison between experimental and FEM of series I.	54
Figure 3.1. Connector layout of Beam 3 and actual image of the beams before concrete casting	64
Figure 3.2. Schematic plan of the supports at the early and later state of the beam	65
Figure 3.3. Accelerometer layout with the hammer impact location	66
Figure 3.4. Cross-section of notched beams	68
Figure 3.5. Composite beam FEM model	72
Figure 3.6. Mesh sensitivity, data labels represent the corresponding element size	72
Figure 3.7. Frequency response functions (FRF) from 24 measurement points of bare CLT beams and CCC beams 28 days after concrete casting.....	74
Figure 3.8. Proposed design criterion with subjective evaluations of CCC floors [127] and calculated results of this study	79
Figure 4.1. Minimum and maximum floor composition	90
Figure 4.2. Connector layout of the tested CCC specimen [155]	90
Figure 4.3. Design variable and objectives of the optimization.....	93
Figure 4.4. Fitness value and Hyper volume of the optimization	99
Figure 4.5. Pareto front of CLT-concrete solution for 9 m floor span.....	100
Figure 4.6. Parallel coordinate of the solutions for 9 m floor span. Detailed version is presented in Annex 5	101
Figure 4.7. Pareto front of different floor span	102
Figure 4.8. Pareto fronts of different ratio Timber/Concrete for 8 m (top) and 9 m (bottom) floor span.....	103
Figure A2.1. Dimensionless distribution of slip modulus K_1 , K_2 , and maximum load F_{max} ...	125

LIST OF ABBREVIATIONS AND ACRONYMS

A_c, A_t	[mm ²]	Cross-section area of concrete and timber
A_i	[mm ²]	Cross-section area of i^{th} layer of CLT panel
$A_{t,net}$	[mm ²]	Cross-section area of longitudinal lamination
a_c, a_t	[mm]	Distance from the centroid of concrete and timber to the centroid of composite section
b, b_c, b_t	[mm]	Width of floor strip, concrete, and timber
$C, C_t, C_c, C_{cnt}, C_i, C_{gyss}$	[cost unit/m ²]	Total cost, cost of timber, concrete, connector, interlayer, and gypsum board
d	[mm]	Deflection (in general)
d_{1kN}	[mm]	Deflection due to 1kN concentrated force
d_{ST}, d_{LT}	[mm]	Deflection due to standard-term and long-term effect
d_{max}	[mm]	Maximum deflection (in general)
$d_{max,ins}, d_{max,LT}$	[mm]	Maximum deflection due to standard-term and long-term effect
E_c, E_t	[MPa]	Elastic modulus of concrete and timber
EI_{eff}	[N.mm ²]	Effective bending stiffness
F_b, F_v, F_t	[MPa]	Bending, shear, and tensile factored strength
$F_{max} (F_{max,cnt})$	[kN]	Maximum shear resistance of the connector
f_1	[Hz]	Natural frequency of first mode, or fundamental frequency
f_c	[MPa]	Concrete compression strength
h	[mm]	Thickness of composite section
h_d	[mm]	Effective distance between timber and concrete centroid
h_c, h_t	[mm]	Thickness of concrete, timber layer
$h_i, h_{i,eff}$	[mm]	Interlayer thickness and effective interlayer thickness
$h_{t,long}$	[mm]	Thickness of longitudinal laminations
I_c, I_t	[mm ⁴]	Inertia moment of concrete and timber layer
K or K_2	[kN/mm ²]	Unitary elastic stiffness of shear connector
$K_{creep,cnt}, K_{creep,t}, K_{creep,c}$	[-]	Creep coefficient of connector, timber, and concrete
K_D	[-]	Load duration factor
K_{fi}	[-]	Fire resistance factor
K_H	[-]	System factor
$K_{r,b}$	[-]	Bending factor, 0.85
K_{Sb}, K_{St}, K_{Sv}	[-]	Service condition factor
K_T	[-]	Treatment factor
L	[mm or m]	Beam length
M_f	[N.mm]	Factored bending moment
M_r	[N.mm]	Bending moment resistance of composite

$M_{r,\gamma,c}, M_{r,\gamma,t}$	[N.mm]	Equivalent bending moment resistance due to concrete, timber
$M_{r,t}$	[N.mm]	Bending moment resistance of timber
m_v	[kg/m]	Mass of the floor-strip per length unit
m	[kg/m ²]	Mass of the floor-strip per surface unit
n	[row]	Number of connector row
P	[N]	Total concentrated load applied on the beam
q	[kN/m ²]	Distributed load (in general)
q_D, q_L	[kN/m ²]	Dead load and live load
s	[mm]	Spacing between connectors
$T_{r,t}$	[N]	Tensile resistance of timber
t	[minutes]	Fire exposure duration
t_{fi}	[minutes]	Fire protection duration of type-X gypsum board
t_n	[mm]	Notch depth
V_f	[kN]	Factored shear force
$V_{f,conn}$	[kN]	Factored shear force at the critical connector position
V_r	[kN]	Shear resistance of composite
$V_{r,c}, V_{r,t}$	[kN]	Shear resistance of concrete and timber
$V_{r,\gamma,conn}$	[kN]	Equivalent shear resistance of composite
$V_{r,\gamma,c}, V_{r,\gamma,t}$	[kN]	Equivalent shear resistance of composite
$x_{c,n}, x_t$	[mm]	Char depth for notional charring and zero-strength layer depth
x_r	[mm]	Effective char depth
β_n	[mm/min]	Nominal charring rate
γ_c, γ_t	[-]	Gamma coefficient of concrete and timber
ϕ	[-]	Resistance factor

TCC	Timber concrete composite
CLT	Cross-laminated timber
CCC	Cross-laminated timber concrete composite
FRF	Frequency response function
EWP	Engineered wood product

INTRODUCTION

SCIENTIFIC AND INDUSTRIAL CONTEXT

Pierre-Eugene Gauthier invented cross-laminated timber (CLT) in 1950 and patented it in 1952 [10]. It was redeveloped in Austria in the early 1990s [11], saw much broader usage in Europe by the 2000s, and newly introduced to North America. As a result, many CLT production lines were implemented in Canada and, more recently, in France with different processes. In 2017, France and Canada initiated the WoodRise project, a global network on research and development to promote medium- and high-rise timber buildings.

Since the construction of Murray Grove tower [12] (completed in 2009, London, England), a 9-story building entirely built from prefabricated solid timber, CLT was proved a viable solution for high-rise timber buildings. Recently, Canada witnessed many successful applications of CLT in the construction of medium and high-rise buildings, including Brock Commons Tallwood House [13] (completed in 2017, Vancouver, British Columbia), the highest residential building in timber construction with 17 stories in CLT panels, and Origine [14] (completed in 2017, Quebec City, Quebec), a 12-story building based on a concrete podium, constructed entirely by CLT and glued-laminated timber. In France, the high-rise timber towers, such as Sensations (Strasbourg), Silva tower (Bordeaux), are already or being built [15]. The world's tallest timber building is the HoHo tower [16] (completed in 2019, Vienna, Austria). The record of 84 m height will soon be break by many projects around the globe, and CLT will continue to play an essential role in constructing these projects.

In Canada in 2011, the CLT handbook [11] was published by FPInnovation as a guideline for the design of CLT structures. In 2015, CLT was incorporated into the National Design Specification (NDS 2015) [17] for wood construction. In addition, the use of CLT was included in the International Building Code (IBC 2015) [18] and in the Canadian standard of Engineering designs in wood (CSA O86- 14) [19]. Therefore, CLT is now a code-compliant construction material. These actions have paved a vital way for engineers to adopt this product as a highly potential and sustainable building material.

CLT panels are multi-functional and used as the building's main load-bearing element. In addition, they can be used to build structures above the ground like walls, intermediate floors, and roofs. CLT's benefits include dimensional accuracy, easy handling during construction. This factor leads to effective, time-saving implementation and reduces the need for storage space in the worksite [11].

In terms of vibration, test results at FPInnovation [11] shown that bare CLT floors can have their area density varying from approximately 30 kg/m² to 150 kg/m² and a fundamental frequency above 9Hz. However, the design criterion was different between a traditional lightweight wood joisted floor and a massive concrete slab floor. Therefore, Hu *et al.* proposed a new criterion for the design of CLT floors. It is based on the concept of limiting the floor span in correlation with objective human perception. This method was introduced in the CLT handbook and then adopted in CSA O86-14, reprinted version June 2017 [19]. However, the current form of the design method applies to CLT floors without topping or without composite action between the topping and CLT.

PROBLEM STATEMENT

The conventional CLT floor usually has a maximum clear span of about 6-7 m. Beyond that, serviceability conditions, *i.e.*, vibration and deflection, are the factors that control mainly the design process. Thus, the composite floor of concrete and CLT are adopted to satisfy those conditions. The concept comprises a CLT layer, a concrete one, and a shear connection between the layers to transfer the shear stress developed at the interface. By achieving the composite action, the mechanical performance of the structure is generally higher than those of its components. This approach results in highly efficient use of materials, the concrete slab supporting compression stresses while the timber part mainly holds the tension stresses.

However, the concrete was usually added as a topping layer on the CLT floor without composite action. The reasons are the high cost of the composite connector and lack of knowledge about the impact of collaboration effect on the vibrational performance of CLT-concrete floors. The project is dedicated to the research of composite action and the vibration performance of CLT-concrete floor structures. The study also focuses on long-span structures that can vibrate with greater amplitude at low frequency.

OBJECTIVES

One of the two objectives of the research project is to evaluate the vibrational behavior of CCC floor structures. This evaluation aimed mainly at the long-span floor structures because their designs are usually governed by vibrational performance. The evaluation is divided into two steps: connection and composite beams.

Understanding the behavior of connector systems of CLT-concrete composite structures: A solution for the connector system of CLT-concrete composite

floor structures will be proposed and evaluated. This objective includes a numerical model to predict the performance of the connector. In addition, a method to uninstall the screws will be tested as a feasible solution for deconstructing the floors.

Understanding the vibrational behavior of CLT-concrete composite beams:

The primary parameters of the study are the connection system, the effective bending stiffness of the section, and the span of the beams. A comparative analysis will be performed based on analytical and numerical models. The main goal is to determine the correlation between the primary parameters and the dynamic responses, such as fundamental frequency and damping ratio. Design criteria defined in Eurocode 5 and CSA-O86 for the lightweight timber floor will be validated using the experimental results.

The second objective is to build a toolbox to optimize the CCC floor design.

Optimization multiobjective of the CCC floors design:

The evaluation step information will be fed into multiobjective optimization to obtain the optimized designs of CCC floors. The objective functions are the mass, thickness, and total cost of constructing the floor. In addition, optimized designs are also subjected to the structural constraint functions of serviceability and ultimate limit state.

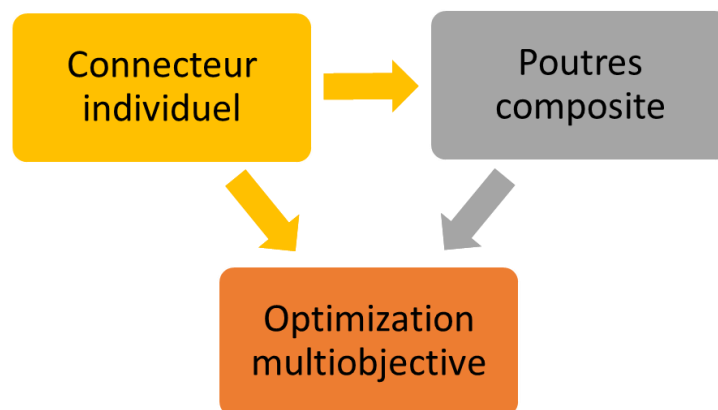


Figure I.1. Structure of the research

ORIGINALITY OF THE RESEARCH

The notched connector performance is studied regarding its principal parameters, such as notch depth and length of the loaded edge. Furthermore, the mentioned connector is also deconstructable, thanks to the implementation of screws systems. Therefore, using notch connectors could be a competitive solution for a TCC floor in terms of cost and performance.

This research will evaluate the application of the notched connector for the CLT-concrete floor. Since the demand for using CLT-concrete for a long-span floor structure at a reasonable cost is rising recently, this study will focus on vibration composite beams elements regarding the effect of composite connectors.

CLT-concrete structures are conditioned by many parameters such as their materials, the dimension of constituent elements, and the connectors. This research will demonstrate the optimization process to obtain the optimal floor design regarding the construction cost and structural performance.

THESIS ORGANIZATION AND RELATIONSHIP BETWEEN THE CHAPTERS

This thesis is mainly composed of three scientific articles written during the research project. The introduction covered the scientific and industrial context, the problem, and the objectives. Besides, the research methodology and the critical results are also presented in French in the “Résumé étendu” section.

The literature review section focused on state-of-the-art timber-concrete composite structures and methods for vibration control for lightweight floors. In addition, experimental tests on the performance of the individual composite connector and the cross-laminated timber-concrete composite beam were discussed in this review.

The first article discussed the performance of screw-reinforced notch connectors and the influence of geometric variables on connector stiffness and strength. The finite element model for determining the stiffness and strength of the connector at the notch was presented and validated by the experimental results.

The second article focused on long-span cross-laminated timber-concrete composite beams using notch connectors. The static and dynamic experimental tests on three composite beams were carried out and analyzed. Calibration of the stiffness of the cross-laminated timber panels shows the influence of the notches on the panel stiffness and, therefore, the beam frequency and deflection.

The third article dealt with the optimization aspect of the research project. A multiobjective optimization relating to the design of cross-laminated timber-concrete floors was carried out. The objective functions are mass, thickness, and cost. In addition, the structural constraint functions have been adopted: service, ultimate, vibration, and fire constraints.

1. LITERATURE REVIEW: VIBRATION OF CROSS-LAMINATED TIMBER – CONCRETE COMPOSITE FLOORS

1.1. TIMBER-CONCRETE COMPOSITE

Timber was used with concrete as a composite structure (Timber Concrete Composite - TCC). This concept results in the highly efficient use of materials. The concrete slab support compression stresses while the timber part experiences the tension stresses. In addition, shear connectors were introduced between two layers to acquire a high composite level and increase the structure's strength and stiffness.

The steel scarcity after World War I and II motivated the TCC concept. As a result, many efforts were made to renovate and preserve the timber buildings in Europe and build highway bridges in the United States and Canada [20]. In 1922 and 1939 [21], proprietary connectors for TCC were patented. In the 1950s, bridge constructions in Australia and New Zealand began using the TCC technic [22]. However, the attention on TCC was only re-built in the early 1990s, and the TCC construction was embraced for bridges, upgrading timber floors for renovation, and new buildings.

Typically, the TCC structure involves traditional engineered wood products like glued-laminated timber (glulam) or laminated veneer lumber (LVL). However, the use of cross-laminated timber (CLT) and other EWP products like dowel-laminated timber (DLT) nailed-laminated timber (NLT) for TCC structures are still in development. One successful CLT-concrete composite (CCC) application was the Design Building at the University of Massachusetts [7].



Figure 1.1. CLT panels with preinstalled HBV connectors, at the UMass Olver Design Building, University of Massachusetts, Amherst, USA. Image courtesy of Alex Schreyer.

In this building, the floor span ranged from 6 to 8 m, with the section comprising 175 mm of 5 ply CLT panel, 25 mm of rigid insulation, and 100 mm of reinforced

concrete. The connector composite was the well-known HBV® system, a patented product from Germany. Vibration is almost always the designing factor in the case of Design Building as opposed to bending or shear strength [7].

The Earth Science Building at the University of British Columbia [23] adopted the timber-concrete composite floor for spans of up to 6.4 m. Using laminated strand lumber (LSL) with a 100-mm reinforced concrete slab and 25-mm insulation, the floor structures perform well in vibration, sound transmission, structural and thermal requirements while having half the weight of a similar concrete structure. The composite action was assured by the steel plates glued into the timber panel and anchored into the cast-in-place concrete.

1.1.1. Composite action

The timber-concrete composite structures (TCC) combine two different materials with different characteristics to support bending and shear stress. When the structure is subjected to bending, the wood mainly supports the tensile forces, and the concrete is mainly in compression. A multilayer structure without connectors is said to be “non-composite,” as opposed to the one with a perfectly rigid connector system, therefore having “full composite action.” The deformation of the connector systematically leads to a relative sliding between the layers of the composite. This structure, therefore, has a “partial composite action.” To effectively transfer the stress between layers of this multilayer structure requires a shear connector system that connects these layers. The connector performance, *i.e.*, stiffness and strength of the connector, will govern the behavior of the TCC. Therefore, shear connectors are a crucial factor for TCCs.

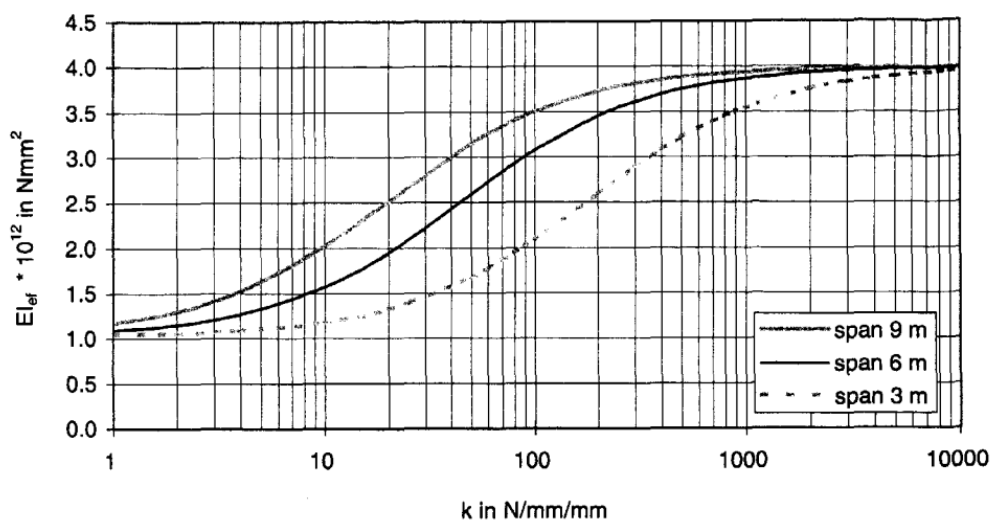


Figure 1.2. Relationship between the effective bending stiffness of the composite beam and the slip modulus on a logarithmic scale, per Van der Linden [24].

Van der Linden [24] presented a graphic showing the influence of connectors on cross-section stiffness (Figure 1.2). The relationship followed an asymptote curve. Thus, increasing the connector stiffness could be the key to obtaining high composite action, but this solution might only be effective to a certain extent.

1.1.2. Effective bending stiffness of the composite section

The effective bending stiffness of the TCC section is essential information needed for any calculation of the TCC structures, especially the deflection and the fundamental frequency. However, since the composite connectors are usually not perfectly rigid due to the deformable nature of timber, the composite action in TCC structures is considered partial in most cases [25].

The most popular method to estimate the effective bending stiffness is the Gamma (γ) method, presented in the Annex of Eurocode 5 [8]. Based on the works of Werner [26], Newmark *et al.* [27], and Mohler [28], this method takes into account the slip between timber and concrete under the sinusoidal distributed load. The model is simple and easy to use despite the constant cross-section, connector properties, and linear behaviors requirements. Many authors proposed different methods to overcome the limitation, from considering different load conditions and nonlinear behaviors [29] to discrete connections [30]. Such new analytical approaches provided closed-form expressions to quantify the static behavior of TCC: slip, moment, shear, axial force, and stress.

In terms of dynamic responses of TCC, the governing differential equations of vibration of partial-composite beams were addressed in the study of Wu *et al.* [31]. Based on the Euler-Bernoulli beam theory, the exact frequency solution for a cross-section with two sub-elements of different materials can be obtained. Furthermore, the effective bending stiffness can be deduced when neglecting the effect of axial force [32]. Although the same limitations as the γ -method were imposed, the expression of the effective bending stiffness is mode- n dependent. This difference means that the natural frequency of the high-order modes could be correctly estimated, unlike the static-based γ -method could only estimate the fundamental frequency. Girhammar *et al.* [33] also found precisely the same expressions to quantify the effective bending stiffness of TCC beams regarding different boundary conditions.

To consider the shear deformation of each layer and the rotatory inertia, Xu and Wu [34] proposed a complete method based on Timoshenko's beam theory to calculate the natural frequency of a simply supported beam. Although, it is worth noting that when

the ratio L/h is high, the effects of shear deformation and rotatory inertia are negligible [34]–[36].

1.1.3. Constituent materials

1.1.3.1. Timber

For TCC applications, the timber elements can have a beam-like form, such as timber joist, glued-laminated timber (GLT), laminated strand lumber (LSL), or laminated veneer lumber (LVL). In addition, the panel-like form could also be employed to create TCC floors by using CLT, LVL, dowel-laminated timber (DLT), and nailed-laminated timber (NLT).

a. Cross-laminated timber panel

CLT is manufactured by gluing lumber board laminations perpendicular to each other. CLT panel could have at least three up to nine layers. The manufacturers and regional regulations vary the panel dimension. Other proprietary CLT products could have their laminations positioned at a different angle than 90 degrees, attached using nails, screws, or wooden dowel.

CLT is very versatile since it could be used as floors, roofs, shear walls, elevator shafts, and cores. Along with its possibility of prefabrication, CLT allowed a precise and quick build-up of the building with less workforce, reduced noise, and waste on the construction site.

From a structural standpoint, the primary advantage of using CLT or timber, in general, is the lightweight characteristic. This aspect could help reduce substantially the weight imposed on bearing structures such as beams, columns, and foundations. In addition, by using CLT, the floor structures' in-plane and out-of-plane strength and stiffness are enhanced. As seen in the reinforced concrete slab, the two-way action could be obtained.

Although being adopted for many construction applications around the globe, CLT still experienced some drawbacks of high fabrication cost and designing regulations, especially in the fire and acoustic aspects.

b. Cross-laminated timber mechanical properties

In North America, the CLT stress grades (or layups), usually comply with the ANSI/APA PRG 320 standard for performance-rated CLT [37]. Canada standard of Engineering Design in Wood, CSA-O86:2014 [9] incorporated the guidelines from PRG 320 for Canadian wood species. In Europe, the properties of CLT vary from one manufacturer to another and comply with the European guideline EN 16351 [38].

However, up to now, it still requires a European Technical Agreement to be delivered to the building market.

The rolling shear strength and stiffness of CLT is considered critical property that may govern the design and the performance of CLT structures. The rolling shear deformation in CLT is caused by the low vertical shear modulus of the transverse laminations [40] while subjected to perpendicular tangential stress. Despite being influenced by many parameters, such as wood density, annual ring width, cutting patterns, lamination size, the rolling shear modulus of lamellas is assumed in Standards to be equal to 1/10 of parallel to grain shear modulus [39].

Some analytical methods can estimate the bending stiffness of CLT along the major strength axis. The most popular and widely adopted methods are Shear Analogy (SA) [41] and Gamma (γ) method [8]. The shear Analogy method, presented by Kreuzinger in 1999, took into account the shear deformation of longitudinal and transversal layers that could accurately and adequately predict the stiffness of CLT panels. This method was used in ANSI/APA PRG 320 [37] and CSA-O86:2014 updated 2016 [9]. The total deflection of the CLT panel would be due to both bending and shear deformation components. Gamma method [8], as previously presented in Section 1.1.2, was initially used for Mechanically Jointed Beams [42], which could determine the bending stiffness of the CLT panel. However, this method was deemed less accurate since it does not account for the shear deformation of longitudinal layers. According to the Canada CLT handbook [39, Ch. 3], the Gamma method was suggested when the cross-section is unsymmetrical due to different thicknesses and materials.

Using a notched connector in CLT-concrete composite floor would cause some issues due to the rolling shear phenomenon and the reduced bending stiffness of the CLT panel. First, the rolling shear would influence the stiffness of the notched connector, causing some reduction in stiffness when the notch cuts further into the upper-most lamination. This phenomenon was reported in Section 2. Second, another issue is that the notch cut on the CLT panel will likely cause some reduction in moment inertia and hence the bending stiffness of the CLT panel. This aspect was discussed further in Section 3.

1.1.3.2. Concrete

a. Concrete properties

Concrete was adopted for TCC structures for its density and high compression strength. Many types of concrete can be used for TCC structures, varying from standard concrete up to high-performance one (compression strength of 250 MPa) [43],

reinforced with steel bars or fibers. However, in terms of vibration, the impact of concrete mass could be unfavorable. The fundamental frequency can only increase to a certain extent then decrease when the concrete thickness increases [44]. The use of concrete for TCC structures, especially when notched connectors are involved, would require the concrete to be self-compacting [45], using concrete with plasticizers or superplasticizers and fine aggregates. The superplasticizers are usually added to the concrete mixture to enhance the workability while keeping the ratio of water-to-cement low.

A side benefit of reducing water in the concrete is limiting the moisture transfer between the timber and concrete. This phenomenon occurred at the early age of cast-in-place concrete is an ongoing question. Lamothe *et al.* [46] used plastic film to prevent moisture transfer and assure concrete and timber quality. However, the geometry form of notched connectors could be jeopardized due to unsettled plastic film, and hence the TCC strength and stiffness could be reduced. Song *et al.* [47] found that exposing CLT to wet concrete could deteriorate timber quality and degrade and delaminate the CLT. The authors suggested that epoxy adhesive could effectively prevent the moisture from penetrating the CLT. Although, it is worth noting that introducing any additional layer between timber and concrete would drive the TCC cost up and negatively impact its competitiveness. Nguyen *et al.* [48] showed that the high-performance concrete with low water amount could help avoid moisture transfer prevention measures.

b. Lightweight and high-performance concrete

Many researchers studied the influence of high-performance concrete on the performance of timber-concrete composite (TCC). In general, high-performance concrete, such as lightweight concrete, steel fiber reinforced concrete, high strength concrete, and self-compacting concrete, was deemed more advantageous than standard concrete. The timber design with such concretes shows some edges in terms of mass, stiffness, resistance, and thickness but comes with a higher cost.

Steinberg *et al.* [49] used lightweight concrete to minimize the total mass of the structures. It was concluded that the structures were affected by the low modulus of elasticity of lightweight concrete, and this causes the reduction of the effective bending stiffness. A denser connector layout could be used to compensate for this reduction. The lightweight concrete did not affect the stiffness and resistance of the proprietary connector “Tecnaria” [21] since the timber properties governed the connector performance. However, a higher grade lightweight concrete was also recommended [50] to assure connection efficiency.

Steel fiber reinforced concrete was used in the study of Kieslich and Holschemacher [51] to reduce the thickness of the concrete slab. Results from the push-out test showed that shear strength and initial stiffness are increased compared to regular reinforced concrete. Lamothe *et al.* [52] stated the same conclusion based on the experimental tests of the TCC notched connector using ultra-high performance fiber reinforced concrete. The notch connector was more rigid, more robust, and helped avoid shear failure of concrete.

Using lightweight concrete could reduce floor mass. The steel fiber reinforced concrete is a potential solution to minimize floor thickness while retaining the same performance, consequently limiting the floor mass. However, the floor mass reduction could lead to inferior vibration performance based on Ghafar's study [44] about the impact of concrete thickness on the natural frequencies.

For notch connectors, shrinkage of concrete in the early days of curing duration will result in a gap at the outer edge of the connection. The phenomenon caused undesired initial permanent deflection of the composite beam. Therefore, it is recommended to use low shrinkage concrete to minimize this unwanted phenomenon while obtaining high workability and flowability [53], [54].

1.1.4. Shear connector

There are three intrinsic components to a TCC floor: (i) concrete layer, (ii) bearing timber components, like timber beams, joist or CLT layer, and (iii) connection system. Besides these components, there are also many other elements like boundary condition, coating and covering layers, insulation interlayer, affecting how a composite floor performs in vibration.

Combining many connector types is the best way to maximize advantages while avoiding and compensating for disadvantages. For example, notch reinforced by screw or steel plate with glue. However, the mixed-use of connectors requires both machining and on-site effort and could lead to extra cost when applied to the floor structure. The most potential combination is a notch with reinforcement. Dias *et al.* [25] compared popular composite connection solutions. The load slip curves in Figure 1.3 shows that the notch with the dowel is a balance solution, adequately stiff while providing some degree of ductility, *i.e.*, plastic deformation before total rupture. It corrects the disadvantage of ductility lack on the notch and low rigidity of dowel type connector. Boccadoro [55] demonstrated two primary advantages of the notch connector: the high stiffness in elastic conditions minimizes the deformations at the service level; the ductility

of the notch at the failure level could be assured if a compressive failure of timber is governing.

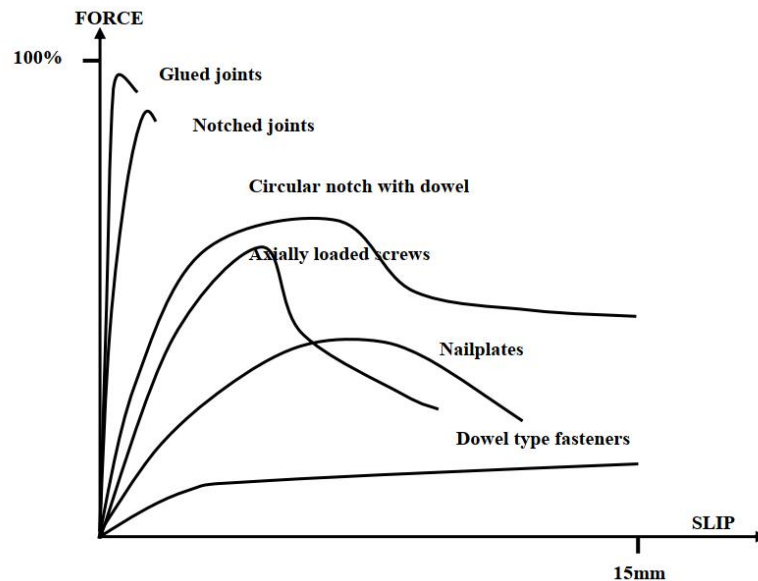


Figure 1.3. Comparison of different types of typical TCC connectors by Dias [25].

The interlayer between timber and concrete has specific influences on the strength and stiffness of the connector. This practice increases the stiffness without increasing the overall mass and, more importantly, enhances the thermal and acoustic performance. Adding an interlayer between timber and concrete could mean a trade-off between acoustic and structural performance. The rigid contact between timber and concrete could impact the acoustic aspect of the floor. A fully floating concrete slab that has composite action is inherently impossible. Lamothe *et al.* [52] found some reduction in stiffness in the individual bird-mouth notch connector when introducing the interlayer into the TCC. However, the authors remarked that the moment of inertia enhancement in the TCC cross-section could compensate for the stiffness loss of the connectors. Djoubissie Denouwe *et al.* [56] also concluded that the presence of interlayer reduced the shear strength and stiffness of the composite connector with threaded bar. Mirdad and Chui [57] found that the stiffness of screw composite connectors could heavily be suffered even for minimal interlayer thickness. The connector strength is more sensitive to other parameters, such as screw insertion angle and embedment length.

Dowel-type fastener

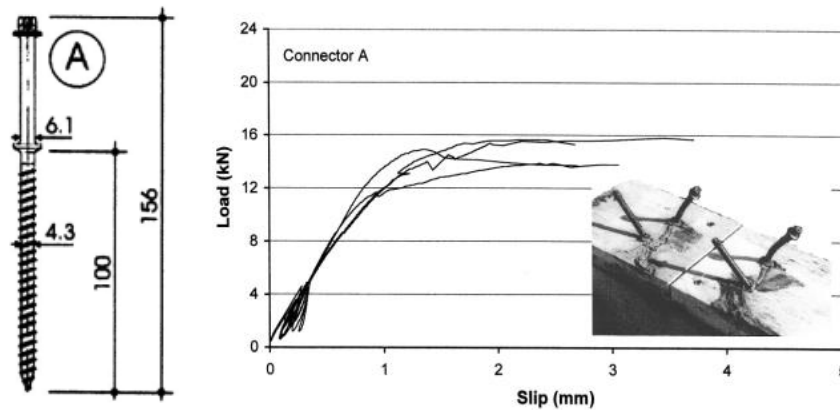
The mechanical fastener shear connector was a straightforward method to connector concrete to the timber layer. This method involves the penetration of a part of the fastener in the timber element. The other part was anchored in concrete. This

fastener could be nails, screws, lag-screws, or bolts. The main advantage a screw has over a nail is its additional withdrawal capacity.

a. Screws

Recently, inclined screws have gained some interest as a timber-concrete connector due to their high withdrawal strength and stiffness compared with the screw installed perpendicular to the grain. Many researchers have tested the VB screw, or SFS screw, a connector specifically developed for TCC structures. The best performance is achieved when placing the screws pairwise, inclining the screws within the pair at 45° and 135°, respectively. The two inclined screws would utilize the fastener's more considerable axial tensile stiffness than the shear stiffness if the fastener only provides dowel action. Unfortunately, the SFS screws failed in a brittle manner, and they remain uninfluenced by the presence of an interlayer, as indicated by Deam *et al.* [58].

Steinberg *et al.* [49] have tested the shear performance (stiffness and resistance) of inclined regular screws and inclined SFS screws in a series of five specimens (Figure 1.4). The experimental results were presented for a single connector, *i.e.*, a pair of screws. The load resistance fluctuated from 15 to 22 kN, while the initial stiffness was 10 to 15 kN/mm. The performance of SFS screws was consistent, their initial stiffness was less, but they had greater strength than the regular screws.



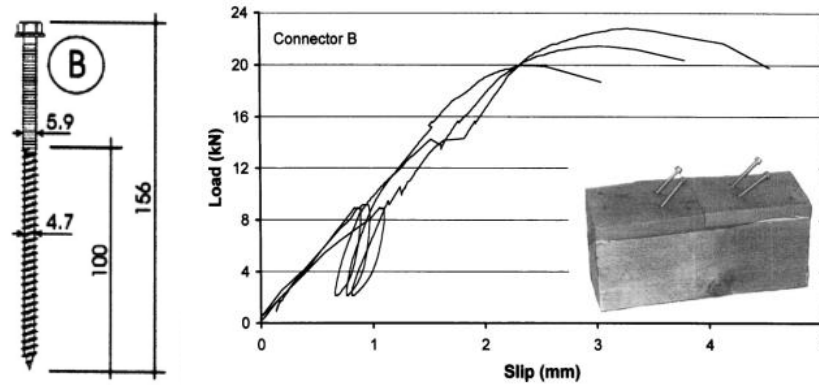


Figure 1.4. Load-slip curves of SFS screws (A) and regular screws (B) by Steinberg *et al.* [49]

Gerber [59] conducted a series of shear tests on self-tapping screws Assy VG CYL with many modifications of timber material (LSL, LVL, and CLT), installation angle of the screw (30° and 45°), and insulation interlayer (Figure 1.5). Fully threaded STS Assy VG with a 10 mm diameter and 240 mm long were used. The test results showed high strength and stiffness with little or no residual displacement under service loads.

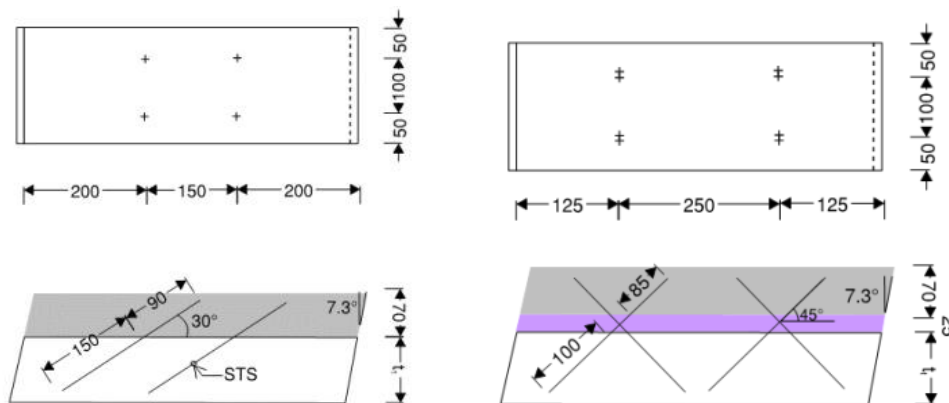


Figure 1.5. Specimens with STS at 30° and pairs of STS at 45° with insulation layer, by Gerber [59].

Mai *et al.* [4] conducted a series of shear tests on six CCC specimens using bolt connectors and five other specimens using SFS screws. Each specimen has a different configuration in screw angles and concrete thickness. In this study, the screw series showed relatively ductile behavior, while the SFS screw series showed brittle and quite brittle modes of failure, respectively. There was no considerable difference in terms of shear strength and slip modulus. However, it seemed that the connections using the SFS screw had a slightly bigger shear capacity compared with the regular screw, especially for inclined connections.

b. Bolts

Lag screws are some of the most rigid types of screws. They are generally used to connect heavy lumber and other materials that bear an intense load. Deam *et al.* [58] have stated that the average type of failure of the lag screw is ductile. The ultimate load of the lag screw with a diameter of 16 mm was higher than the one of 12 mm because the load was distributed into timber over a larger area (Figure 1.6). The $\Phi 16$ -screw also caused the LVL to split longitudinally. The yielding of the steel and crushing of the wood resulted in substantial deformations (22 mm) before the peak strength was reached. This phenomenon would prevent the screws from developing their full strength in a flooring system.



Figure 1.6. Lag screws connectors, by Deam *et al.* [58]

Mai *et al.* [4] conducted a series of shear tests on four CCC specimens using bolt connectors (Figure 1.7). Each specimen has its configuration that differentiates from others in an installed angle, concrete thickness. Bolt connectors exhibited an almost brittle behavior in these measurements. The connector installed at 90° to timber grain witnessed the lowest slip modulus in the series.

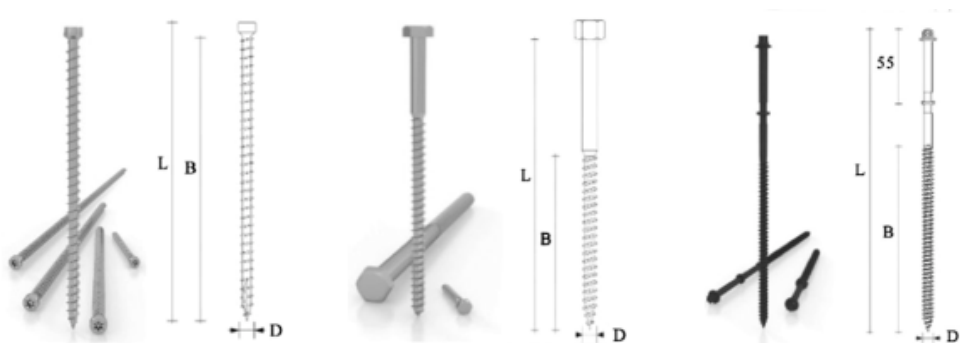


Figure 1.7. Screw, bolt, and SFS screw, by Mai *et al.* [4]

Longitudinal connector

Glued-in steel connector system Holz-Beton-Verbund (HBV) (Figure 1.8) has recently gained attention from engineers and researchers. This connector is the most viable option in achieving strength, stiffness, and ductility. However, there are some

concerns regarding the assurance of stringent quality control measures, the complexity of applications at the worksite, and high costs [59]. However, the installation of steel mesh *in situ* raised some concerns about worker security. Furthermore, considering that this connector is a patented product, the cost of using HBV could be high, and the quality control is somewhat tricky.

In a recent study on the shear capacity of the connector on LVL-concrete and CLT-concrete specimens, Gerber [59] found the specimens with 25 mm of insulation layer exhibited a less stiff behavior and a failure at lower loads as compared to those without the interlayer. These results could be due to the insulation's lack of lateral restraint; hence the mesh had to deal with longer buckling length.



Figure 1.8. HBV installation, by Gerber [59]

Yeoh [60] investigated the shear performance of a double-sided toothed metal plate in the double LVL-concrete specimens. The connector was easy to construct, and it exhibited a ductile plate tearing failure with high strength and stiffness. Furthermore, the strength prediction of this connector could base on plate yield strength and length.

Notched connectors

a. Notched connectors only

The notch connection for TCC systems is obtained by creating a notch in the timber, and the concrete pouring in the notch will create an interlock between two materials. The geometry form of the notch is usually rectangular, as it is straightforward for machining. Many other forms, like bird-mouth (rectangular), trapezoidal, round, and dovetail, were also investigated by researchers. This connector type was reported to have high strength and stiffness but low ductility. Deam *et al.* [58] tested the round notch's shear performance with a diameter of 48.5 mm and a depth of 20 mm (Figure

1.9). The connector produced significant strength and stiffness due to the LVL and concrete notch interface. The behavior of the notch at failure is classified as brittle.



Figure 1.9. Round notch (or plug) connector, by Deam *et al.* [58]

Three geometric types of notch connectors were investigated by Yeoh [60] (Figure 1.10). The triangular-shaped notch was comparable to the rectangular one when comparing the maximum shear capacity. As expected, the failure of these connectors tends to have low ductility compared to the connector of the same geometric form with lag screws.

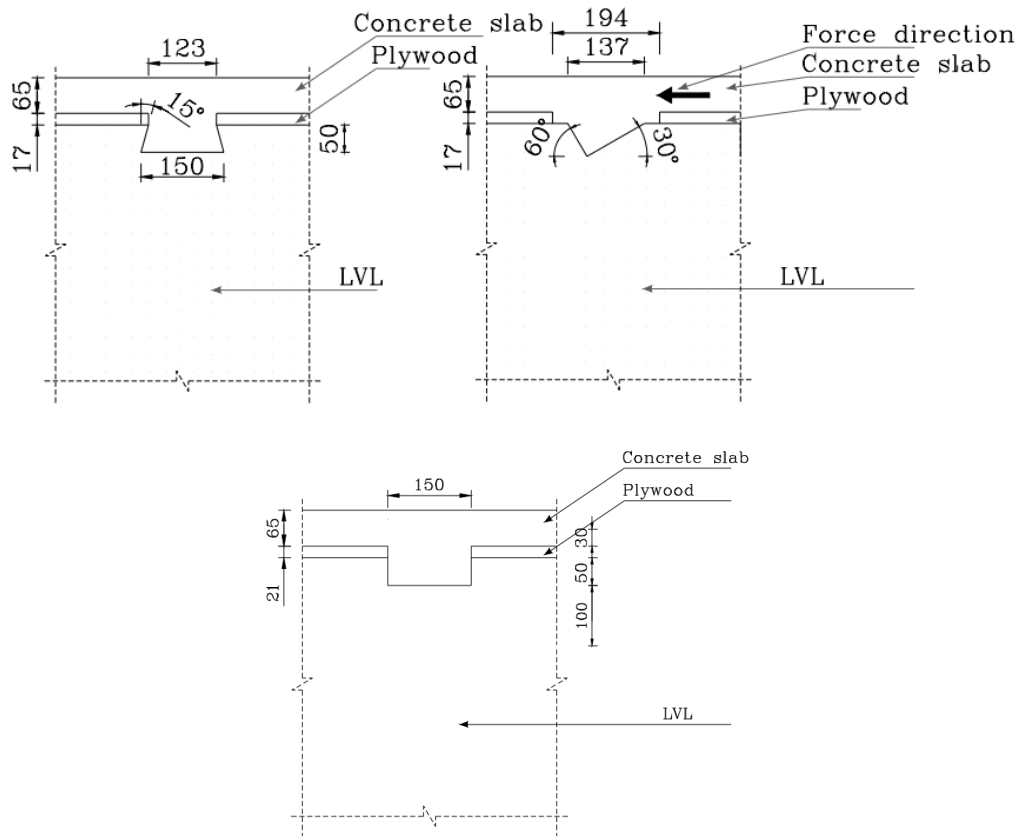


Figure 1.10. Three geometry form of notch connectors, by Yeoh [60]

b. Notch reinforced with fastener

Notch connector is a prominent solution for TCC structure using mass timber panel. Notches cut could be made by a simple CNC machining process during the fabrication of timber panels. In addition, the notch with vertical screws could be a remedy to the low ductility of the notch connector [25]. However, the ductility of individual connectors depends on the type and the number of screws, and a ductile connector could not ensure the ductile behavior of a whole structure [43].

In the study of Rijal [61], it was concluded that the bird-mouth type connections exhibited higher strength and stiffness than the trapezoidal notch connections. The failure mode of bird-mouth notched connections was different from trapezoidal notched connections. The latter had to crush and splitting failure in the LVL and bending of the lag screw, while the former had no damage in the notch and no bending of the lag screw. This difference in the failure mode could probably be due to the high tensile strength of the lag screw used in these series.

A combination of notch and lag screw was investigated by Deam *et al.* [58]. A lag screw could increase the performances of the specimens with the round concrete notch. The rectangular notch with the lag screw provided greater strength and stiffness

with a larger notch area. The failure mode of these two types of a combination is reported to be the same as the lag screw appeared to hold the fractured surfaces of the concrete together. The strength dropped when the lag screw eventually fractured.

Gutkowski *et al.* [62] tested the shear performance of many configurations of notch size with Hilti dowel and Borden resin (Figure 1.11). The result shows that the notch dimension affected the slip modulus and strength of 2x4 specimens and made no significant effect on 4x4 specimens. Various failure modes were observed in the slip test, with none being predominant.

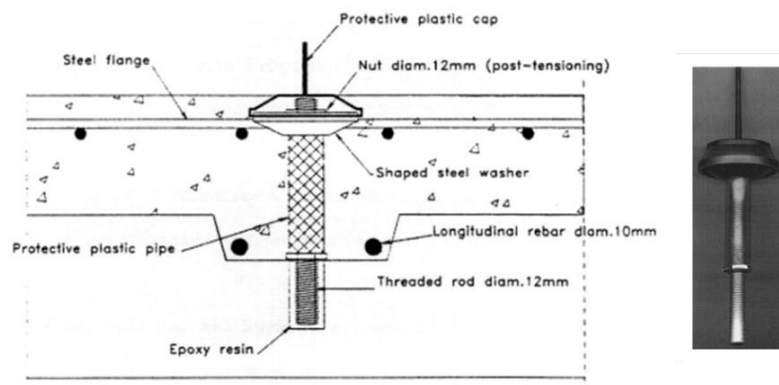


Figure 1.11. Notch with dowel connectors and image of Hilti dowel, by Gutkowski *et al.* [62]

Auclair *et al.* [63] developed the notched connector made of ultra-high-performance fiber-reinforced concrete (UHPFRC) with a steel rod core (Figure 1.12). The notch could be prefabricated and installed before the concrete casting. In addition, the composite connector provided a ductile behavior with excellent shear strength. Thus, a high serviceability stiffness could be obtained, although the variation could be improved by introducing gap fillers and ameliorating the fabrication process. The design was initially aimed for TCC beams, and an application on CLT-concrete floors would require some modifications.

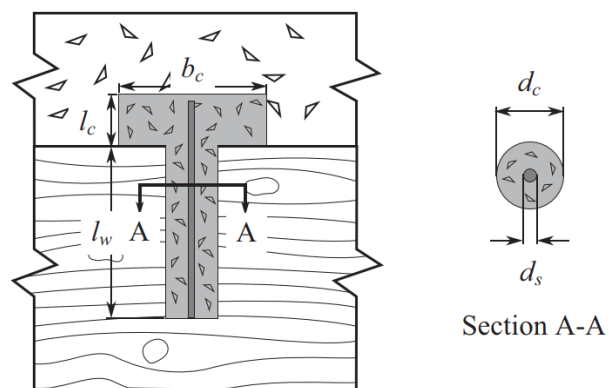


Figure 1.12. Notched connector geometry, by C. Auclair *et al.* [63]

1.2. VIBRATION OF TIMBER FLOORS

1.2.1. Vibration theory

Dynamics considers the behavior and effect of motion on a body. Vibration is a specific part of dynamics that considers cyclic motion [64]. Specifically, floor vibration is the up-and-down motion caused by forces that are directly applied to the floor by the people or machinery or by vibrations transmitted through building columns, other floors, or the ground [65]. The most usual and essential source of dynamic excitation is pedestrian traffic. A person walking at a regular pace applies a periodically repeated force to the floor, which may cause a buildup of response.

A body is said to vibrate when it describes an oscillating motion about a reference position. The simple spring-mass model is an easy device to use in thinking about vibration. With only one mass moving in one direction, this system is called single-degree-of-freedom (SDOF). There is also multi-degree-of-freedom (MDOF) systems that feature several parts, and each part has multiple directions in which it can move. Those systems, in general, are also called lumped-parameter systems compared to distributed-parameter systems. To describe the die out and reduce to zero motions of oscillation systems, the theory of differential equations suggests that adding a term $c\dot{x}(t)$ to $m\ddot{x}(t) + kx(t) = 0$, where c is called damping coefficient, will result in a solution $x(t)$ that dies out: $m\ddot{x}(t) + c\dot{x}(t) + kx(t) = 0$. The two-mass system provides an example of a two-degree-of-freedom system (Figure 1.13).

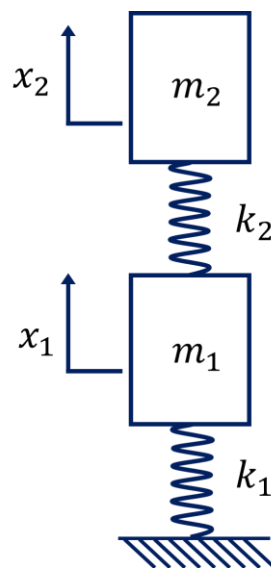


Figure 1.13. A simple two-degree-of-freedom system model.

By summing forces on each mass in the horizontal direction yields: $m_1\ddot{x}_1 + (k_1 + k_2)x_1 - k_2x_2 = 0$ and $m_2\ddot{x}_2 - k_2x_1 + k_2x_2 = 0$. Rewrite these equations in the form of vectors and matrices yields

$$[M]\{\ddot{x}\} + [K]\{x\} = 0 \quad (1.1)$$

Assuming a harmonic solution is assumed of the form $x(t) = \mathbf{u}e^{j\omega t}$, where \mathbf{u} is a non-zero vector of constants to be determined, ω is a constant to be determined and $j = \sqrt{-1}$. By substitution of this assumed the form of solution into matrix equation of motion, Equation (1.1), yields

$$(-\omega^2[M] + [K])\{\mathbf{u}\}e^{j\omega t} = 0 \quad (1.2)$$

Applying the condition of singularity to the coefficient matrix of Equation (1.2) yields the result for non-zero solution \mathbf{u} to exist

$$\det(-\omega^2[M] + [K]) = 0 \quad (1.3)$$

Consider the results of Equation (1.3) are $\pm\omega_1, \pm\omega_2$, there are four solutions of $x(t)$ made of four values of ω and vectors \mathbf{u}_i .

$$\begin{aligned} x(t) &= \mathbf{u}_1e^{j\omega_1 t}; x(t) = \mathbf{u}_1e^{-j\omega_1 t}; \\ x(t) &= \mathbf{u}_2e^{j\omega_2 t}; x(t) = \mathbf{u}_2e^{-j\omega_2 t} \end{aligned} \quad (1.4)$$

This solution defines mode shapes, where u_1 and u_2 are called the first and second mode shapes of the system. Each mass in this system oscillates at two frequencies ω_1 and ω_2 called the natural frequencies of the system.

1.2.2. Parameters of vibration

Stiffness – This parameter decides both the static and dynamic performance of the floor structures in serviceability states. High stiffness leads to less deflection when applied static or dynamic forces. The timber floors are usually highly orthotropic, so longitudinal flexural stiffness is much higher than transversal flexural ones. Dynamically, this would cause vibrations modes to be clustered with smaller spacing in between. As a result, the systems will have many modes under 40 Hz, contributing to the vibration amplitude. The 40 Hz threshold is an arbitrary value proposed by Ohlsson [66] as the author suggested that the contributions to the total motion of higher than 40 Hz modes are insignificant [67]. For instance, using plate-liked engineered wood products CLT or LVL could help reduce this phenomenon [68].

Damping – This means specific internal damping of all materials constitutive of the structure. Damping is even more complicated to predict because it involves the joints, contacts, connectors. Many design standard proposals use a damping ratio of

0.01 – 0.02 (1% - 2%), which is very conservative. The in-situ floors possess a higher level of damping than those in laboratory conditions. Timber structures are reported to have higher damping than steel or heavy concrete structures.

Boundary conditions – This parameter influences the dynamic properties of a floor. It was found that the natural frequencies are higher for a simply supported condition at four edges than at two opposite edges in CLT panels [69]. As a result, the deflection of the structures decreases due to the additional support stiffness [68]. However, this gain in frequency is less critical in the slab systems with double CLT panel half-lap jointed [69] or in the case of long-span floors [68].

Mass – Conventional timber floors usually have lower mass compared to concrete floors. This feature is desirable since it will significantly decrease the charge on the supporting systems (beams, walls, columns, and foundations) and the seismic design and labor gains at the worksite. However, lower mass implies that floors will have greater vibration amplitude for an equal stiffness.

1.2.3. Human perception toward floor vibration

The human perception of floor vibration is complex and challenging to measure. The sensitivity and subjectivity of the human body lead to the fact that no limit is stated for acceptable vibration levels in the design of the building, but only guidelines were developed. The sensitivity of human perception on the floor vibration can be evaluated by the acceleration and the velocity responses to the fundamental natural frequency. Many correlations of subjective perception to an easy-to-use design guideline were found in the literature and discussed in Section 0. These guidelines focus on different vibration responses such as fundamental frequency, number of natural frequencies below 40 Hz, damping, mean acceleration, peak acceleration, velocity, and deflection under a specified static load.

Negreira *et al.* [70] conducted an extensive psycho-vibratory evaluation of timber floors in laboratory conditions using multilevel regression. The authors demonstrated the relationship between the subjective answers of the floor occupants and many measured vibration responses of the floors. The results showed that the best indicator for vibration annoyance is the fundamental frequency (calculated based on EC5 guidelines [8]) and Hu and Chui's ratio [71] (calculated using the fundamental frequency and the deflection of the floor under 1kN point load). On the other hand, for vibration acceptance, the best indicator is the Maximum Transient Vibration Value (a computed based on the acceleration experienced by the test subjects, as per Standard ISO 2631-1:1997 [72]).

1.2.4. Design criteria

The design criteria to limit the annoyance due to floor vibration could be static, dynamic, or mixed. The criteria presented herein would explain how the design limits change over time.

Static response parameters were the earliest effort to establish vibration design criteria. Onysko [73]–[75] proposed that the static deflection due to concentrated load of 1kN d_{1kN} was a better parameter of human response to floor vibration. The criterion was later adopted in the 1990 National Building Code of Canada [76] for floors built with solid timber joists. Canadian Construction Materials Centre (CMCC) adopted this approach for other engineered joist products [67].

Another approach of limiting the fundamental frequency f_1 was proposed by Dolan *et al.* and Johnson [77]–[79]. The criterion suggested that the fundamental frequency f_1 of occupied and unoccupied timber floor should be at least 14 Hz and 15 Hz. It was shown that these criterions is analogous to the limiting of deflection under distributed dead load. They were also too conservative for timber floors with heavy topping or semi-heavy one [80]. Ljunggren [81] stated that humans are significantly affected by an extra frequency component, *i.e.*, second or third mode frequency, under certain conditions.

The mixed approaches consisted of limiting both static and dynamic parameters. The static parameter is usually the deflection under a point load. The dynamic parameters could be peak velocity due to unit impulse, fundamental frequency f_1 , frequency weighted root mean square (RMS) acceleration.

Ohlsson [82], [83] proposed to limit the deflection under 1kN and the peak velocity due to unit impulse. The first requirement was aimed to reduce the effect of low-frequency components (< 8 Hz), and the second one was for the impact of high-frequency components (from 8 up to 40 Hz). The actual Eurocode 5 [8] vibration criterion for timber floors was based on the Ohlsson approach. Many concerns were raised in the adoption of this approach: the “unit impulse” is a mathematical expression and not a response that could be experimentally measured and validated, the calculation of the number of vibration modes less than 40 Hz was deemed to be complicated and less accurate, the 8 Hz frequency constraint was too conservative for semi-heavy floors [67]. For example, in the case of steel-concrete composite, such absolute frequency constraints are not employed. Instead, the peak acceleration must not exceed the recommended acceleration limit for the walking excitations, and a minimum acceptable

frequency level was suggested as a function of the peak acceleration and the occupancy type for the rhythmic excitations [84].

Smith and Chui [85], [86] proposed a combination of limiting the fundamental frequency f_1 and frequency weighted rms acceleration a_{rms} . The first requirements was like the Ohlsson approach with constraints on the use of long span or semi-heavy timber floors. The second requirement on limiting frequency weighted rms acceleration was carried out based on single-degree of freedom systems. Negreira *et al.* [70] stated that frequency weighted RMS acceleration is not the best indicator for vibration annoyance and vibration acceptability.

In the recent work, Hu *et al.* [87] proposed the design criterion for controlling vibration of wood-concrete composite floors, using the same approach as in the work of Hu and Chui [71] for timber floors, by limiting the empirical ratio between fundamental frequency f_1 and the deflection d_{1kN} . This criterion was established for TCC floors based on multiple experimental tests of specimens with a width of 5m, and the clear span ranged from 8m to 8.65m.

New proposals of Eurocode 5 [88] for the design by vibration include both the timber and timber-concrete floor. The requirements are divided into two categories by the fundamental frequency f_1 limit of 8 Hz. For those floors that have the fundamental frequency f_1 as least 4.5 Hz up to 8 Hz, the verification of acceleration a_{rms} should be calculated and for the floor with fundamental frequency f_1 higher than 8 Hz, the velocity criteria v_{rms} should be applied. Six floor performance levels was defined based on the deflection d_{1kN} and response factor R ($R = a_{rms}/0.005$ or $R = v_{rms}/0.0001$). Investigations and validations [89] have been carried out based on the new guidelines.

Table 1.1 summarizes some of the design criteria for timber and timber-concrete floors. The three criteria in bold were considered most relevant for the design of CCC floors.

Table 1.1. Summary of criteria for the vibrational design of timber floors

Authors	Parameters	Criterion	Application
Onysko (1985) [73]	Deflection due to 1 kN point load at the mid-point of the floor	$w_{1kN} < \min \left\{ \frac{8}{L^{1.3}} (mm) \right.$	Timber floors
Dolan <i>et al.</i> (1999) [78]	Fundamental frequency	For occupied floors: $f_1 > 14 \text{ Hz}$ For unoccupied floors: $f_1 > 15 \text{ Hz}$	Timber floors
Ohlsson (1988) [82]	Deflection due to 1 kN point load at most flexible point Maximum impulse velocity response due to a 1 Ns impulse, by considering fundamental frequency and damping ratio RMS value of vibration velocity	$w_{1kN} < 1.5 (mm)$ Restriction for $h'_{max} = \frac{40(0.4 + 0.6n_{40})}{gBl + 200}$ For habitation: $v'_{RMS} < 0.015 (m/s)$ For office: $v'_{RMS} < 0.010 (m/s)$	Timber floors
Smith and Chui (1988) [86]	Fundamental frequency Frequency-weighted RMS acceleration during first second	$f_1 > 8 (Hz)$ $a_{RMS} < 0.45 (m/s^2)$	Timber floors
Hu (2002) [90]	Ratio between fundamental frequency and deflection, based on measurements	$\frac{f_1}{w_{1kN}^{0.39}} \geq 15.3$	Timber floors
Hu and Chui (2004) [71]	Ratio between fundamental frequency and deflection, for analytic design	$\frac{f_1}{w_{1kN}^{0.44}} \geq 18.7$	Timber floors
EC 5 (2003) [8]	Fundamental frequency Instantaneous vertical deflection due to force F Impulse velocity	$f_1 > 8 (Hz)$ $w/F \leq a (mm/kN)$ $v \leq b f_1 \zeta^{-1} (m/N s^2)$	Timber floors
Hamm <i>et al.</i> (2010) [91]	Fundamental frequency Deflection due to a 2 kN point load	High demands: $f_1 > 8 (Hz)$ Low demands: $f_1 > 6 (Hz)$ High demands: 0.5 (mm) Low demands: 1.0 (mm)	Timber floors
Hu and Gagnon (2012) [92]	Ratio between fundamental frequency and deflection, based on measurements	$\frac{f_1}{w_{1kN}^{0.7}} \geq 13.0$	CLT floors
Hu <i>et al.</i> (2016) [87]	Ratio between fundamental frequency and deflection, based on measurements	$\frac{f_1}{w_{1kN}^{0.34}} \geq 6.23$	TCC floors
New EC 5 (2019) [88]	Fundamental frequency Impulse velocity Acceleration Deflection due to 1 kN point load	Six performance levels based on Response factor R $w_{1kN} \leq [0.25 - 1.6]$ $f_1 \geq 4.5 \text{ Hz}$ $a_{rms} \leq R \times 0.005$ $v_{rms} \leq R \times 0.0001$	Timber and TCC floors

1.3. EXPERIMENTAL METHOD

1.3.1. Experimental studies on CCC structures in literature

Many researchers conducted experimental tests on the CCC flooring structures to determine the static and dynamic properties. Before conducting investigations on CCC beams, an assessment of composite connectors was usually performed.

For example, Mai *et al.* [93] performed dynamic and static tests on 6-m CCC beams based on an experimental investigation on a screw composite connector [4]. Higgins *et al.* [5] test CCC beams using screw connectors at Oregon State University. Lamothe *et al.* [52] tested 9m beams of CLT-HPC (High-performance concrete) composite. The authors used a bird-mouth notched connector with reinforced screws. Zhang *et al.* [45], [94] focused on the influence of geometry on the notched connector of

CCC floors. Jiang and Crocetti [6] tested the notched connector's shear properties and the CCC beam's bending resistance using this type of connector.

The static aspects of CCC beams were studied extensively recently, and the results showed that this construction system could robustly withstand short- and long-term loading. On the other hand, CCC beam dynamic behavior was less studied even though vibration performance usually governs the CCC design, especially for the long-span beams and floors.

1.3.2. Shear tests on connectors

The performance characteristics of connectors for serviceability and ultimate limit state (SLS and ULS) can be determined through the direct shear push-out test according to standard EN 26891:1991 [95]. The strength is quantified as the maximum shear load F_{max} applied when the failure occurs in the push-out specimen and defined as the highest value of shear force monitored during the test for slips not larger than 15 mm. Maximum shear resistance F_{max} is estimated before conducting the test. The stiffness is quantified by the slip modulus at three different load levels (40, 60, and 80% of the mean maximum load) corresponding to the service, ultimate, and near-collapse load levels [60] (Figure 1.14). As the vibrational problems lie in the serviceability limit, the behavior of the structure is considered linear elastic. Therefore, the vibrational performance of the composite timber-concrete structure highly depends on the stiffness, or more specifically, the stiffness at 40 % of estimated failure load, of the connection systems.

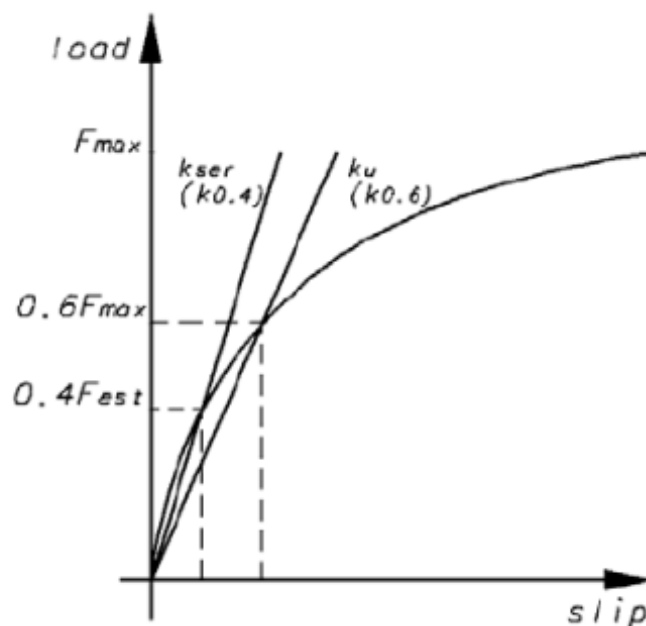


Figure 1.14. K_u and K_{ser} , by Lukaszewska [96]

Two test configurations are available to assess the shear properties of composite connectors: symmetric and non-symmetric.

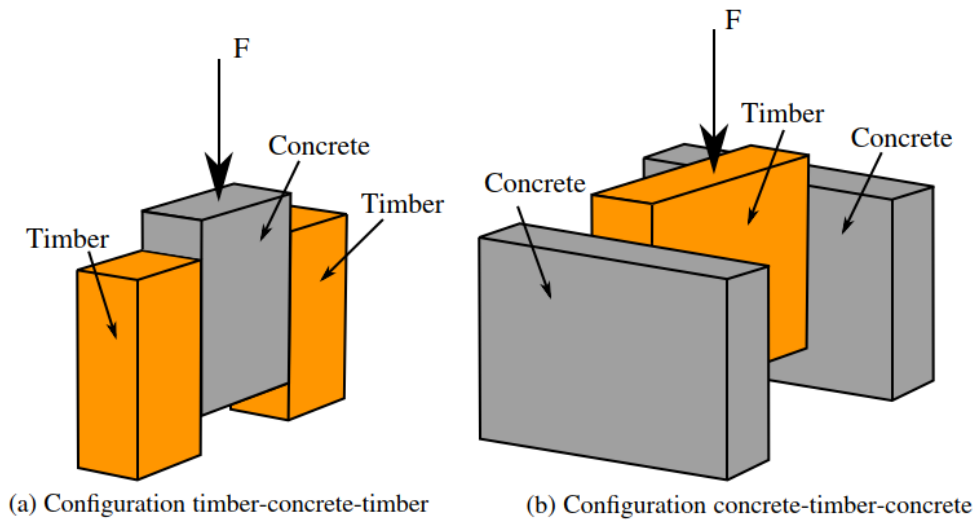
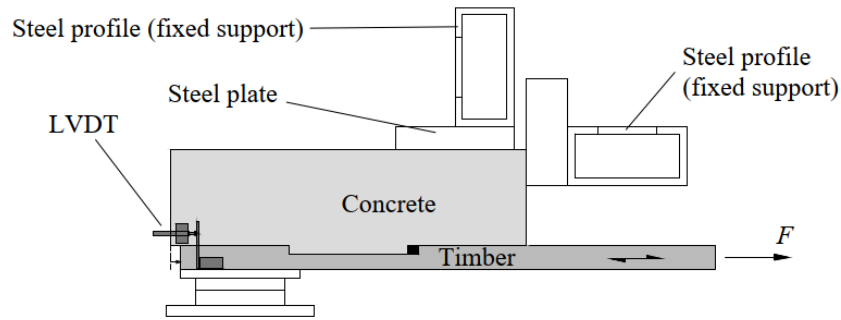


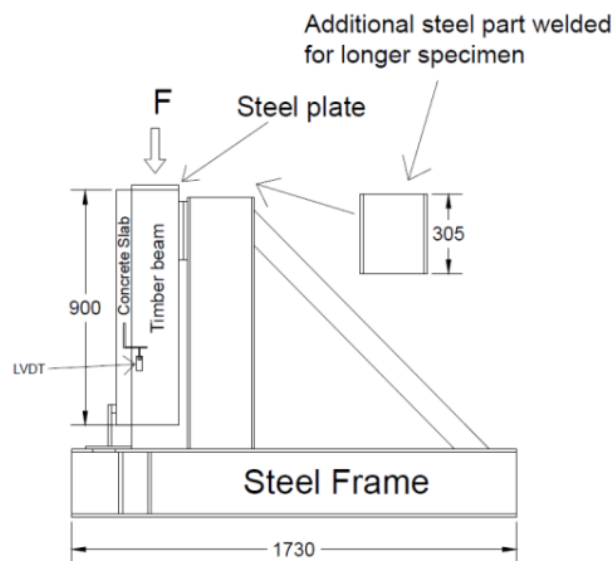
Figure 1.15. Configuration symmetric for shear connector tests, adapted by C. Auclair [43]

The symmetric configuration could be timber-concrete-timber or concrete-timber-concrete, as presented in Figure 1.15. Carvalho and Carrasco [97] concluded that the concrete-timber-concrete is a better configuration since they represent the condition of composite beams and are closer to the normalized steel-concrete composite test. Furthermore, the symmetric configurations allow testing on two individual connectors simultaneously. The response is the average one. Hence, each connector's defects or local phenomenon could be minimized [43].

The non-symmetric configuration allowed the force applied in the horizontal direction [55] or vertical one [52] (Figure 1.16). Thus, the measured response is from one individual connector. This configuration also required less fabrication effort than the symmetric one means that the number of test specimens could be increased for the same amount of material. However, the eccentric nature of this configuration amplifies the connector stiffness by 10% [96].



(a) Horizontal force



(b) Vertical force

Figure 1.16. Configuration non-symmetric for shear connector tests, (a) Boccadoro [55], (b) Lamothe [52]

1.3.3. Vibration tests on beams

There are two different ways of calculating the modal parameters. First, the theoretical approach for the modal analysis assumes the knowledge of the structural matrices, the stiffness matrix K , the mass matrix M , and the damping matrix C . Second, the experimental approach insists on measuring the system responses either in the time domain (e.g., acceleration) or frequency domain (e.g., frequency response functions - FRFs). Then, the measured data will go through the modal identification to obtain the natural frequencies and mode shapes. This approach is called “experimental modal analysis” (EMA) or, in short, “modal testing.”

A vibration measurement generally requires several hardware components. The essential hardware element consists of a source of excitation, called an exciter, for

providing a force to the structure, a transducer to convert the mechanical motion of the structure into an electrical signal [64].

A signal conditioning amplifier to match the characteristics of the transducer to the input electronics of the digital data acquisition system and an analysis system (or analyzer) in which signal processing and modal analysis computer programs reside. For a large structure like the floor, enough input energy must be set to activate the floor vibration. However, this leads to the risk of nonlinear behavior. A heavily damped structure could also cause a response peak hard to detect. For a laboratory test, the damping of the structure is significantly lower than an on-site one, so this problem could hardly occur [81].

Experimental modal analysis (EMA) is a technique to determine experimentally the dynamic of the structure involved in testing components or structures intending to obtain a mathematical description of their dynamic or vibration behavior [98]. The conditions to perform this technique are [99]:

- The structure must perform a linear dynamic behavior.
- The structure's dynamics must be time-invariant.
- The structure's dynamics must be observable.
- The structure should obey Maxwell's reciprocity principle – the response at a point p caused by force applied at the reference point q is equal to the response at the point q resulting from the same force applied at point p .

The linear dynamic behavior allows the relationship between the input force and the response of the system $X_j \cdot H_{jk} = F_k$. The Fast-Fourier Transform allows the input force and the response to be described in the frequency domain $X_j(t) \xrightarrow{FFT} X_j(\omega); F_k(t) \xrightarrow{FFT} F_k(\omega)$. By solving the equations of motion when harmonic forcing is applied, the complete solution can be described by a single matrix, "frequency response matrix" or FRF, $[H(\omega)]$. The element of this matrix, $H_{jk}(\omega)$, represents the harmonic response, X_j , in a degree of freedom, j , caused by a single harmonic force, F_k , in another degree of freedom, k .

$$H_{jk}(\omega) = \frac{F_k(\omega)}{X_j(\omega)} = \sum_{r=1}^N \frac{A_{jk_r}}{\lambda_r^2 - \omega^2} \quad (1.5)$$

where λ_r^2 is the eigenvalue of the r^{th} mode (its natural frequency and damping combined); A_{jk_r} is the modal constant, and N is the degree of freedom of the system. Data extraction from an FRF is performed by curve-fitting theoretical models to the

measured FRF data. This process is called “modal analysis identification.” Numerous identification methodologies have been proposed in the literature, like Least-Squares Frequency Domain, Ibrahim Time Domain, Stochastic Subspace Identification [100]. The application of these methods will be performed in LMS Test.Lab program, which is compatible with the measurement hardware from Siemens.

1.4. CONCLUSION

Many aspects of timber-concrete floors have been studied based on the available information in the literature since researchers around the globe continuously push the knowledge boundaries on the TCC. The present study on CCC inherently profits from this vast and solid base. The CLT possesses different characteristics than other wood engineering products on the market, hence the intrinsic advantages and disadvantages.

This study needs to address the connector performance to carry out successfully the evaluation and optimization objectives. The influence of the connector geometry should be quantified. This first step will provide crucial information for the evaluation performed on a larger scale: long-span CCC beams. Since the number of specimens will be limited, the connector design will be carefully chosen. Finally, the optimization will employ all the information acquired from the literature and the evaluation steps to make a case for CCC structures. This study will generally promote the CCC floor construction in terms of structural performance and economic competitiveness.

2. PERFORMANCE OF NOTCH CONNECTOR FOR CLT-CONCRETE COMPOSITE FLOORS

Résumé : Les systèmes de planchers mixtes bois lamellé collé croisé (cross-laminated timber - CLT) - béton sont des solutions pour les bâtiments en bois avec un plancher de longue portée. Il permet une réduction de l'empreinte carbone et même une structure éco-responsable à la fin de sa durée de vie. Cette étude va évaluer la performance mécanique des connecteurs à l'entaille pour les planchers composites en CLT - béton, comprenant la rigidité, la charge maximale et le comportement à la rupture. Les paramètres du plan de test sont la longueur du bord chargé (longueur du talon), la profondeur de l'entaille, l'épaisseur du béton et la longueur de la vis. D'autres variables secondaires sont également évaluées, telles que les différents cycles de chargement, la vitesse d'essai et la teneur en humidité du bois. Les résultats expérimentaux prouvent que les performances du connecteur dépendent de manière significative mais non linéaire de la profondeur de l'entaille et de la longueur du bord chargé. Le connecteur avec une entaille plus profonde et un talon plus court sera plus rigide et plus robuste, mais il a également tendance à avoir une rupture fragile. Les résultats des tests aident également à valider une solution pour les systèmes de connecteurs déconstructibles. Un modèle d'éléments finis non linéaire du connecteur est construit et validé. Il donne des résultats corrélés avec les expériences en termes de résistance et peut capturer la relation charge-glissement.

Abstract: Cross-laminated timber (CLT)-concrete composite floor systems provide timber buildings with long-span floors. It yields a carbon footprint reduction and even an eco-friendly structure at the end of its service life. This study will evaluate the structural performance of notched connectors in the CLT-concrete composite floor, such as the serviceability stiffness, maximum load, and behavior at failure. The test plan parameters are the loaded edge length, the notch depth, the concrete thickness, and the screw length. Other secondary variables are also assessed, such as different loading sequences, test speed, and timber moisture content. Experimental results prove that the connector performance depends significantly but not linearly on the notch depth and the length of the loaded edge. The connector with a deeper notch and a shorter heel will be stiffer and more robust, but it also tends to have a brittle rupture. The test results also help validate a solution for deconstructable connector systems. A nonlinear finite element model is built and validated versus the experimental results. It yields reasonably good predictions in terms of resistance and can capture the load-slip relationship.

2.1. INTRODUCTION

French engineer Pierre-Eugene Gauthier developed cross-laminated timber (CLT) and then patented it in 1952 [10]. It was redeveloped in Austria in early 1990 [39] and saw much broader usage in Europe by the 2000s. CLT is particularly suitable for floor system applications. There have been many successful applications of CLT in the construction of mid-rise and high-rise buildings. Brock Commons (Vancouver, BC, Canada) is the highest residential building in timber construction with 17 stories in CLT. Origine Project (Quebec City, QC, Canada) is a 12-story building based on a concrete podium constructed using CLT panels and glued-laminated timber beams.

The idea of timber-concrete composite (TCC) was used for bridge structures in the 1940s and, recently, for timber structures renovation [96]. TCC has been an objective for many extensive studies regarding short-term [101], and long-term behavior [102], [103], fire resistance performance [104], and prefabricated solutions [96], [105]. These studies emphasized the advantages of the TCC solution: resistance and rigidity, fire and seismic resistance, easy and rapid installation, dry site, prefabrication capacity, acoustic and thermal isolation, environmental and deconstruction. TCC is an excellent balancing solution from an economic and environmental standpoint, rather than using all-reinforced concrete or all-timber floors. CLT-concrete composite (CCC) structures inherit the advantage of a TCC one. CCC is notably more beneficial in mid-rise and high-rise buildings than a TCC system, *i.e.*, wooden beam-concrete slab, because we could lose up to 30 cm for each TCC floor compared to a CCC one. This means one floor per 10 story building for a defined total height. The uses of CLT in timber-concrete composite structures are still in development. A successful CCC application is at the Design Building, University of Massachusetts (Amherst, MA, USA). In this building, the floor span ranged from 6 to 8 m, the floor section comprised 175 mm of 5 ply CLT panel, 25 mm of rigid insulation, and 100 mm of reinforced concrete. The connector composite was the patented HBV system [7].

The connector system is the means to obtain the mentioned composite action. Since the timber-concrete connector would be deformable rather than infinitely stiff, the full composite section is impossible to achieve. Slip between timber and concrete layer results in a partial composite action. Many connector solutions for TCC are available, such as shear interlock, bolts, screws, metal plates [106]. They have been widely studied for four decades [1]–[3], [24]. These solutions are all applicable for CCC structures; some require minor modifications. There were many recent studies dedicated to CCC structures and their connector systems. Gerber [107] tested two types of connectors: screws, and HBV mesh, on timber-concrete composite panels (CLT, LVL, LSL). The

study showed that the analytical expressions could reasonably predict dynamic properties. Mai *et al.* [4] conducted shear tests on the individual screw connectors and applied them to the full-scale CLT-concrete beams. The authors observed a higher dynamic and static performance on composite structure than on bare CLT floor [93]. In the Oregon State University report [5], Higgins *et al.* carried out short-term and long-term tests on a full-scale CLT-concrete composite floor. They found that HBV mesh possesses a superior performance. Recently, Jiang and Crocetti [6] studied the performance of a single notched connector and a full-scale CLT-concrete beam. Lag screws and steel stirrup reinforced the notched connectors. The authors confirmed that this solution is reliable, robust, stiff, and inexpensive.

Timber material has undeniable advantages in terms of carbon footprint; however, some sustainability issues remain when considering the end of service life. Since we opt for a hybrid solution due to the mentioned reasons, a TCC floor with permanent connector systems would spawn solid waste with an incredibly low possibility of reusing after the dismantling. Furthermore, this would cause a mixture of concrete and timber, making timber lose its environmental-friendly characteristic. Hence, an adaptation for the deconstructable connector will facilitate the dismantling of the CCC structure and enhance the reusability of materials [108].

This study conducted a shear test on a reinforced notched connector of CCC structures. The main objectives are to investigate and compare the influence of many variables on the load-bearing capacity, the stiffness modulus, and the post-peak behavior that could be associated in some way with its ductility. Furthermore, a deconstructable connector for CCC structures is proposed and tested. Finally, a finite element model was also built in this study to understand the involved mechanisms, and the experimental result would validate this model.

2.2. SPECIMEN GEOMETRY AND MATERIAL

2.2.1. Materials properties

The CLT material used in this study, provided by Nordic Structures® (Montréal, QC, Canada), was a 5-ply CLT and had a thickness of 175 mm. Its lamella configuration is 35L-35T-35L-35T-35L, where “35” is the thickness in mm while “L” and “T” are the longitudinal and transversal directions, respectively. The timber specimens were E1 grade, complying with the standard ANSI/APA PRG-320-2019 [37]. E1 grade CLT should have 1950f-1.7E (the term “1950f-1.7E” represents the bending stress parallel-to-grain, 1950 lb/in², and the modulus of elasticity, 1.7 × 10⁶ lb/in²) Spruce-pine-fir MSR

lumber in all parallel (longitudinal) layers and No. 3 Spruce-pine-fir lumber in all perpendicular (transversal) layers. The panel was face-glued by Purbond® HD E202 adhesive (Henkel Canada Corporation, Mississauga, ON, Canada) and not edge-glued [109]. Table 2.1 presents the characteristic values of the CLT material.

Table 2.1. Properties of CLT and concrete.

Property	Unit	CLT * Longitudinal Layer	CLT * Transversal Layer	Concrete **
Compression strength, f_c	MPa	23.6	8.5	36.8
Modulus of elasticity, E	GPa	11.7	9.0	22.3
Density	kg/m ³	514	514	2262

* Standard properties of CLT given by the manufacturer [109]. ** Experimentally measured on five cylindrical specimens according to the ASTM C39/C39M—18 standard [110].

After each shear test, the moisture content of the timber was measured at six different randomly chosen locations on the two sides of the CLT part. The average moisture content of all tested specimens had a mean of 15.7%, with a coefficient of variation (CoV) of 14%. The high moisture content of the wood is because the specimens were stored in an uncontrolled environment, and the measurement technique only allowed sampling up to 1 cm from the timber surface.

The moisture exchange between timber and concrete is an open-ended question. Roughly speaking, if the timber absorbs water too much from concrete or vice versa, the stiffness and strength of both materials will be affected [55]. Polyethylene film was considered in the design since our knowledge of the moisture exchange between timber and concrete is limited for CLT-concrete composite. Moisture isolation, in this case, is necessary. The thickness of the crystal polyethylene film was about 50 μm (Figure 2.1.a). This film would also reduce a certain amount of friction between timber and concrete and compensate for the phenomenon of eccentricity. In the full-scale floor, this friction phenomenon is minor, and therefore the necessity of this layer lies in its capacity for moisture isolation. Once we control this unknown variable for a built floor, removing this film (if it is a case) would not cause any significant difference between the laboratory test and actual behavior.

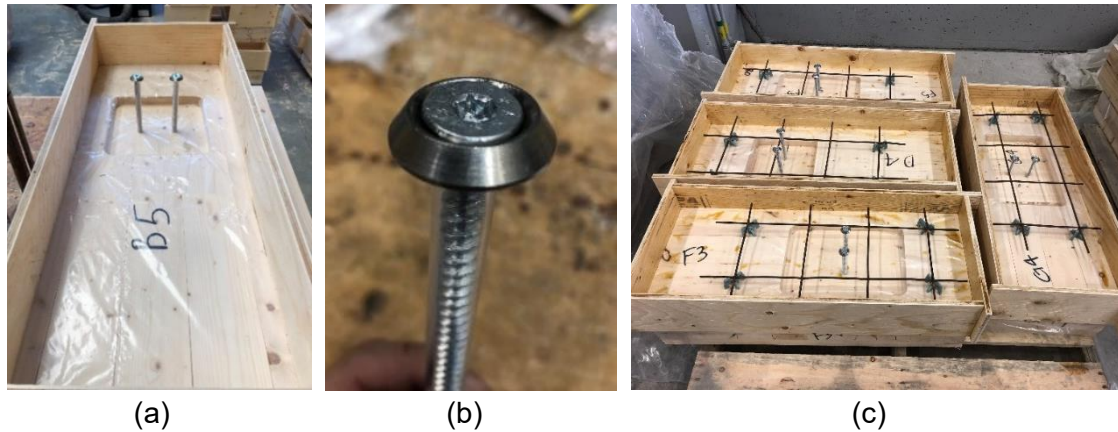


Figure 2.1. Specimen with preinstalled polyethylene film (a), vertical attachment part with a threaded screw, counter-sunk washer and plastic sleeve installed (b), reinforcing steel mat of the specimens (c).

A local supplier provided the concrete material with the indicated class of C35. The nominal aggregate size was 14 mm to assure a complete concrete fill in the minimum notch's depth of 20 mm. There was also a water-reducing admixture in the mix to achieve the same objective. Standard ASTM C39 [110], the test method for compressive strength of cylindrical concrete specimens, was used to measure the compression strength and the modulus of elasticity of concrete. The last column of Table 2.1 indicates the properties of the concrete material. Screws or bolts were adopted as the vertical attachment [6] to prevent the uplift phenomenon. For deconstructable composite floors, these screws must be easy to uninstall. According to Gutkowski *et al.* [62], some adjustments were made to simplify the implementation. The vertical attachment systems comprised a screw, a plastic sleeve, and a washer (Figure 2.1.b). ASSY VG countersunk head screws (My-Ti-Con Ltd., Surrey, BC, Canada) were used in the tests with a diameter of 8 mm and full-length threaded. They had an identical outer diameter and facilitated the installation of the sleeve. A 90° washer put on each screw head was to compensate for the bearing load lost due to the sleeve. The head of the screw was at the same level as the top surface of the concrete layer. The plastic sleeve prevented contact between the screws and the concrete. This solution provided easy access to the head of the screw to uninstall it.

2.2.2. Test specimens

The “connector” is the zone that transfers the force from one material to another. The “connector” term in this study was used interchangeably with the “connector system,” which implied the assembly of the timber female part, the male concrete part, and screws. CLT panels of 175 mm thickness were all cut into pieces of 300 mm by 750 mm. A rectangular notch was then cut into the CLT specimen using the round drill bit. The four corners of the notch were round at a radius of 20 mm. The concrete layer had

a thickness of 80 mm or 100 mm. In this study, the part in front of the loaded edge was called the heel of the connector; the timber part supported the compression and shear force transferred from the male concrete part. In our study, the heel part usually comprised more than two lamellas and the round edge of the loaded side. Heel length had three possible levels: 300-, 350-, and 400-mm. Notch depth has three levels: 20, 25, and 35 mm, without exceeding the maximum thickness of the first CLT layer. Two self-tapping screws reinforced each connector. The length of the screw was 160 mm or 220 mm. A reinforcing steel mat of 150 mm of square spacing and a diameter of 6 mm were put in place to prevent a premature crack in concrete due to shrinkage. Sixty specimens were distributed into thirteen series and tested in two phases. The first phase comprises eight series from A to H and five series from I to M in the second phase. Table 2.2 and Figure 2.2 present the detailed parameters of each series.

Table 2.2. Parameters of test series, in mm.

Serie	No. of Specimens	Heel Length (a) in mm	Notch Depth (b) in mm	Screw Length (c) in mm	Concrete Thickness (d) in mm
A	5	400	20	160	80
B	5	400	20	220	100
C	5	400	35	160	100
D	5	400	35	220	80
E	5	300	20	160	100
F	5	300	20	220	80
G	5	300	35	160	80
H	5	300	35	220	100
I	6	400	25	220	80
J	3	300	25	220	80
K	3	350	20	220	80
L	3	350	35	220	80
M	5	350	25	220	80

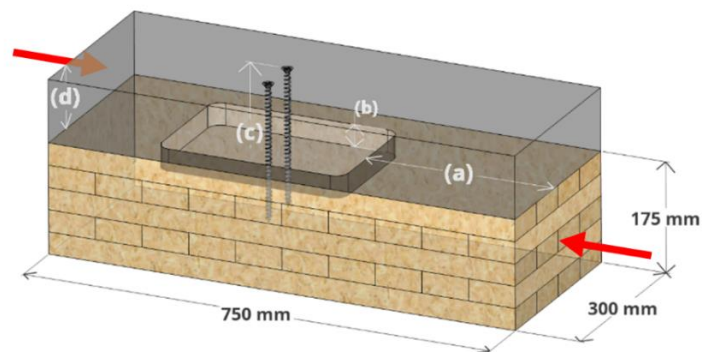


Figure 2.2. Diagram of a typical specimen, with indicated (a) heel length, (b) notch depth, (c) screw length, (d) concrete thickness.

Four variables were considered for the experimental plan: the length of the heel part, the length, depth, width of the notch, and thickness of the timber and concrete layer:

- The screw length was included in the plan to study the screw influence and validate the unscrewing option.
- A study in the LVL-concrete individual notched connector [55] showed that the length of the notch is not a significant issue in terms of stiffness and strength.
- The eccentricity aspect and the derived compression between timber and concrete were much related to the length of the heel part.
- The notch depth was a critical parameter since the characteristic of CLT is sensitive in the depth direction, *i.e.*, one layer is perpendicular adjacent to the other.
- Since the notch depth was not exceeded the thickness of the first layer of the lamella, this layer's characteristic was uniform transversally. Therefore, a fixed notch's width of 200 mm was chosen.
- The thickness of the concrete layer was included in the testing plan. This variable was to verify the influence of the eccentricity (between axial force in timber and concrete).
- We chose to use 5-ply-CLT and hence fixed the thickness of the timber layer to 175 mm. This is because a thinner (three plies) or thicker (seven plies) CLT would not be suitable for our future application of long-span composite floor systems (~9 m span).

2.2.3. Test setups

The configuration adopted for the shear test is an asymmetrical specimen system. This configuration was cheaper to fabricate than the symmetrical one, and a more significant number of the specimens could be tested. The difference is that the asymmetrical test would estimate the shear stiffness and strength higher than the symmetrical one [24]. The eccentricity moment occurred when the testing machine applied on the timber part; this would generate compression force and the friction between timber and concrete on the upper part of the specimen [1]. For TCC connector systems, Lukaszewska [1] estimated that the stiffness and strength difference between the asymmetric specimen and the symmetric one was about 10%, depending on the specimen dimensions. In this study, since there was a thin polyethylene film at the material interface, the effect of this phenomenon might be lessened.

The bench adaptor is comprised of two I-profiles welded perpendicular to each other. The specimen was placed on a fixed metal plate, only by the concrete part. The moving part of the testing machine transferred the load on a metal plate then distributed the charge to the timber part of the specimen. Teflon plate was put on the vertical I-profile to reduce the friction between the sample and the I-profile (Figure 2.3). The testing machine, driven by a defined displacement rate, could produce a maximum charge of about 445 kN.

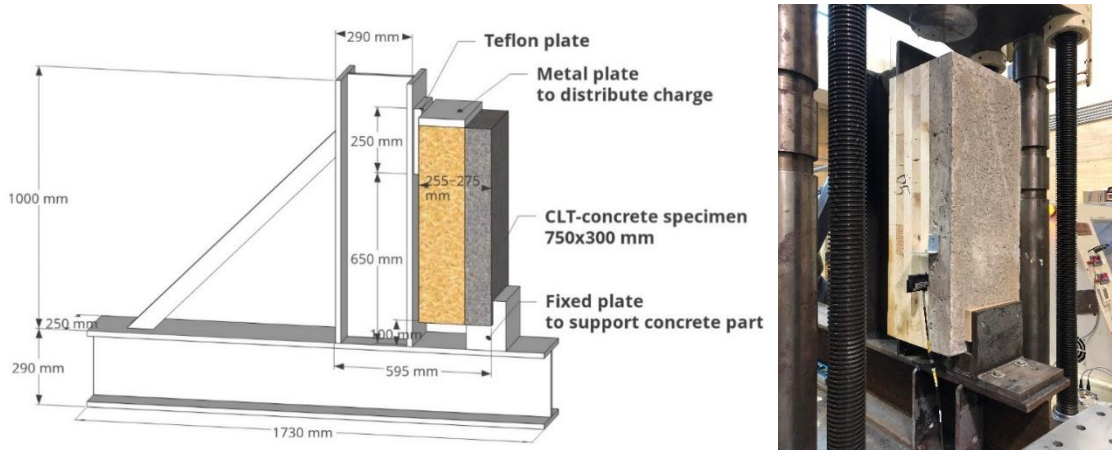


Figure 2.3. Adaptor for the asymmetrical CLT-concrete specimen (left). Actual image of adaptor (right).

Two analog laser sensors (ALSs) were fixed on two sides of the sample to capture the relative displacements between the two layers. The ALSs were fixed on the timber part by screws. The install area of the two ALSs was about 150 cm to the edge of the sample. This location was where the loaded edge of the notched commences. The ALSs were connected to amplifier units before transmitting the data to the computer. Another displacement sensor was integrated into the testing machine to measure the total displacement of the timber part. Finally, the vertical charge applied to the specimen was measured by a sensor of the testing machine.

Standard EN 26891 [95] proposed a protocol to determine resistance characteristics of the timber connector subjected to static loading. The total time for testing was about 15 minutes. The condition for the ending of the test was whether the charge had a significant drop or the relative displacement reached 15 mm. We used a customized forklift to put the specimen into the bench adaptor. Once the sample was in place and well-positioned, the speed test was set by turning the dial manually. The loading speed of the test was average 1.3 mm per minute, and it fluctuated greatly due to manual handling. However, the result shows no correlation between the magnitude of loading speed and the stiffness or resistance. After the tests, we measured the

moisture content and then dismantled some specimens for further study. The specimen disassembling helped us look at the failure mechanism and define the type of failure.

According to Standard EN 26891 [95], the slip modulus of the service state limit k_s is defined on the initial modified displacement, from 10% to 40% of the maximum load. This definition was proposed only for the first loading sequence. The range from 0% to 10% of the maximum load comprised the first loading sequence; the contacts between connector elements were not assured.

In this study, we used the notation K_1 and K_2 as the slip modulus of the first loading sequence and second loading sequence, respectively (Figure 2.4). By applying the linear regression $y = \beta y + \alpha$ on all the data points between the modified displacement, K_1 and K_2 were obtained as the slope of the regression line. The maximum load F_{max} was the load reached at the curve peak or 15 mm of displacement. Both K_1 and K_2 were defined over the range from 10% to 40% of the maximum load. The modulus K_1 had the same meaning as k_s , although we used the regression slope instead of an arbitrated displacement point for the modulus determination. On the other hand, K_2 had no counterpart in the standard in terms of physical meaning (modulus of second loading sequence). From our point of view, K_2 is more suitable for the calculation of vibration behavior since the structure is more stabilized after the first load sequence and exhibited the behavior close to the actual structure.

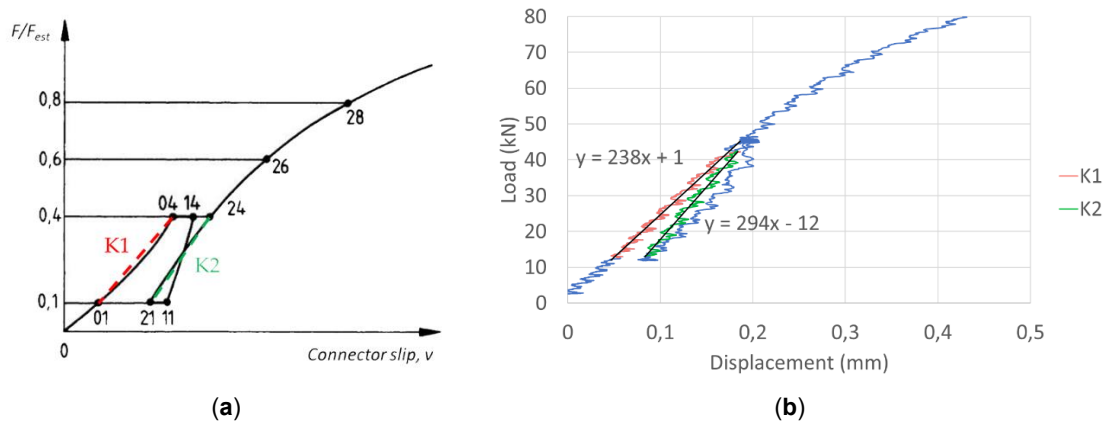


Figure 2.4. Theoretical loading procedure from EN 26891 [95] (a) and stiffness K_1 (red) and K_2 (green) determination of specimen A2 (blue) on raw data representation (b).

2.3. EXPERIMENTAL RESULTS AND DISCUSSION

2.3.1. Overview

Three different failure types were observed: ductile failure of the specimen due to the compression in the timber contact zone (type timber ductile - TD), brittle failure of

the specimen due to the shearing-off of the timber lamellas in the heel (type timber brittle - TB). Furthermore, there was a combination of type TD and TB. The specimen had crushed timber and a part of its lamella sheared-off (type TD + TB). Brittle failure of the specimen due to the shear failure of the concrete part was noted as CB (type concrete brittle). The average stiffness and strength of the 13 series are presented in Table 2.3, with the corresponding coefficient of variation (CoV).

Table 2.3. Summary of tested series

Series	K1		K2		F _{max}	
	Mean	CoV	Mean	CoV	Mean	CoV
	kN/mm	%	kN/mm	%	kN	%
A	224	13	294	5	127	10
B	213	18	303	15	140	9
C	248	8	311	8	221	5
D	238	12	315	5	221	11
E	199	16	258	7	140	4
F	202	4	256	6	151	7
G	208	9	274	11	211	7
H	195	19	254	13	217	9
I	242	13	326	13	177	4
J	208	1	286	7	169	5
K	202	1	270	13	158	7
L	205	7	291	17	238	6
M	212	12	311	14	175	10

As compared to the results of other studies [4], [107], [111], [112], the notched connector stiffness was on average higher than for the screw connector but still lower than HBV mesh. For example, a pair of screws could have a shear stiffness that varies from 0.14 kN/mm² to 0.3 kN/mm², while HBV mesh was about 0.825 kN/mm². The experimental results of this study showed that the stiffness ranged from 0.34 to 0.43 kN/mm². The unit kN/mm² indicates the shear stiffness (kN/mm) per connector length (mm). Figure 2.5 presents the load-displacement curves of 60 specimens distinguished by their series. The resistance ranged from 108 kN to 253 kN depending on the notch geometry, especially the depth of the connector.

There were distinct gaps between the curve family with the heel length of 400 mm (Figure 2.5.a). However, the post-peak behavior was less consistent in other series of 350 mm and 300 mm heel length (Figure 2.5.b and c). This observation was because the shorter heel length specimens have few materials to dissipate the charge and more likely sustain the timber softening.

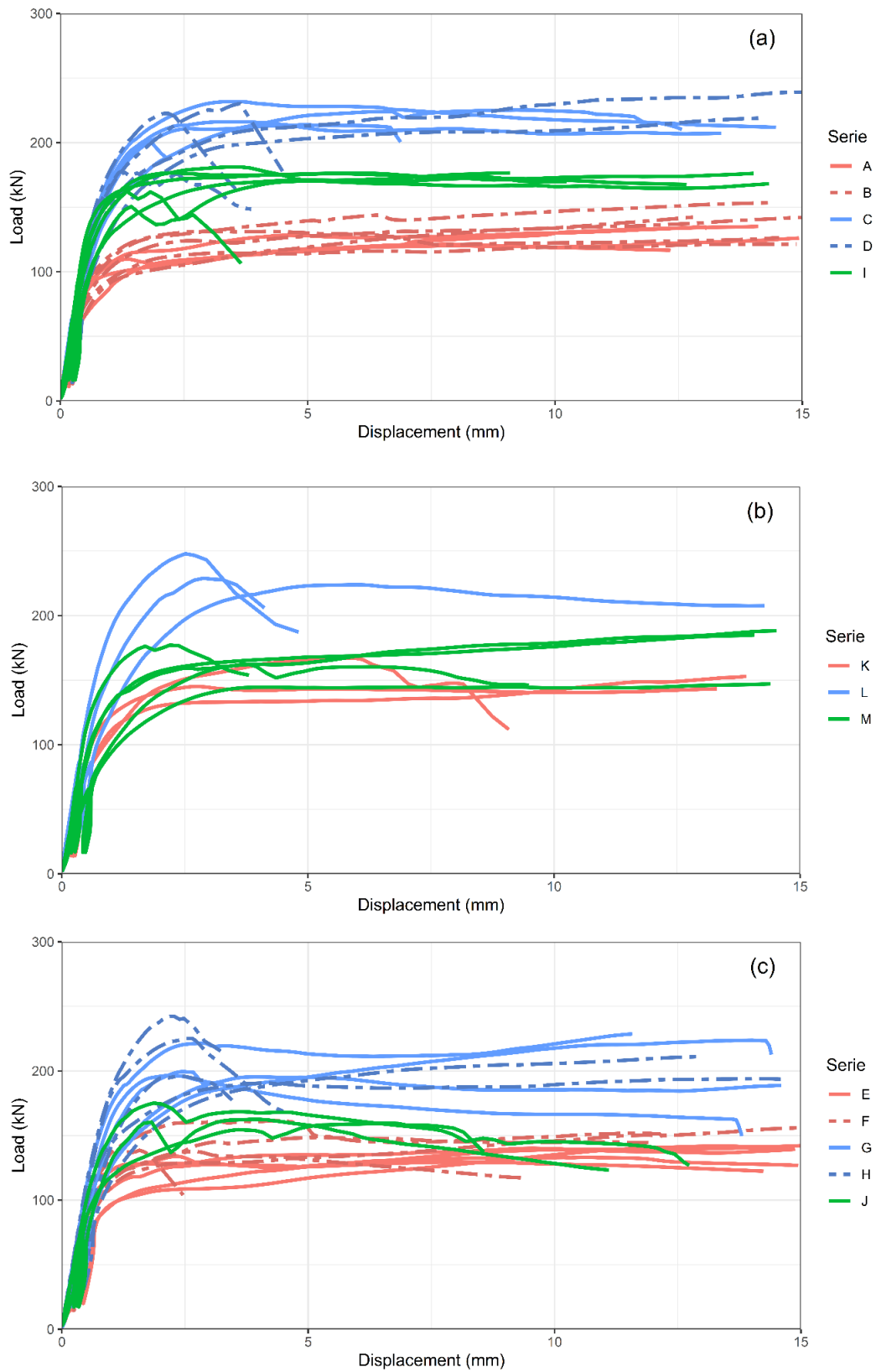


Figure 2.5. Load-displacement curves of specimens that have (a) 400 mm, (b) 350 mm, (c) 300 mm heel length, curves in red indicate 20 mm notch depth specimens, 25 mm in green, and 35 mm in blue.

2.3.2. Influence of heel length

Figure 2.6 exhibits the relationship between the heel length and the variables of interest, namely K1, K2, and Fmax. One can see an increase of about 15% of the stiffness K1 and K2 when the heel length increases from 300 mm to 400 mm (Figure 2.6.a and b). Heel length was assumed not to influence either the stiffness or strength of the connector (Figure 2.6.c). This slight increase was probably because of the asymmetrical properties of the test. The lengthy heel magnified the eccentricity and the friction between concrete and timber. The resistance of the connector of different notch depths distinguished clearly from each other's; they developed almost independently regarding their heel length. Modulus K2 was more consistent than K1 since the specimen was stabilized after the first loading sequence. In terms of the effect of heel length on the failure type, a specimen with a shorter heel tended to have its lamellas sheared off at failure. The error bars in the graphs represent the 95% confidence interval of the mean value \bar{x} . They are calculated as $\bar{x} \pm t_{n-1} \cdot s/\sqrt{n}$, with s is the standard deviation of the sample, n is the sample size, and t_{n-1} is the upper $(1-0.95)/2$ critical value for the t distribution with $(n-1)$ degrees of freedom. Since the standard error was significant in some average data points, the evolution of K1 and K2 was challenging to be verified.

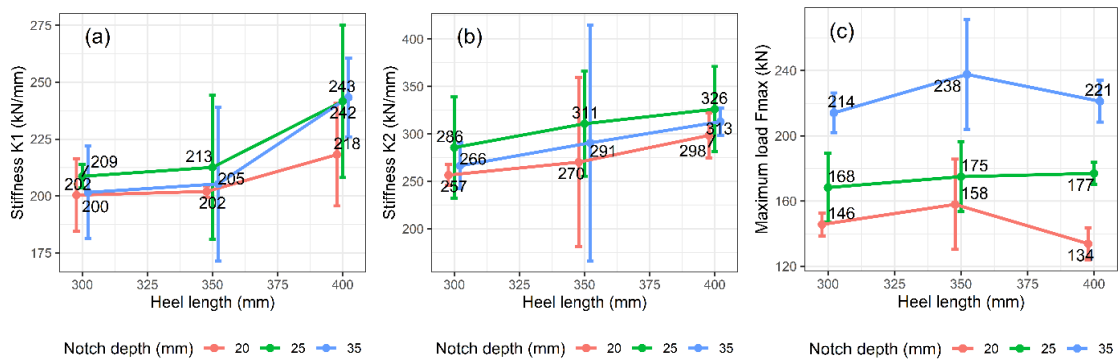


Figure 2.6. Stiffness K1 (a), K2 (b), and maximum load Fmax (c) of different notch depths.

2.3.3. Influence of notch depth

Figure 2.7.a and b show the evolution of slip modulus when the notch depth increases. A deeper cut did not yield a stiffer connector. The notch with 25 mm depth had the highest stiffness in most cases. In the notch with 35 mm of depth, the timber material of the first layer of the lamella was extracted entirely, and the second layer, which laid in the direction perpendicular to the first one, was weaker in terms of modulus perpendicular to the grain. The transversal timber lamellas were also not glued edgewise. They could be the reason for the “peak” trend of the slip modulus curves.

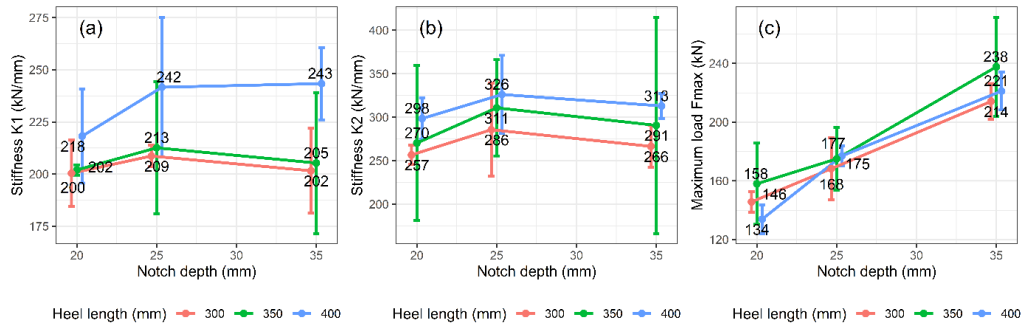


Figure 2.7. Stiffness K1 (a), K2 (b), and maximum load Fmax (c) of different heel lengths.

Figure 2.7.a and b show the stiffness K1 and K2 per notch depth. The modulus gained per millimeter of notch depth was higher in the less deep notches. The shallow notch used the material more effectively in terms of stiffness, and further extraction of material in the topmost longitudinal layer would reduce the effectiveness of the connector. The linear correlations between the stiffness per depth and the notch depth were also observed (Figure 2.8).

The resistance of the connector is higher for the deeper cut (Figure 2.7.c). An increase of the resistance of about 50% was observed when the cut was deeper. The correlation between notch depth and the maximum load Fmax was almost linear. The notch depth had a more significant effect on maximum load than the effect of heel length in Figure 2.7.c. The coefficient of variations of mean data points of the maximum load was considerably smaller than the other two responses (*i.e.*, modulus K1 and K2). It meant that the experimental measurement of stiffness was difficult, and the maximum load of the notch would be more straightforward to be predicted by the variable of notch depth. A shallower notch connector tended to have the loaded edge crushed rather than the shear-off lamellas (*cf.* Section 3.7). Hence, the curves of these specimens had a more prolonged post-peak displacement that ranged from 10 to 15 mm. Optimization of the notch depth will have to balance between the performance and the post-peak behavior.

For a CCC notched connector, Jiang *et al.* [6] reported a serviceability stiffness per 25 mm notch-depth of 15.3 kN/mm² and the resistance per depth of 7.1 kN/mm, while the corresponding results of our study were 12.5 kN/mm² and 7.0 kN/mm. Furthermore, the notch connectors in this study featured rounded corners at the loaded edge, while Jiang *et al.* tested a full-width square notch. This detail generated a transverse component of the applied force exerted on the notch. It might be the reason for the less stiff connector observed in this study.

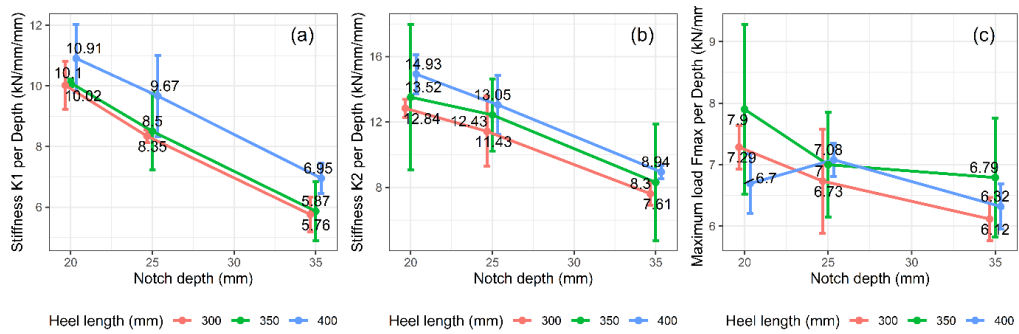


Figure 2.8. Stiffness K1 (a), K2 (b), and maximum load Fmax (c) per notch depth of different heel lengths.

2.3.4. Influence of concrete thickness and screw length

Figure 2.9 shows some minor changes (about 10% maximum) of the stiffnesses and the resistance of the connector in terms of concrete thickness and screw length. It could be concluded that these two variables do not influence the overall performance of individual notch connectors. Since the implementation of the deconstructable screw part yielded no difference in terms of the structural performance of the connector, this solution was possible for CLT-concrete floors systems. The uninstalling of the screws was carried out without any difficulty (Figure 2.10) by using a wired screwdriver.

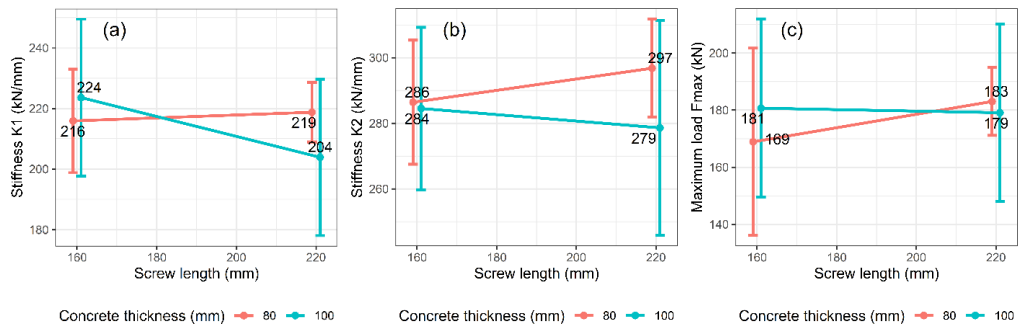


Figure 2.9. Stiffness K1 (a), K2 (b), and maximum load Fmax (c) in terms of screw length and concrete thickness



Figure 2.10. Screw uninstallation

2.3.5. Influence of loading sequence

The modulus of the second loading sequence K2 was 35% higher than for K1. This is because the contact between the connector component was well established after the first loading sequence. Any possible gaps between them were closed, and the material was stabilized. Modulus K2 in terms of the heel length and the notch depth, had almost the same and more transparent tendencies than modulus K1. However, it is worth noting that the confidence interval of the mean values was still considerable. The stiffness results were not more consistent after the first loading-unloading cycle. The loading speed was manually set for each specimen and constant in the loading sequences. This variable fluctuated significantly but did not significantly affect the stiffness and the maximum load.

2.3.6. Influence of moisture content of timber

The moisture content of timber was measured after the test, as it was considered an essential variable. Some specimens showed minor color change spots and no significant deformations of the upmost timber layer. However, most of the series had stiffness K1 reduced when the timber moisture increased (eight over 13 series). The same phenomenon could be observed in K2 (ten over 13 series) and Fmax (eight over 13 series). Therefore, only the correlations between stiffness K1 and moisture content are shown in Figure 2.11.

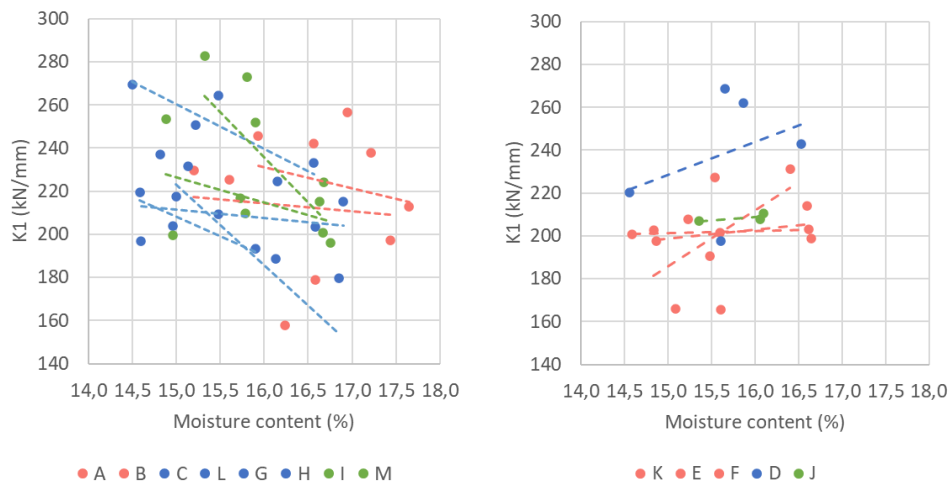


Figure 2.11. Correlation between stiffness K1 and moisture content of timber of different series. 20 mm notch depth specimens are represented by the red points, 25 mm in green, and 35 mm in blue.

2.3.7. Failure types

Three principal failure types were observed. Figure 2.12 shows the typical load-slip curves of different failure types, and Figure 13 presents photos of these failure types.

In this study, most of the tested specimens had the failure type with a compression zone principally in the heel (47 over 60 tested samples). Therefore, they were classified as type TD.

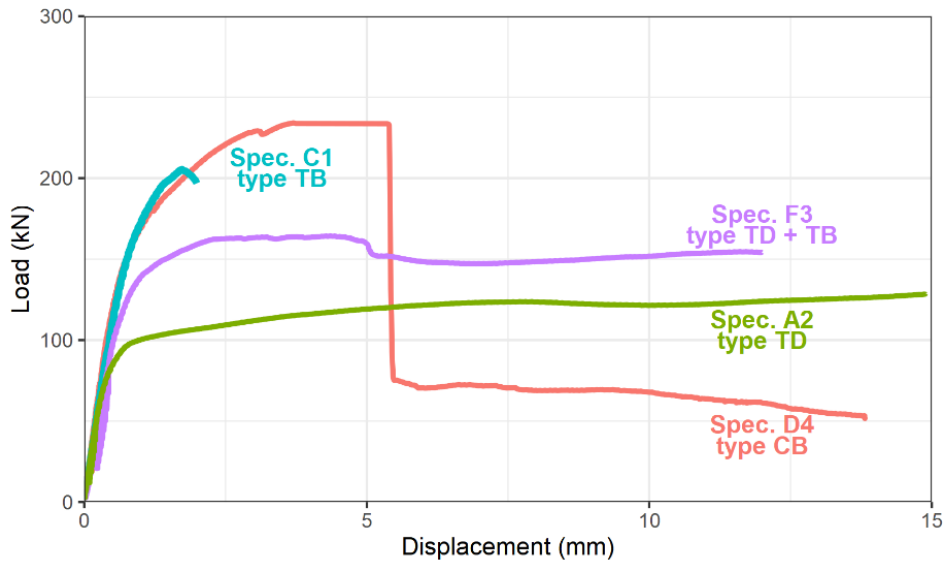


Figure 2.12. Load-slip curves of different failure types.

The failure type TB occurred when the lamellas of the heel got sheared-off at the displacement from 2 mm to 3 mm. The full measured curves of type TB could reach a significant displacement at a relatively high load. This is because, firstly, when the testing machine pushed to the timber part, it held the sheared-off lamellas in place. This is because the metal plate, designated for distributing the load from the testing machine, covered the surface of the timber upper part. When the timber lamellas of the heel part were sheared-off, the metal plate held the lamellas in place and caused a load increase in the load-displacement curve. Secondly, at a significant slip, only the screws bear the load. The sleeve between screws and concrete would prevent the contribution of the screws to the shear loading from initial up to 2 mm of displacement. Considering this artifact, we assumed that the specimen failed at the first drop in terms of load.

In the specimens classified as type TD + TB, one could observe a minor drop in the load after the sample reaches its peak load at the slip of about 2 mm to 6 mm. However, the specimens still carried on and achieved a significant displacement (10 mm or more) because a portion of the heel was still glued to the transversal layer, got crushed at the loaded edge, and held the charge. Hence, we considered this type as a sub-category of type TD.

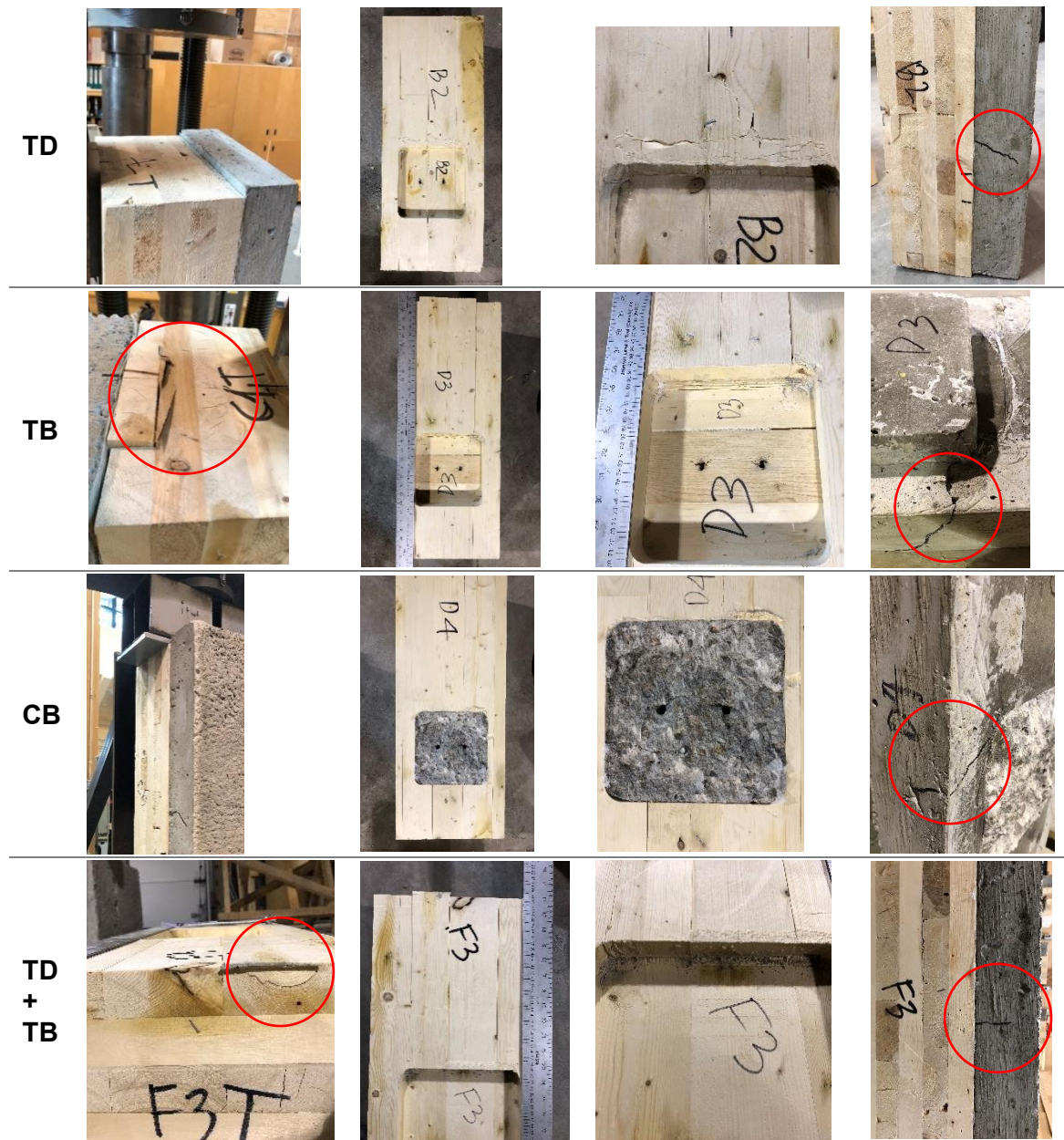


Figure 2.13. Typical different failure types.

The notched concrete part was sheared-off in the specimens classified as type CB, while the load increased. Thus, after the failure, the screws held the residual charge. It is worth noting that the concrete has rebar steel mesh, and the two screws rigidly attached the two parts altogether. Therefore, the connector in this study was less likely to have the failure type CB (two over 60 specimens).

Almost every specimen had diagonal cracks at failure. These cracks took place in the corner between timber and concrete shortly before the load reached its peak. They developed at an angle from 30° to 45° to the concrete's surface. In addition, a plastic hinge was observed in the screw at the interface location. However, this only contributed to the post-peak behavior and helped extend the slip. Firstly, the reasons are that an

individual screw was much less rigid than the notch itself. Secondly, there was a gap between the screw and the concrete due to the plastic sleeve; it prevented the screw from contributing to the connector rigidity.

Figure 2.14 shows the failure types distribution for only one variable; the data labels represent the number of specimens. The percentage of failure type TD reduced from 73% to 61% when the heel length decreased from 400 mm to 300 mm. Thus, the timber imperfection was likely to be manifested heavily by a brittle failure in the specimens with a shorter heel. In terms of notch depth, one could observe a significant reduction from 87% at 20 mm depth to 48% at 35 mm depth.

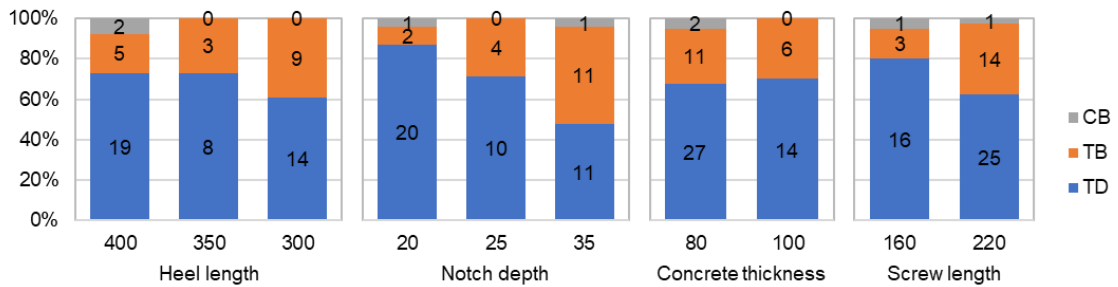


Figure 2.14. Number of specimens with different failure types.

The deeper notch must withstand greater shear force and more likely fail in a brittle manner. This shows differences in load transmission depending on heel length and notch depth. As lamellas were not edgewise glued, the sheared area must be significant enough not to be the weakest (brittle) link versus the compressed (ductile) parallel-to-grain area. Potential future design rules will have to prevent brittle failure. One could see that the thickness of the concrete layer did not influence the distribution of failure type. The longer screw might have caused a brittle rupture of the connector, from 15% to 35% of the specimen's number (three over 20 specimens versus 14 over 40 specimens). Further investigation is needed to confirm this phenomenon.

2.4. FINITE ELEMENTS MODEL VALIDATION

Many authors have used different techniques to model timber material regarding connection, whether for notched or dowel connectors. Dias *et al.* [113] used Hill's criterion to characterize the anisotropy of timber material. The method was helpful in modeling elastic-plastic behavior and was later employed in CCC by Jiang *et al.* [6] for notched connectors and Mai *et al.* [4] for screw connectors. Models with damage mechanics were also adopted in the literature, such as using continuum damage mechanics to obtain brittle and ductile failure modes (Sandhaas and van de Kuilen

[114]), using Hashin failure criterion for the laterally loaded nail of CLT bracket connection (Hollenbeck [115]), cohesive elements to simulate cracking in timber bolted connection (Franke and Quenneville [116]). User-defined features (such as subroutine in Abaqus) are required for such applications and raise computational costs. In this study, we will focus on the estimation of the shear stiffness of the connector, hence a FE model using 3D orthotropic element will be used. The damage mechanics with post-peak behavior will be omitted based on the scope of the study.

2.4.1. Materials

a. Timber

Timber was modeled as an orthotropic elastic-perfect plastic material. According to Dias *et al.* [113], Hill's criterion, which is an extension of von Mises's function, could be used for orthotropic material to characterize the yielding phenomenon:

$$f(\sigma) = F(\sigma_{22} - \sigma_{33})^2 + G(\sigma_{33} - \sigma_{11})^2 + H(\sigma_{11} - \sigma_{22})^2 + 2L\sigma_{23}^2 + 2M\sigma_{31}^2 + 2N\sigma_{12}^2 \quad (2.1)$$

where σ_{ij} is the components of the stress tensor in three dimensions and $F, G, H, L, M,$ and N are constants determined experimentally:

$$F = \frac{(\sigma^0)^2}{2} \left(\frac{1}{\bar{\sigma}_{22}^2} + \frac{1}{\bar{\sigma}_{33}^2} - \frac{1}{\bar{\sigma}_{11}^2} \right); \quad (2.2)$$

$$G = \frac{(\sigma^0)^2}{2} \left(\frac{1}{\bar{\sigma}_{33}^2} + \frac{1}{\bar{\sigma}_{11}^2} - \frac{1}{\bar{\sigma}_{22}^2} \right); \quad (2.3)$$

$$H = \frac{(\sigma^0)^2}{2} \left(\frac{1}{\bar{\sigma}_{11}^2} + \frac{1}{\bar{\sigma}_{22}^2} - \frac{1}{\bar{\sigma}_{33}^2} \right); \quad (2.4)$$

$$L = \frac{3}{2} \left(\frac{\tau^0}{\bar{\sigma}_{23}} \right)^2; \quad (2.5)$$

$$M = \frac{3}{2} \left(\frac{\tau^0}{\bar{\sigma}_{13}} \right)^2; \quad (2.6)$$

$$N = \frac{3}{2} \left(\frac{\tau^0}{\bar{\sigma}_{12}} \right)^2. \quad (2.7)$$

The definition of the potential coefficients R_{ij} is:

$$R_{11}, R_{22}, R_{33}, R_{12}, R_{13}, R_{23} = \frac{\bar{\sigma}_{11}}{\sigma^0}; \frac{\bar{\sigma}_{22}}{\sigma^0}; \frac{\bar{\sigma}_{33}}{\sigma^0}; \frac{\bar{\sigma}_{12}}{\tau^0}; \frac{\bar{\sigma}_{13}}{\tau^0}; \frac{\bar{\sigma}_{23}}{\tau^0} \quad (2.8)$$

where $\bar{\sigma}_{ij}$ is the measured yield stress value when σ_{ij} is applied as the only nonzero stress component; σ^0 is the reference yield stress and $\tau^0 = \sigma^0/\sqrt{3}$. The problem was defining the yield stress σ^0 and the yield stress ratio R_{ij} . Considering σ^0

as the yield strength in the direction parallel to the grain of the timber, Dias *et al.* [113] proposed the coefficients R_{ij} for spruce $R_{11} = 1; R_{22} = R_{33} = 0.19$ and $R_{12} = R_{13} = R_{23} = 0.38$. The Wood Handbook [117] suggests $R_{11} = 1; R_{22} = R_{33} = 0.11$ and $R_{12} = R_{13} = R_{23} = 0.39$ (mean value) for Canadian SPF. The model used value from this reference [117].

The preliminary modeling showed that the resistance of the notched connector depends heavily on the “shear” ratio R_{12}, R_{13} rather than the “orthogonal” ratio R_{22}, R_{33} . The lamellas of the third and fifth layers of CLT specimen were extracted and subjected to the compression tests, based on standard ASTM D143-2014 [118] for a small clear timber specimen. Table 2.4 presents the extreme case value of σ^0 and E_{xx} obtained from the experimental tests [32] with direction xx is the direction parallel to grain. Other properties $E_{yy}, E_{zz}, G_{xy}, G_{zx}, G_{yz}$ were derived from E_{xx} as the indications of EN 338 [119] for softwoods:

$$E_{xx} = 30E_{yy} = 30E_{zz} \quad (2.9)$$

$$16G_{xy} = 16G_{zx} = 0.5(E_{xx} + E_{yy}) \quad (2.10)$$

$$16G_{yz} = 0.5(E_{yy} + E_{zz}) \quad (2.11)$$

Table 2.4. Summary of the timber parameters of the FEM model

Parameters	Value	Parameters	Value	Parameters	Value
σ^0	37.5–25.8	E_{xx}	18200–9340	ν_{xy}	0.4
R_{11}	1	E_{yy}, E_{zz}	607–311	ν_{xz}	0.3
R_{22}, R_{33}	0.11	G_{xy}, G_{zx}	588–302	ν_{yz}	0.3
R_{12}, R_{13}, R_{23}	0.39	G_{yz}	59–30	(–)	(–)

b. Concrete

Concrete was modeled as an isotropic elastic material without any plasticity properties. The experimental test provided the modulus of elasticity of concrete (*cf.* Table 2.1). The impact of plasticity characteristics of concrete was considered minimal to the model based on preliminary modeling. This simplification helped reduce the computational cost and increased the possibility of convergence of the model.

2.4.2. Models

The finite element model of the notched connector was performed with the commercial software Abaqus [120]. The tie constraint was used for the glued contact between the lamellas (rigid contact). The non-glued surface and the one between timber and concrete had “hard” contact in the normal direction and “frictionless” in the tangential direction. The finite elements were eight-node cubic with reduced integration C3D8R. The reduced integration minimized the computational effort but raised some problems in terms of “hourglass.” Hourglass is a nonphysical, zero-energy mode of deformation that produces zero strain and no stress. This occurs in the reduced integration elements, with only one integration point in the middle (e.g., C3D8R). To minimize it, we used the default hourglass control algorithm of Abaqus. The fine mesh of 4 mm-element was applied to the concrete and timber contact zone down to the second layer. The coarse mesh of 12 mm was for the rest of the model (Figure 2.15). In addition, the local failure criteria of the materials were not implemented. Furthermore, we imposed a criterion of global relative displacement of 10 mm between timber and concrete. Hill’s criteria were used for the sake of yielding phenomenon in orthotropic material, *i.e.*, timber in our case.

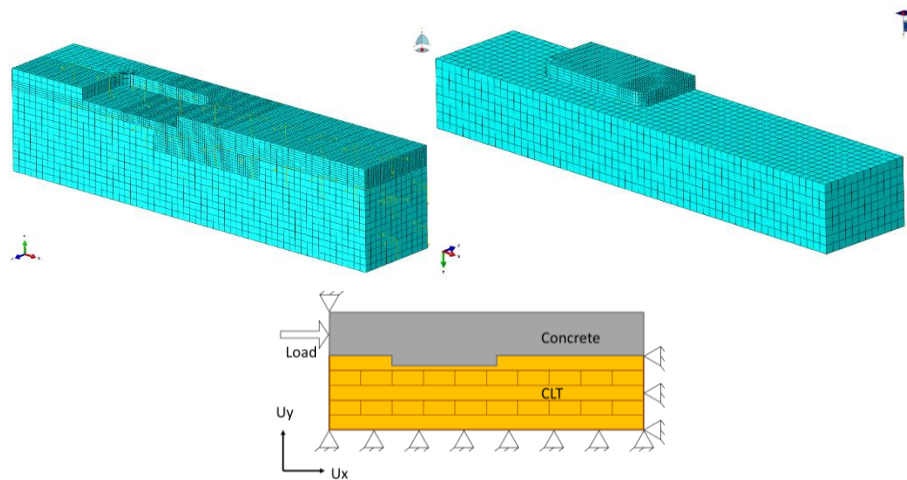


Figure 2.15. Mesh definition of timber and concrete part and boundary conditions.

The screws were omitted because of their minimal impact on the overall performance of the connector. Only half of the specimen was modeled to reduce the computational cost. The charge was placed on the concrete part. The boundary condition was set to imitate the specimen's behavior on the bench test. The CLT part was limited in the translational displacement U_y and U_x , while the concrete part was constrained in the U_y of the loaded end (Figure 2.15). The model was built based on the standard/implicit calculation regime. Abaqus would check for the convergence of the model at each iteration. The convergence of the model was quite good for displacement

from 0 to 4 mm. Beyond this, there were some cases where the model aborts the calculation due to the divergence. The excessive displacement of the element at the loaded edge of the notch might be the reason for this divergence.

2.4.3. Results

For the stiffness of the connector, the model could capture the trend in terms of notch depth. Figure 2.16 shows that the stiffness per depth decreases when the notch depth increase. The model yields a better prediction for K2 than for K1.

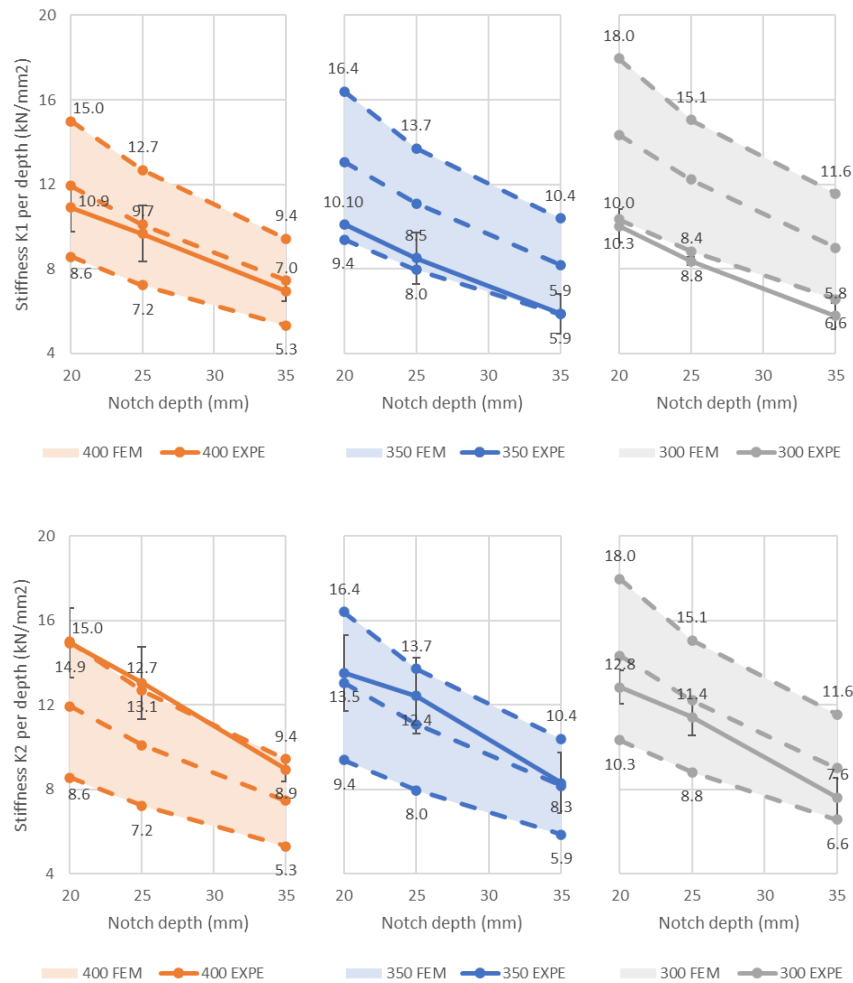


Figure 2.16. FEM envelop of stiffness K1 and K2 per depth of multiple heel length.

These results showed that the test's initial loading and unloading step might impact the specimen (close the contact and stabilize the material). However, it exhibited an opposite trend in terms of heel length. The experimental stiffness (K1 and K2) decreased for a smaller length; the model stiffness increased. Therefore, it could be explained that our model assumed the same modulus of elasticity for both compression and traction behavior of timber.

The model could characterize the trend of maximum load in terms of notch depth and heel length (Figure 2.17). The envelope of maximum load created by the model was consistent in heel length and increased when the depth of the cut was deeper. Furthermore, the model over-estimated the load even though we used the experimental compression data of lamellas of the tested CLT.

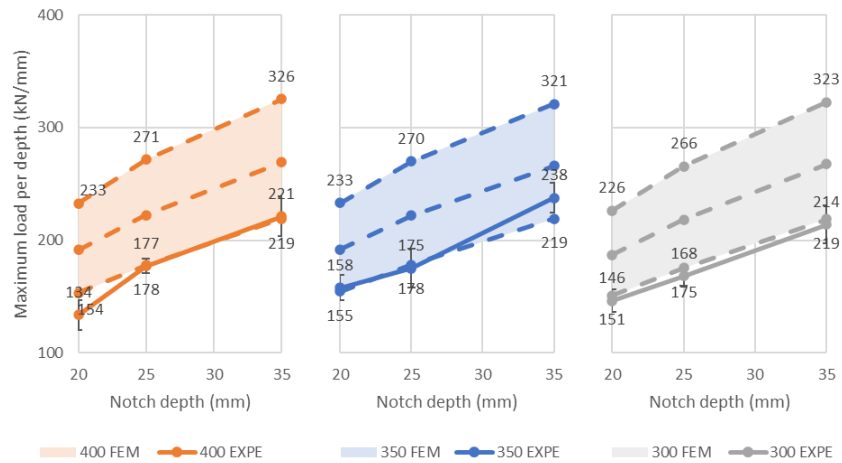


Figure 2.17. FEM envelop of maximum load F_{max} per notch depth.

The comparison between the experimental and modeled load-displacement curves of series I is shown in Figure 2.18. The model strength was overestimated when using the upper bound of the reference yield strength σ^0 (37.5 MPa, cf. Table 4) while it showed some agreement up to the displacement of 6 mm at lower strength bound (25.8 MPa).

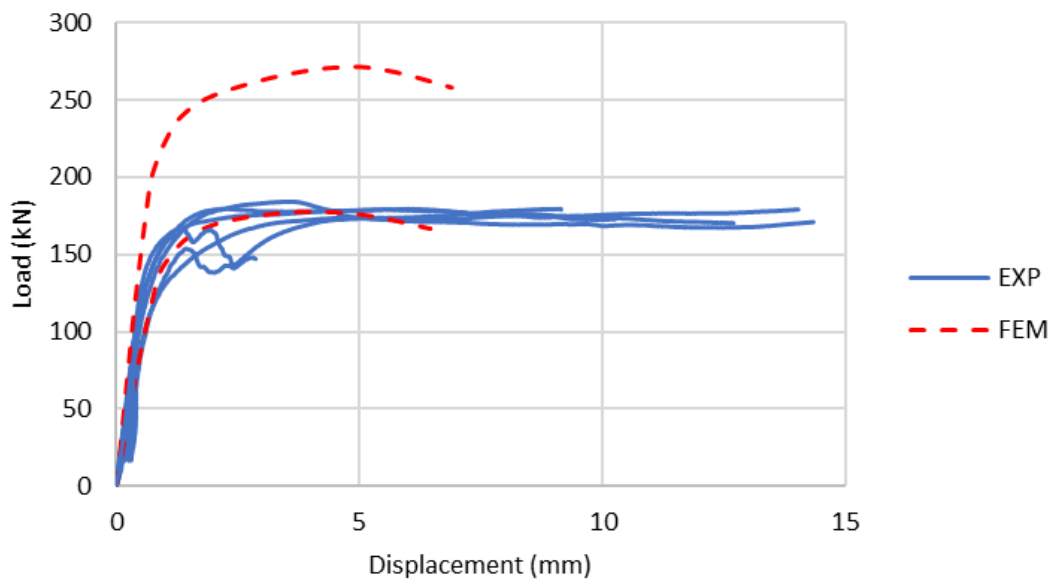


Figure 2.18. Load-displacement curves comparison between experimental and FEM of series I.

2.5. CONCLUSION

We have investigated and compared the influence of four variables on the overall mechanical performance of the notched connector. The variables tested were heel length, notch depth, screw length, and thickness of the concrete layer. The following conclusions were drawn from the results of the study:

1. Based on the load-displacement behavior of the specimens, the notched connector with reinforced screws could withstand a load from 120 kN to 240 kN. The resistance of connectors depended on the geometry configuration. The stiffness of the notched connector was higher than the screw connectors but lower than the HBV mesh. Furthermore, most of the specimens exhibited ductile rupture with significant post-peak displacement.

2. By comparing the results of different configurations, the geometry variables, heel length, and notch depth significantly influenced the connector stiffness and maximum load than other variables. The connector's performance was not increased proportionally with a deeper notch cut. Screw length and concrete thickness only had minor influences that are difficult to spot since the number of tests was limited.

3. The finite element model could capture the tendency of both stiffness and maximum load in terms of notch depth. The model would need to characterize different timber modulus of elasticity for compression and traction to predict stiffness better. Such implementation requires user-coded material in Abaqus, which is out of the scope of this study.

4. The results showed that the length of the screw did not impact the overall results. After the test, the specimens were successfully disassembled and separated using a simple screwdriver. This connector system could be employed if there are concerns about the reusability at the end of the structure service life.

This study gave more information about the performance of individual notched connectors of different geometry configurations. The finite-element model could produce a reasonably good prediction, though it could not entirely capture the experimental phenomenon due to an over-simplified timber material. Since our next step would focus on the vibrational behavior of full-scale specimens, this study provided a basis to create a simplified parametrical model of the connector for a global optimization application. For future research, full-scale testing of long-span CCC beams will adopt this type of connector. The presented findings on individual behavior (strength, stiffness) and other aspects such as group effect, number of connectors, and distance between the connectors will be considered. One of the objectives of our research project is to propose

a solution to a deconstructable connector. It involved a vision at the scale of beams, floors, and entire structures. This solution will also be validated in-depth on a full-scale beam test.

ACKNOWLEDGEMENT

The authors are grateful to Natural Sciences and Engineering Research Council (NSERC) of Canada for the financial support through its IRC and CRD programs (IRCPJ 461745-18 and RDCPJ 524504-18), the Region Nouvelle Aquitaine for the financial support (ref. 2017-1R10223), and the industrial partners of the NSERC industrial chair on eco-responsible wood construction (CIRCERB).

3. VIBRATIONAL BEHAVIOR OF CLT-CONCRETE COMPOSITE BEAMS USING NOTCHED CONNECTORS

Résumé : La solution de plancher bois lamellé collé croisé (cross-laminated timber – CLT) - béton composite (CCC) est attractive car elle possède de nombreux avantages d'un système de plancher composite bois - béton à une faible épaisseur. Cependant, les critères de vibration sont généralement un obstacle dans le processus de conception, en particulier plus onéreux pour les planchers de longue portée. La présente étude se concentre sur les performances vibratoires des poutres CCC dotées de connecteurs à l'entaille. Trois poutres composites ont été fabriquées et testées. Les fréquences naturelles expérimentales ont été comparées aux résultats analytiques et numériques. Une certaine amélioration en termes de fréquence fondamentale et d'amortissement modal a été trouvée dans les poutres CCC par rapport aux poutres de CLT nus. Un écart important entre la fréquence fondamentale expérimentale et théorique a été observé dans le cas de la poutre non composite. L'amortissement modal était négativement corrélé au nombre d'entaille usinée sur les poutres. Enfin, l'analyse a été étendue à d'autres études dans la littérature pour valider nos résultats expérimentaux et numériques.

Abstract: The CLT-concrete composite (CCC) solution is appealing since it possesses many advantages of a timber-concrete composite flooring system with a small thickness. However, the vibration performance is usually an obstacle in the design process, especially more onerous for the long-span floor. The present study focus on the vibrational performance of CCC beams featured notched connectors. Three composite beams were fabricated and tested. The experimental natural frequencies were compared with analytical and numerical results. The fundamental frequency and modal damping improvement were found in the CCC beams compared to bare CLT beams. However, a significant gap between the experimental and theoretical fundamental frequency was observed in the case of a non-composite beam. Furthermore, modal damping was negatively correlated to the number of notches of the beams. Finally, the analysis was expanded to other literature studies to validate our experimental and numerical results.

3.1. INTRODUCTION

Timber-concrete composite (TCC) structures are an excellent way to benefit from timber and concrete advantages. The timber elements resist the tensile stress, and the concrete elements hold the compression stress. Intensive studies on TCC structures were carried out in the last decade to demonstrate the advantages regarding short-term and long-term behavior [96], [102], [103], performance on fire, seismic, acoustic, and vibration [121], [21], [104], prefabrication ability [96], [105]. TCC is also a more balanced solution for economic and environmental than all reinforced concrete or timber floors. CLT-concrete composite (CCC) structures are a variant of TCC; therefore, they inherit the mentioned advantages. Moreover, a CCC floor using timber panels would have a limited depth, an asset for mid-rise and high-rise buildings [57], which means that there would be a potential gain of one floor over ten floors built.

Timber floors are prone to have inferior vibration comfort compared to traditional concrete or steel-concrete composite floor. Concrete topping added to the lightweight timber floor enhanced the floor performance in fundamental frequency and modal damping. Performance of TCC structures in vibration and benefit of the additional concrete layer was proven in many studies [44], [93], [122]. However, the concrete mass might cause a reduction in performance [44].

TCC floors have three principal elements: concrete deck, timber panel or timber beams, and connector systems. Hence, the characteristic of materials, *i.e.*, modulus, density, and connector stiffness, are required to assess the vibration performance of TCC floors. Dynamic characteristics of TCC floor, such as fundamental frequency and damping, have been studied by many authors in the literature [93], [123]–[125]. For example, Ghafar *et al.* [124] found that the natural frequency and damping were lower in laminated-veneer lumber (LVL)-concrete than the bare LVL beam. Santos *et al.* [123] also found a decrease in fundamental frequency after adding the concrete layer on the glulam beams. For the non-geometric parameters, the authors found that an increase of concrete class, timber class, and connector stiffness would augment the fundamental frequency of a TCC floor. The composite action between concrete topping and timber is crucial in TCC floors. Lukaszewska *et al.* [125] tested prefabricated TCC beam of 4.8 m span. The tested floor could have the fundamental frequency exceed 8 Hz. It is worth noting that these are experiments on traditional TCC floors with timber beams connected to the concrete slab. In the case of the CCC floor, Mai *et al.* [93] found that the fundamental frequency of CLT floors could increase significantly by adding 100 mm concrete topping along with a shear connector system. Recently, in terms of human-induced vibration response of TCC floor, Xie *et al.* [126] conducted dynamic experiments

to analyze the vibration response of the TCC floor subjected to different walking loads. The peak acceleration of the floor increased with an increase in step frequency and the number of pedestrians. Loading and support conditions are also the factors that need to be considered in the design of floor vibration comfort.

TCC floor could be regarded as semi-lightweight. They are heavier than traditional timber floors, have a lower fundamental frequency, and worsen in a long-span structure. Since there is no dedicated vibrational design guide, the design of long-span TCC floor must be carefully considered in terms of vibration. Recent efforts have proposed an appropriate design criterion for this floor system [87], [127]. This criterion was derived using the method defined in ISO/TR 21136:2017 [128], was validated by limited data, and would require further investigation. Another version of this criterion for the CLT floor [92] was adopted in the Canadian Standard CSA-O86:2014, updated June 2017 [9].

Limiting the fundamental frequency is the most popular solution to assure lightweight timber floor vibration comfort [81] because the human body is more sensitive to low frequencies than higher ones. Hence, a high damping ratio is desirable and is usually contributed by the non-structural element (insulation, dropped gypsum board, plumbing). However, damping is challenging to estimate correctly and is assumed in the design with uncertainty [129]. Therefore, the fundamental frequency and damping predictions are the most critical objective parameters in assessing vibration performance. The peak acceleration estimation is also suggested by EN 1995-1-1 [8]. However, based on the psycho-vibratory evaluation of Negreira *et al.* [70], this objective parameter is not the best indicator for vibration annoyance. Therefore, the fundamental frequency is one of the best candidates for assessing vibration performance considering parameter convenience and reliability in the design phase.

An experimental study [130] quantified the performance of the notched connectors. In terms of serviceability limit state, notched connectors were relatively stiff and robust for the long-span floors. Therefore, this solution was adopted for the long-span floor in this study. The main goal is to evaluate the dynamic properties (fundamental frequency and damping) of long-span CLT-concrete composite beams using the notched connector. This goal is interpreted into three steps:

- Analyze the experimental results, from static and dynamic tests, of CCC beams built using a notched connector.

- Propose a FE model that can characterize the vibrational behavior of CCC beams. This model would be straightforward while offering static loading analysis and even non-linear analysis.
- Evaluate the natural frequencies prediction of analytical expression and the FE model vis-à-vis the experimental results.

3.2. MATERIALS AND METHODS

3.2.1. Materials properties

The CLT has grade E1 complying with the standard ANSI/APA PRG-320-2019 [37]. The properties of CLT was presented in Table 1. The CLT panel was face-glued and not edge-glued [109]. The local supplier provided the concrete material with the indicated class of C35. The compression test conducted on the cylinder specimens yielded a mean compression strength f_c of 36.8 MPa and a mean modulus of elasticity E_c of 26773 MPa.

Table 3.1. Properties of CLT and concrete.

Property	Unit	CLT Longitudinal Layer *	CLT Transversal Layer *	Concrete **
Compression strength, f_c	MPa	23.6	8.5	36.8
Modulus of elasticity, E	GPa	11.7	9.0	26.8
Density	kg/m ³	514	514	2262

* Standard properties of CLT given by the manufacturer [109]. ** Experimentally measured on five cylindrical specimens according to the ASTM C39/C39M—18 standard [110].

3.2.2. Specimens

Three CCC beams with dimensions 9.0×1.0 m (length×width) were fabricated. The beams had different composite levels. The first one (beam 1, icon as ) had no notch; hence, non-composite. The two others (beam 2  and beam 3 ) had a different number of notches (beam 2  has one row of 10 connectors while beam 3  has 26 connectors distributed in 3 rows), consequently have low- and high-level composite. The beam span L , or distance between the supports, was 8.7 m. Figure 3.1 presents the plan of beam 3.

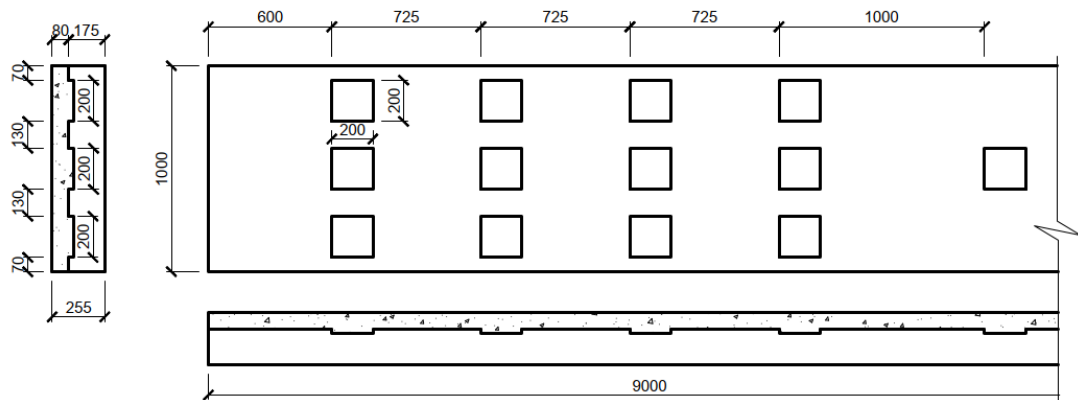


Figure 3.1. Connector layout of Beam 3 and actual image of the beams before concrete casting

The CLT panels were delivered with pre-cut notches. Their dimensions are 200×200×25mm (length×width×depth). We put the polyethylene film on each beam, especially the notched surface, to limit the moisture transfer between timber and concrete. Two screws were installed at each notch position. The panels were then ready for concrete casting when the steel mat (150×150 mm) was in place. The individual notched connector specimens were fabricated and tested under a test campaign to determine their stiffness and resistance. The connector stiffness k was obtained from the static shear test (push-out test). After six repetitions (serie I), the stiffness of the single notch connector yielded 242 kN/mm with a coefficient of variation (CoV) of 13%. The load-slip curves of six specimens tested could be found in [130].

3.2.3. Supports

Supports for CLT-concrete beams were fabricated from the rectangular wood logs, steel tubes, and steel plates. The upper plates placed between the tube and the timber part were not soldered or fixed. The friction between this plate and timber would hold it in place while the contact with the steel tube provided sufficient displacement for the beams. The supports are distinguished as pinned and roller by mean of the welding tube-bottom plate. The CCC beams were placed above four supports in the early days.

The two intermediate supports were removed seven days after the casting, and the composite structures then worked as a simple beam on two supports (Figure 3.2).

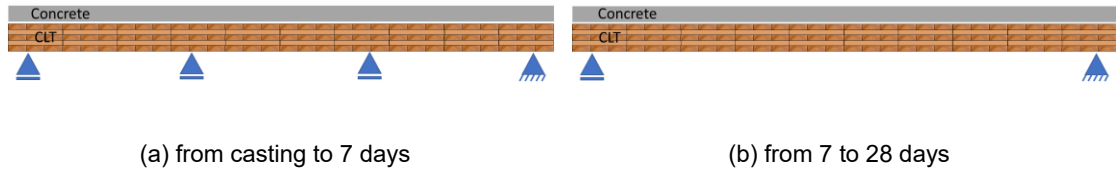


Figure 3.2. Schematic plan of the supports at the early and later state of the beam

3.2.4. Test procedure

3.2.4.1. Deflection test

The beams were subjected to the non-destructive deflection test. This test was conducted by applying a concentrated load of approximately 1 kN at the beam midpoint. The total testing time is less than 5 minutes. The deflection tests were conducted on the simple support beams for CLT panels and CCC 28 days after casting. The deflection of the tension edge was measured using two LVDTs installed at mid-span. The deflection, called global displacement [131], is the average of two measured values. The apparent flexural stiffness EI_{app} of bare CLT panels could be calculated as:

$$EI_{app,CLT} = \frac{PL^3}{48d_m} \quad (3.1)$$

The effective bending stiffness of the beam EI_{eff} could be deduced from EI_{app} based on indications of 2015 National Design Specification, Section 10.4.1.1 [132], (Equation (3.2)). The effective shear stiffness GA_{eff} of bare CLT panel is assumed unchanged between the three panels and equals $15 \cdot 10^6$ N [133]. K_s is a constant dependent on support conditions and applied load. K_s for simply supported beams under concentrated load at the mid span equals 14.4. Beam span L equals 8700 mm.

$$EI_{eff,CLT} = \frac{EI_{app,CLT}}{\left(1 - \frac{K_s EI_{app,CLT}}{GA_{eff,CLT} L^2}\right)} \quad (3.2)$$

3.2.4.2. Vibration test

A vibration measurement generally requires several hardware components. The essential hardware element consists of a source of excitation (exciter) for providing a force to the structure, a transducer to convert the mechanical motion into an electrical signal [81]. Experimental modal analysis (EMA) is a technique to determine the structure

dynamic involved in testing components or structures to obtain a mathematical description of their dynamic or vibration behavior [98].

The free vibration tests using an impact hammer were conducted on the simply supported bare CLT beams and CCC beams 28 days after concrete casting. Figure 3.3 shows the grid of acquisition points on the beams. The tests were performed with the accelerometers and the impact hammer measuring the responses perpendicular to the beam surface. The desired frequency range conditioned the longitudinal spacing of the grid. In our case, it is up to the fifth bending mode, *i.e.*, ~ 100 Hz. All the vibration tests had point 15 as a reference point. In addition, there were four points (13, 15, 16, 18) that could provide the same results. Hammer hitting at these points allowed the excitation of both bending and torsional mode without coinciding with the modal node (point 10, 12, 19, 21) or too far from the other side of the beam (point 4, 6, 7, 9, 22, 24, 25, 27).

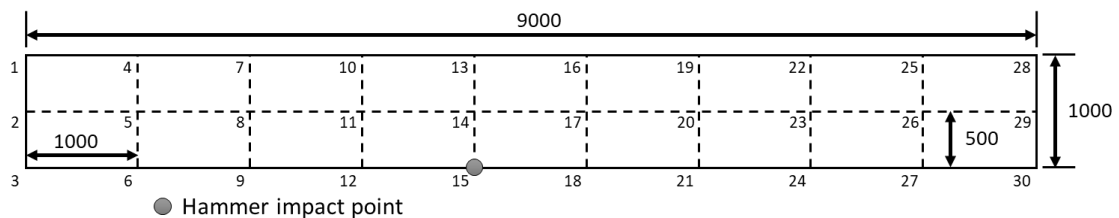


Figure 3.3. Accelerometer layout with the hammer impact location

A total of six uniaxial low-frequency accelerometers was used for the vibration test. The accelerometers, model 626B02 from ICP-PCB Piezotronics, are uniaxial ceramic shear ICP accelerometers with a sensitivity of 500 mV/g and a frequency range from 0.2 to 6000 Hz. Roving-accelerometer method was adopted [98], [134]. The hammer would hit the same place on the beam, and the six accelerometers would be displaced after each hit to cover the whole structure. The results of measurement points from 4 to 27 were presented in Figure 3.7. The impact hammer, model 086D20 from ICP-PCB Piezotronics, is equipped with a uniaxial force sensor with a sensitivity of 0.23 mV/N, a measurement range of ± 22.2 kN, and a super soft plastic tip, was employed to generate the vibration force. The acquisition box was LMS SCADAS with eight channels. The software used for data acquisition was LMS.ImpactTesting. Frequency, damping, and mode shapes were identified in LMS.TestLab using PolyMAX as the modal parameter identification method [135]. This method yielded clear stabilization diagrams, direct results with minimum computational efforts.

3.3. ANALYTICAL AND NUMERICAL MODELING

3.3.1. Bending stiffness of bare CLT panels

CLT properties are essential to the assessment of dynamic properties. In a parametric study carried out on TCC beams, Santos *et al.* [123] concluded that the timber class (*i.e.*, modulus E_t) has an influence on the fundamental frequency. In the case of notched beam, the timber loss would also impact the moment of inertia I of the cross-section; hence, the effective bending stiffness EI_{eff} of bare CLT beams. Moreover, the implementation of notched cross-sections into a simplified FE model or analytical expression is complex. For these reasons, the evaluation and calibration of bending stiffness EI_{eff} of CLT panels are important and were conducted. The primary purpose is to determine the actual stiffness of the CLT panel with the notched connectors.

3.3.1.1. Analytical methods

The Gamma (γ) method could be adopted to determine the CLT bending stiffness [39]. The calculation assumed that the longitudinal lamellas contribute to the load carrying, and the transversal one is the “imaginary shear connector” through their rolling shear stiffness. For example, a 5-ply CLT panel with a span of 8.7 m, a width of 1.0 m could have the connector efficiency of layers 1, 3, and 5 as

$$\gamma_1 = \frac{1}{1 + \left(\pi^2 \cdot \frac{E_1 A_1}{l^2} \cdot \frac{t_2}{G_{y2} b_y} \right)} = 0,97 \quad (3.3)$$

$$\gamma_3 = 1 \quad (3.4)$$

$$\gamma_5 = \frac{1}{1 + \left(\pi^2 \cdot \frac{E_5 A_5}{l^2} \cdot \frac{t_4}{G_{y4} b_y} \right)} = 0,97 \quad (3.5)$$

The bending stiffness along the major direction could be calculated as

$$(EI)_{eff,y} = \sum_{i=1}^n (E_{yi} I_{yi} + \gamma_i E_{yi} A_i z_i^2) \quad (3.6)$$

The CLT bending stiffness could be calculated based on the Shear Analogy (SA) method [39]. This method is relatively accurate and used to determine the CLT panel stiffness in many standards [9], [37]. The stiffness in the mentioned standards was obtained by neglecting the stiffness transversal layers, *i.e.*, $E_{90} = 0$ for layers 2 and 4 of 5-ply CLT. For the CLT panel with n layers, the bending stiffness along the major direction could be evaluated by

$$(EI)_{eff,y} = \sum_{i=1}^n \frac{E_i b_y t_i^3}{12} + \sum_{i=1}^n E_i b_y t_i z_i^2 \quad (3.7)$$

The irregular cross-section (rectangular section with notches) was taken into account (Figure 3.4). Since the notch's depth t_n is 25 mm, the top layer of CLT was divided into a "notched layer" of 25 mm and a "no-notched layer" of 10 mm. The width $b_1 = b_{y1} + b_{y2} + \dots$ of "notched layer" are 1000, 800, and 400 mm for Beam 1, 2, and 3, respectively.

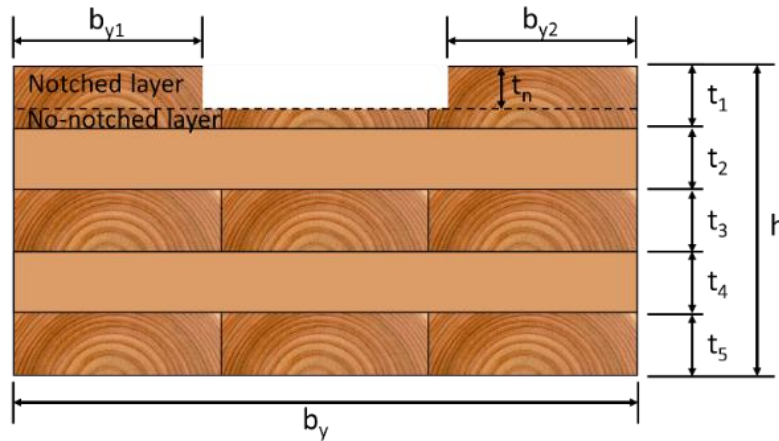


Figure 3.4. Cross-section of notched beams

Table 3.2 presents the calculation of both two presented methods for the notched section of beam 2.

Table 3.2. Calculation of effective bending stiffness by two analytical methods

Layer	Depth t [mm]	Orientation [°]	Width b [m]	E_t [GPa]	z_t [mm]	$EI_{eff_t}(SA)$ [$\times 10^{12} \text{Nmm}^2$]	γ [-]	$EI_{eff_t}(\gamma)$ [$\times 10^{12} \text{Nmm}^2$]
1.1 - notched	25	0	0.8	11.7	-75	1.33	1.00	1.33
1.2 - intact	10	0	1.0	11.7	-57.5	0.39	0.99	0.38
2	35	90	1.0	0	-35	0.00	-	0.00
3	35	0	1.0	11.7	0	0.04	1.00	0.04
4	35	90	1.0	0	35	0.00	-	0.00
5	35	0	1.0	11.7	70	2.05	0.97	1.98
						3.81		3.74

3.3.1.2. Experimental method

Dynamic-based: Zhou *et al.* [136] proposed a method for calibration of the CLT elastic constants based on the free vibration of orthotropic Mindlin plate simply supported at two opposite sides. The inverse problem would determine the effective bending and shear stiffness from a set of specified modal frequencies. The genetic algorithm (GA) was chosen as the optimization technique. Objective function $F(X)$, or fitness function, for GA, is defined as the sum of the relative difference between the experimental and calculated natural frequency of N selected input mode.

$$F(X) = \sum_{i=1}^N \left| \frac{f_{\text{exp}_i} - f_{\text{cal}_i}}{f_{\text{exp}_i}} \right| \quad (3.8)$$

The input modal frequency f (m, n) combination suggested in the work of Zhou *et al.* are “Lower-5-Freqs” (2,0), (2,1), (2,2), (2,3), (3,0); “Higher-5-Freqs” (3,0), (2,1), (2,3), (2,4), (4,0); or “7-Freqs” (2,0), (2,1), (2,2), (2,3), (2,4), (3,0), (4,0), with m and n are number of nodal lines including the simple supports in x and y direction. These combinations are suitable for plate-like structures with a relatively low ratio of length/width per thickness. For our case, the panels with beam-like form had a particularly high ratio L/h (*i.e.*, 9.0 m / 0.175 m = 51). The bending mode in the width direction was almost impossible to obtain through an impact hammer vibration test. The chosen combination for calibration was (2,0), (3,0), (4,0), (2,1), (3,1), namely the first, second, third bending mode in the longitudinal direction, and first, second torsional mode.

Static-based: CLT longitudinal bending stiffness $EI_{eff,CLT}$ was determined based on static vertical displacement; see Section 3.2.4.1.

3.3.2. Bending stiffness of CCC beams

The experienced floor vibration is assumed to be a result of the fundamental frequency [81]. The higher frequency means better dynamic performance since the human bodies are only sensitive to a specific frequency range. Eurocode 5 [8] proposed the calculation for rectangular timber floor simply supported all *four* edges, although the formula implied no contribution from the transversal component. The frequency for any n^{th} flexural vibration mode of a simply supported uniform beam is given by:

$$f_n = \frac{n^2 \pi}{2} \sqrt{\frac{EI_{eff}}{mL^4}} \quad (3.9)$$

The estimation of EI_{eff} of a composite cross-section would require materials, geometry, and shear connector properties. Since vibration criteria usually condition long-span TCC structures, a reliable analytical expression to estimate EI_{eff} is necessary. Eurocode 5 [8] proposed the Gamma method. This method is the most popular and robust expression to estimate the effective bending stiffness [39]. Another analytical method was suggested by Wu *et al.* [31] for free vibration of partial-interaction composite members with axial forces under simply supported boundary conditions. This method was presented under the closed-form expressions.

3.3.2.1. Gamma (γ) method

The Mechanically Jointed Beams Theory, also named the Gamma method [8], suggested the calculation of the effective bending stiffness of a simply supported TCC beam as

$$EI_{eff} = E_c I_c + E_t I_t + \gamma_c E_c A_c a_c^2 + \gamma_t E_t A_t a_t^2 \quad (3.10)$$

with the shear coefficient γ and distance a as

$$\gamma_c = \left(1 + \frac{\pi^2 E_c A_c s}{kL^2} \right)^{-1}; \quad \gamma_t = 1; \quad (3.11)$$

$$a_c = \frac{\gamma_t E_t A_t (h_c + h_t)}{2(\gamma_c E_c A_c + \gamma_t E_t A_t)} \quad (3.12)$$

$$a_t = \frac{\gamma_c E_c A_c (h_c + h_t)}{2(\gamma_c E_c A_c + \gamma_t E_t A_t)} = \frac{h_c + h_t}{2} - a_c \quad (3.13)$$

3.3.2.2. Wu *et al.* method

Wu *et al.* [31] proposed a relation to obtain the effective longitudinal stiffness of a simply supported TCC beam. Based on the Euler-Bernoulli beam theory, the exact solution of frequency for a composite section with two sub-elements of different materials can be obtained as

$$\tilde{\omega}_n^2 = \tilde{\omega}_{n0}^2 \left[1 + \frac{\tilde{H}}{\tilde{N}_{n,cr}} - \frac{\beta^2 - 1}{\frac{\tilde{\alpha}^2}{(n\pi)^2} + \beta^2} \right] \quad (3.14)$$

By neglecting the effect of axial force \tilde{H} , the effective bending stiffness can be deduced as

$$EI_{eff} = \bar{EI} \left[1 - \frac{\beta^2 - 1}{\frac{\tilde{\alpha}^2}{(n\pi)^2} + \beta^2} \right] \quad (3.15)$$

with

$$\tilde{\alpha}^2 = \frac{k}{s} L^2 \left(\frac{1}{E_c A_c} + \frac{1}{E_t A_t} + \frac{h^2}{\Sigma EI} \right) \quad (3.16)$$

$$\beta^2 = \frac{\bar{EI}}{\Sigma EI} \quad (3.17)$$

$$\bar{EI} = \Sigma EI + \frac{E_c A_c E_t A_t}{E_c A_c + E_t A_t} h^2 \quad (3.18)$$

The shear connector between the two sub-elements is assumed continuous and uniformly distributed in the longitudinal direction. Our preliminary study shows that two

analytical methods yielded the exact evaluation of EI_{eff} for the first mode. With mode- n dependent EI_{eff} , Wu *et al.* [31] method could provide better results when shifting to the bending mode of a higher order.

3.3.3. Finite elements model of CCC beams

In this study; a finite element models was developed as an alternative to the analytical one. It needed to be simple for engineering implementation and future optimization study. These models could estimate the natural frequencies of complex composite structures. Many modeling approaches depending on the finite element (beam, shell, or cubic element) could be found in the literature. For example, Glisovic and Stevanovic [137] used the 3D element to model the steel-concrete beam vibrational behavior. Cubic elements modeled the concrete deck, while the steel profile used shell elements. The connector was modeled as a spring element. The authors also elaborated on another model using a beam element for a discrete connector. The overall results show no significant difference between the two concepts. Jiang *et al.* [6] also employed a 3D element to modeling CCC beam behavior under static loading. Santos *et al.* [123] proposed a practical and easy-to-implement 3D FE model for traditional TCC floor (glulam beams, concrete deck). The model used frame elements for the timber beams with spring elements for the connector. The same approach was adopted by Turmo *et al.* [138] for a two-dimensional FE model to simulate the behavior of steel-concrete composite beam with partial interaction.

A unidimensional finite element model was built in Abaqus CAE software [120]. The model used beam elements in a plane B21 (2-node linear beam) for timber and concrete materials. The beam elements are shear deformable and account for finite axial strains. They have three degrees of freedom at each node: two translational and one rotational about the normal to the model plane. Connectors were modeled as spring elements in the horizontal direction. The stiffness of the spring element was defined as a constant. The concrete was modeled as isotropic material. The information about concrete material was based on the compression stress of cylindrical specimens. The average MOE in compression of concrete 28 days after casting was 26.8 GPa. The timber was also modeled as isotropic material with bending MOE along the major strength axis E_b as the modulus. The bending MOE of timber was taken from the following section on stiffness calibration. The concrete Poisson ratio and density are 0.2 and 2262 kg/m³, respectively.

The model schematic of CLT-concrete beams is presented in Figure 3.5, where h_c and h_t are the thickness of concrete and timber layer, respectively.

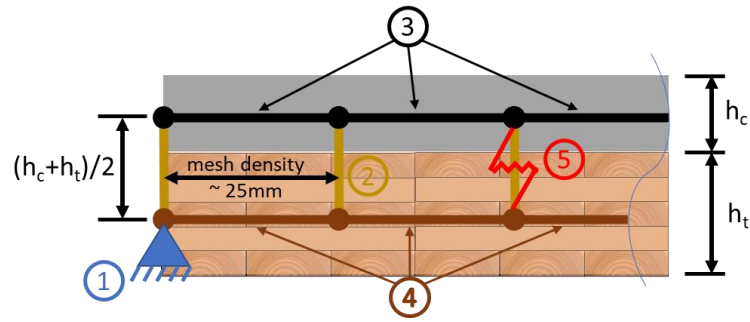


Figure 3.5. Composite beam FEM model

1. Support
2. Vertical strut elements, rigid in terms of axial stiffness
3. Concrete elements
4. Timber elements
5. Horizontal connector elements, a spring-like element with defined horizontal stiffness (connector stiffness)

The mesh density is the question addressed adequately elsewhere [138]. It is known that the distance between vertical strut influences the results of the analysis: the smaller distance would lead to a more accurate result. In this study, mesh density was exhibited through the individual concrete (or timber) element length. The element size (distance between vertical struts) was fixed at 50 mm (beam thickness is 255 mm) based on the mesh sensitivity study (Figure 3.6). The blue points are the calculations based on analytical expressions (Equation (3.1) for the deflection and Equation (3.9) and (3.15)-(3.18) for the fundamental frequency).

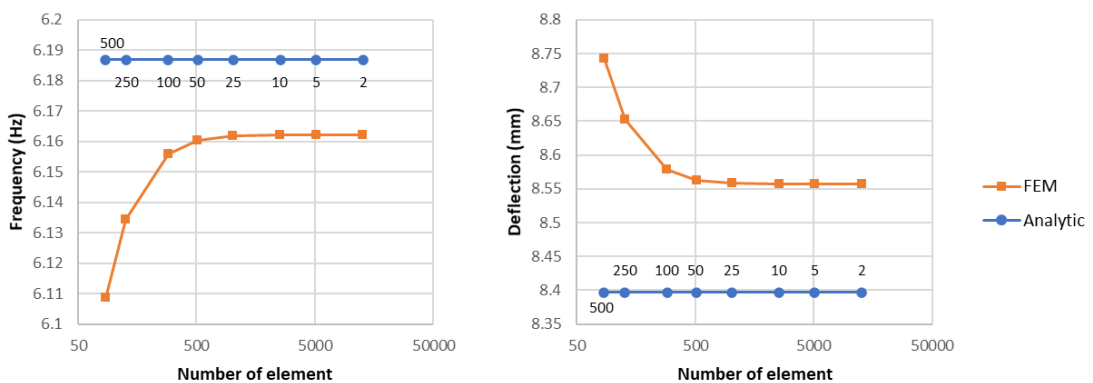


Figure 3.6. Mesh sensitivity, data labels represent the corresponding element size

3.4. RESULTS

3.4.1. Static deflection tests of CLT and CCC beams

The deflection d_m under 1kN of bare CLT and CLT-concrete beams after 28 days are listed Table 3.3. The EI_{app} and EI_{eff} was deduced from experimental deflection d_m by using Equation (3.1) and (3.2). The bare CLT panel (with no notch) has a theoretical stiffness EI_{eff} (using Shear Analogy method) of 4.14 MNm²/m [109], which is 2.7% different from the experimental results, 4.25 MNm²/m of Beam 1.

Table 3.3. Results of static deflection tests (MNm²/m)

Beam	df_{m-1kN} [mm]		EI_{app} [MNm ² /m]		EI_{eff} [MNm ² /m]
	Bare CLT	CCC 28 days	Bare CLT	CCC 28 days	Bare CLT
1 	3.41	2.50	4.02	5.50	4.25
2 	3.62	0.81	3.79	16.83	3.99
3 	3.73	0.75	3.68	18.15	3.87

3.4.2. Vibration tests of CCC and CLT beams

The results exhibited in Table 3.4 are the natural frequencies of bending modes, the beams' modal damping at the state of bare panel, and 28 days old concrete. The FRFs (frequency response functions) of 24 measurement points are presented in Figure 3.7. The mode shapes of bending modes are presented in Annex 6.

Table 3.4. Natural frequencies and damping

Mode	Beam 1 		Beam 2 		Beam 3 	
	Freq.	Damping	Freq.	Damping	Freq.	Damping
Bare CLT beams						
1	4.30 Hz	0.6 %	4.26 Hz	0.5 %	4.17 Hz	0.6 %
2	16.49 Hz	1.0 %	15.70 Hz	0.2 %	15.50 Hz	0.9 %
3	34.62 Hz	1.5 %	32.29 Hz	2.5 %	32.68 Hz	1.3 %
4	58.75 Hz	1.3 %	59.08 Hz	0.9 %	56.93 Hz	1.4 %
CCC beams at 28 days						
1	4.95 Hz	2.1 %	5.27 Hz	1.2 %	5.35 Hz	0.6 %
2	16.02 Hz	2.9 %	18.11 Hz	1.9 %	18.52 Hz	1.6 %
3	28.77 Hz	4.8 %	33.53 Hz	3.8 %	35.62 Hz	2.8 %
4	44.63 Hz	4.6 %	49.70 Hz	3.5 %	52.09 Hz	3.3 %

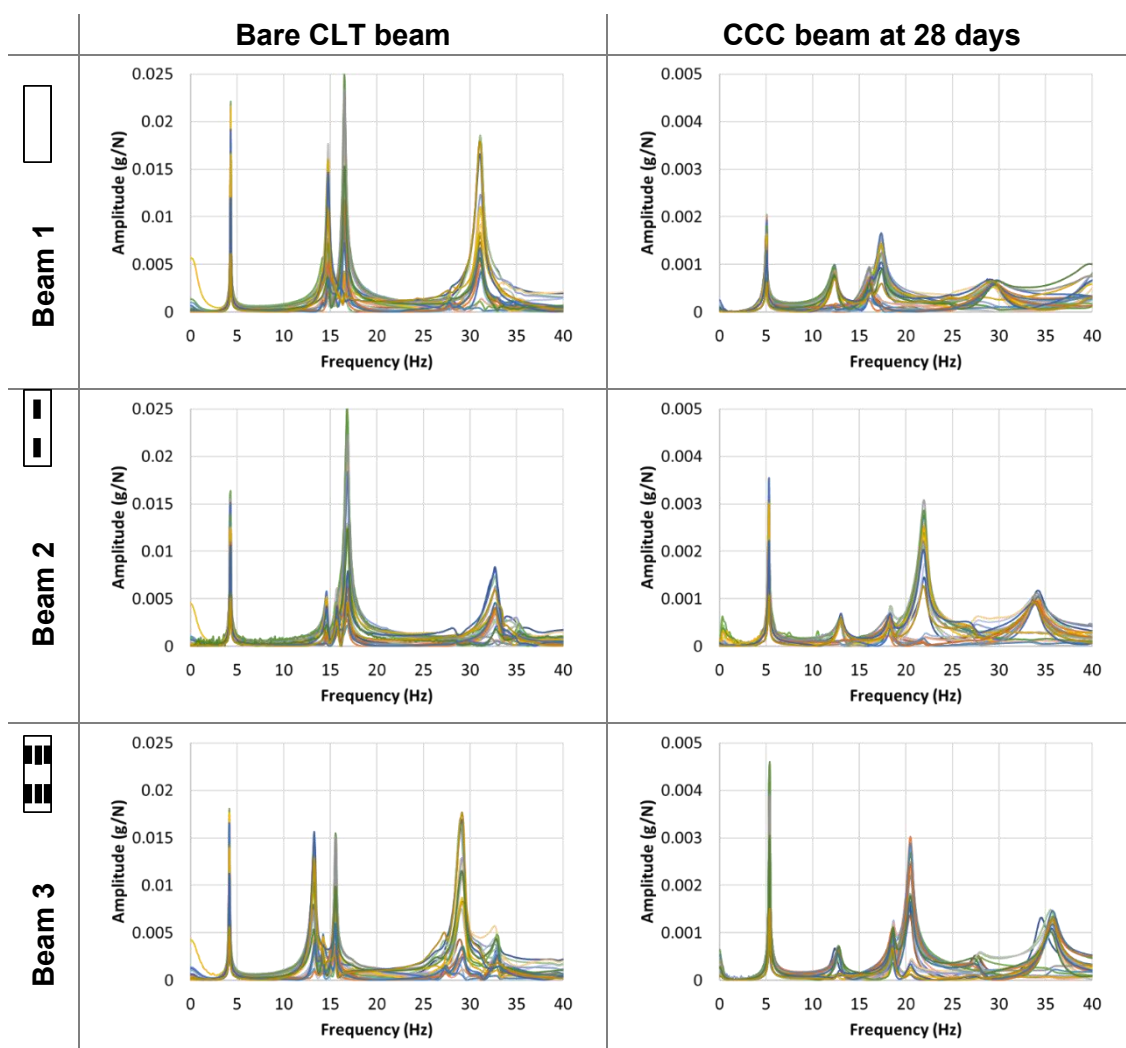


Figure 3.7. Frequency response functions (FRF) from 24 measurement points of bare CLT beams and CCC beams 28 days after concrete casting

3.4.3. Bending stiffness of bare CLT panels

3.4.3.1. Analytical method

The impact of notches could be estimated by analytical expressions using this approach (Table 3.5).

Table 3.5. EI_{eff} of bare CLT beams based on analytic expressions

Beam	Moment of inertia I_t [$\times 10^8$ mm ⁴]	Effective bending stiffness EI_{eff} [$\times 10^{12}$ Nmm ²]	
		Gamma method	Shear analogy
1	4.47	4.07	4.14
2	4.17	3.74	3.81
3	3.54	3.08	3.07

3.4.3.2. Experimental methods

Dynamic-based methods: The original method proposed by Zhou *et al.* [136] for plate structure allows the calibration of E_x, E_y, G_{xy}, G_{xz} and G_{yz} . Since our structures was beam-like, the information of E_y and G_{yz} (transversal modulus) is inaccessible. The calibration herein was performed for E_x, G_{xy}, G_{xz} . The estimations of the elastic constant $X_i = [E_x; G_{xy}; G_{xz}]$ were subjected to the bound constraint such as $X_{i_{min}} \leq X_i \leq X_{i_{max}}$. The lower bound $X_{i_{min}}$ of [9.000; 450; 100] MPa and upper bound $X_{i_{max}}$ of [1.1000; 650; 350] MPa were adopted for the calibration. These values were suggested for the 5-ply CLT panel [139]. The results' convergence of the optimization process could be obtained after 30 generations. In some cases, the algorithm converged after 10-15 generations. The average elastic constants E_x of 20 runs are presented in Table 3.6. The result of E_x, G_{xy} and G_{xz} was consistent with low CoV. This result was acceptable for the next comparison. It is worth noted that the cross-section took account by the inverse solution had no notch. The effective bending stiffness EI_{eff} presented in Table 3.6 were calculated by multiply the E_x by the inertia moment of intact section.

Table 3.6. EI_{eff} of bare CLT beams based on vibration test results

Beam	E_x [MPa]	Effective bending stiffness EI_{eff} [$\times 10^{12}$ Nmm ²]
1 	9.189	4.10
2 	8.990	4.02
3 	8.518	3.80

Static-based methods: CLT longitudinal bending stiffness EI_{eff} was determined based on static vertical displacement, see Table 3.3.

3.5. ANALYSIS AND DISCUSSION

3.5.1. Bending stiffness of bare CLT panels

Theoretical Young modulus of longitudinal lamination equals 11.7 GPa as suggested by CSA-O86:14 (2017) [9] and by the manufacturer [133]. In addition, the transversal lamination contribution has a known parallel to grain modulus of 9.0 GPa and a perpendicular to grain modulus of 0.3 GPa, which was omitted in the theoretical calculation [9], [133]. These are the basic assumptions for both analytic methods, while other moduli (shear and rolling shear) were derived based on European guidelines for softwood [119]. The shear deformation was considered differently by the two methods: calculating two deflection components by the SA method and calculating γ -coefficient

by the γ -method. Hence, the static-based stiffness was comparable with the results issued from the γ -method since they were based on the same assumptions of including shear deformation in the estimation of CLT stiffness. However, because the ratio L/h of the CLT panel was high, the deflection due to shear deformation was negligible when using the analytic methods to quantify the stiffness of the long-span CLT panel. For example, in CLT Beam 1, the deflection due to shear force was about 3.6% of those due to bending moment.

Regarding the influence of elastic modulus variation on CLT panel vibrational response, Zhou *et al.* [140] had recently conducted a sensitivity analysis on the frequency of vibration modes. One could observe that the response of bending mode (*i.e.*, mode (2,0), (3,0), (4,0) and (5,0) as denoted by the authors) depend principally on longitudinal modulus E_x and much less or even none on shear and transversal modulus $E_y, G_{xy}, G_{xz}, G_{yz}$. For example, sensitivity index of mode 1 to E_x , is more than 4.5% while sensitivity index of mode 1 to other modulus was less than 0.2%. Base on these arguments, we suggested that the shear deformation has a low impact on the vibration of CCC beams. The reason is the minimal effect of shear deformation on the responses of the long-span CLT beams. It is worth noting that both SA and γ -method underestimated the static-based stiffness of Beam 3. Hence, taking into account shear deformation would be too conservative and could lead to unrealistic frequency estimations.

Since the specimen number is minimal (one specimen for each configuration), we considered using the no-notched CLT panel (Beam 1) as an anchor point for the investigation. As presented in Table 7, the relative difference between analytic (SA and γ -method) versus static-based CLT stiffness was about 2.7% (4.14 vs. 4.25×10^{12} Nmm²) and 4.4% (4.07 vs. 4.25×10^{12} Nmm²). We concluded that the theoretical method based on presented modulus assumptions was reliable and suggested that the different responses of Beam 2 and 3 were due to the notches cut on these panels. Both analytic and experimental calibrated bending stiffness had the same trend regarding the number of notch cuts on the beam top layer. The intact CLT panel (beam 1) was the most rigid, while those with notch cuts (beam 2 and 3) were less stiff. The analytic and experimental methods registered the stiffness reduction in the most critical case (Beam 1 vs. Beam 3) of about 25 % and 10 %, respectively. Beam 2 and 3 seem to be underestimated by the analytic expressions since notches were assumed throughout the beam length. Some parts of these beams have an intact section; the notches only occupied 4% and 12% of beam 2 and 3 surfaces, respectively. Careful assessment of stiffness is suggested when the notches occupied more than 5% of the CLT surface.

Table 3.7. Comparison between experimentally calibrated and analytic CLT stiffness

Beam	Analytic [$\times 10^{12}$ Nmm ²]		Experimental [$\times 10^{12}$ Nmm ²]	
	Shear analogy	Gamma method	Static-based	Dynamic-based
1 	4.17	4.07	4.02	4.10
2 	3.83	3.74	3.79	4.02
3 	3.17	3.08	3.68	3.80

The stiffness difference (between the beams) due to the notched section is difficult to implement into the simplified unidimensional FE model. The fundamental frequency analysis would be based on these dynamically calibrated values, and the modulus reduction was used to interpret different notched cross-sections. Hence, the FE model would assume the same rectangular CLT section, while the modulus is different between the beams. The calibrated modulus were 9189, 8990, and 8518 MPa for Beam 1, 2, and 3, successively.

3.5.2. Vibration characteristics of CCC beams

The damping ratios reported on beam 1 (Table 3.4) were the highest among the three CCC specimens. Since the beam supports were the same, the stiffest connector systems would influence the beam damping. In composite beams (2 and 3), the connector systems would bind the two layers into a monolithic bloc. Beam 1 was two superimposed layers, and the friction between them might increase the damping. This observation is interesting since the damping ratio is the best indicator of vibration acceptability, per Negreira *et al.* [70]. The floor response amplitude depends on its natural frequency, the excitation source, the mass mobilized, and the damping. Increasing damping would make the amplitude of steady-state response a series of less significant transient responses. Although damping ratios are challenging to predict in the design phase, their dependence on connector systems should be considered (*i.e.*, high connector density might increase the stiffness and reduce the damping ratios). Rijal *et al.* [141] conducted an experimental investigation on the LVL-concrete composite using multiple types of connectors. The authors tested two beams with different connector densities (Beam 3 density was higher than Beam 4's – original notation of the authors). Although the authors did not clarify the impact of connector density on the modal damping, they concluded that an increasing number of notches could significantly affect damping ratios. This statement agreed with our findings.

The comparison between model and experiments was carried out based on the test results of CLT-concrete composite beams. Table 3.8 presents the CLT panel and

connector characteristics and natural frequencies from experimental tests and models. Normalized relative frequency difference NRFD (in %) was defined as:

$$NRFD = \frac{|f_{experiment} - f_{model}|}{f_{experiment}} \quad (3.19)$$

The frequency calculated using two methods, Wu *et al.* [31], and the finite element model, were in good agreement. Moreover, the two could predict the natural frequencies with relatively low NRFD, especially in the low- and high-composite beams. Therefore, according to the present findings, the estimated fundamental frequency might be conservative, provided that the flexural modulus must be correctly estimated.

There was a gap in the natural frequencies between the estimated and experimental results in the non-composite beam. Both analytical and numerical models could not capture this phenomenon. We suppose that this phenomenon would occur only while the beams vibrate since the static test confirmed that the stiffness EI_{eff} was correctly estimated by Wu *et al.* method [31] and the finite element model. However, the viscous-elastic characteristic of material subjected to an instantaneous loading was different from those of long duration loading. Moreover, the non-connected layers of Beam 1 would vibrate independently from each other, and friction at the interface might cause frequency differences.

Vibration criteria were proposed for lightweight floor systems assuming that the floor span is considerably smaller than floor width and bending stiffness in the span direction is more significant than width direction. The beams tested in this study could be considered as a 1-m wide floor-strip at the most unfavorable case, *i.e.*, no bending stiffness contribution whatsoever in the width direction. If the floor width is more significant than its span, the fundamental frequency could still be estimated using the Euler-Bernoulli beam theory [127]. Based on the guideline of Eurocode EN 1995-1-1 [8] about the vibration comfort of lightweight timber floor, both three CCC beams, also known as floor-strips, in this study did not satisfy the preliminary frequency condition ($f_1 > 8.0 \text{ Hz}$). In these cases, EC 5 suggested that a special investigation to demonstrate the design would be necessary. The beams did not satisfy either the guideline on vibration criterion (section A.8.5.3) of Canadian Standard CSA-O86:2014, updated June 2017 [9] for the CLT floor. However, interesting results could be found when applying the new vibration threshold for the wood-concrete floor in general, based on the recent report of C. Auclair [127]. The suggested criterion was presented under the form of an inequality

$$r = f_1 \cdot d_{1kN}^{-0,14} \geq 5,75 \quad (3.20)$$

with f_1 is the fundamental frequency and d_{1kN} is the static deflection under 1kN concentrated load in the middle of the beam. Figure 3.8 shows the curve of Equation (3.20) along with ten experimental subjective evaluations [127] (in blue, red, and green for "unacceptable," "marginal," and "acceptable" ratings, respectively). Although positioned in the "unacceptable" zone, Beam 2 and 3 of this study were remarkably close to the "marginal" subjective rating curve. A modification of beam length (*i.e.*, reduce the span from 8.7 m to 8.0 m) would make Beam 2 and 3 get into the "acceptable" subjective rating. Although, it is worth noted that even if Equation (3.20) was satisfied, the floor might not provide enough vibration comfort for occupants.

The calculated value of fundamental frequency f_1 and deflection d_{1kN} are of full-size floors tested by FPIinnovations. The calculated values of 1-m wide floor strips are the most unfavorable case of the full-size floor. The contribution of the transversal stiffness and supports in the transversal direction is none in this case. Therefore, the comparison made in Figure 3.8 demonstrates the possibility that the worst-case scenario could even satisfy the vibration criteria imposed on the full-size floors

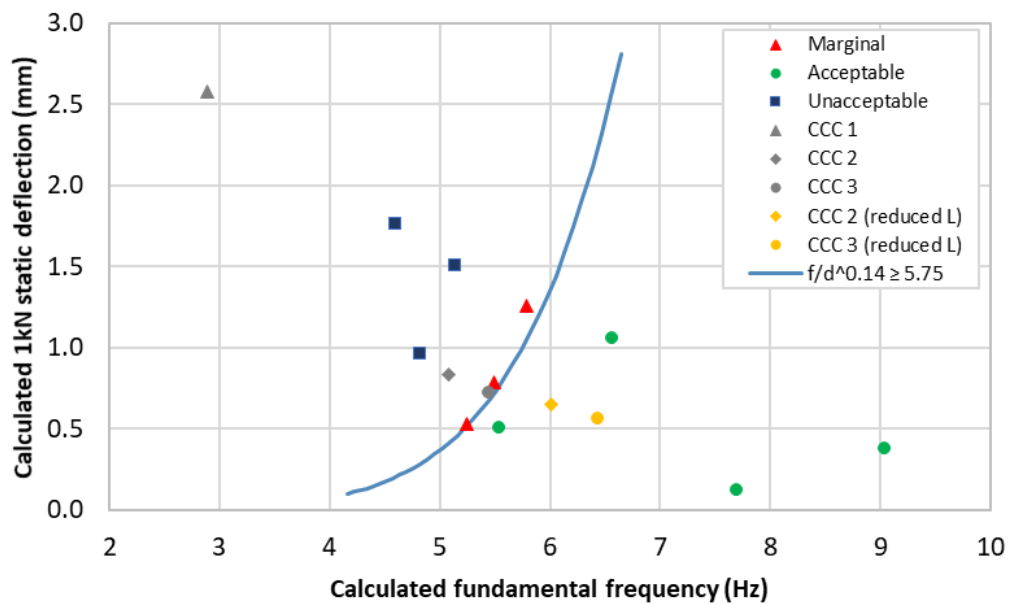


Figure 3.8. Proposed design criterion with subjective evaluations of CCC floors [127] and calculated results of this study

3.5.3. Comparison to other studies on the CCC beams

We expanded our investigation on other comparable studies (*i.e.*, CCC beams subjected to static and dynamic tests) to qualify our approach. We found three other studies [46], [93], [107] on CCC beams with different geometry, CLT, and concrete

material. All results were related to simply supported beams. Lamothe [46] carried out vibration and bending tests on three CCC beams (four beams were fabricated, but only three were subjected to dynamic tests). The author used Ultra-High-Performance Fiber Reinforced Concrete (UHPFRC) in one beam and High-Performance Concrete (HPC) for the other two beams. The employed connector was a bird-mouth notch with reinforced screws. Gerber [107] tested many timber-concrete composite beam configurations in which two of them were CCC (denoted S3 and S8 by the author). Beam S3 used an inclined screw as its composite connector, and Beam S8 used HBV® steel mesh. Finally, Mai *et al.* [93] performed full-scale static and dynamic experiments on CCC beams using inclined bolts (beam B-45-s150) and vertical and inclined SFS screws (three SFS beams). The author also tested a standard bare CLT panel, which gave us more information for comparison.

Table 3.9 presents the geometry, material, and connector information used for the calculation. Column 11 exhibited the experimental results of the fundamental frequency f_1 of the beams. Column 12 and 13 are the results of the fundamental frequency f_1 obtained from the analytical expression (Wu *et al.* [31] method) and the FE model previously presented. Columns 14 and 15 are the effective bending stiffness EI_{eff} of each beam obtained from the experimental tests (of each study) and from the analytical expression (Wu *et al.* [31] method). From Table 3.9, the following observations could be drawn.

- The bare CLT panel results got an excellent correlation between experiments (row 6, 11, 12, 13; col. 11 and 14) and analytical models (row 6, 11, 12, 13; col. 12 and 15). Another study [142] on the vibration of the CLT panel also indicated this observation. The apparent bending modulus E_t of the panels is the most important parameter for such a prediction. This bending modulus E_t could be obtained by the analytic expressions (Gamma method or Shear analogy method) in most cases. However, the notches on the upper surface of the CLT panel indeed reduced the bending stiffness.
- The frequency calculated by using the experimental effective bending stiffness EI_{eff} (col. 12) consistently lower than the experimental one (col. 11). The reason is that the effective bending stiffness was primarily measured in the initial loading sequence (up to 40% of maximum resistance). In comparison, the panel vibration occurred under a much smaller loading (about 1.0 kN in the case of a person normally walking [143]). This observation implied that the interface of materials and the behavior of the connector would cause these differences.

- The minor differences between the analytical method (col. 14) and experimental effective bending stiffness (col. 15) were caused mainly by the underestimated (row 14-16) or overestimated (row 1-5, 7-10) connector stiffness (stiffness of an individual connector and distance between connectors). Thus, under the circumstance where the MOE of the CLT panels was relatively correct to the actual behavior, and both materials density was well measured, the connector stiffness is the only primary parameter that conditions the frequency outcome.
- Comparing the models (FEM vs. Wu *et al.* [31], col. 12 and 13) shows an excellent agreement. Thus, adopting these models in the design process would be appropriate, whether for a quick estimation or a thorough investigation.

1

Table 3.8. Natural frequencies comparison between experiments and models

Beams	CLT	Connector		EI_{eff}		f1			f2			f1		f2	
	E	k	s	Exp*	Wu	Exp	Wu	FEM	Exp	Wu	FEM	Exp-Wu	Exp-FE	Exp-Wu	Exp-FE
	GPa	kN/mm	mm	$\times 10^{12}$ Nmm ²		Hz	Hz	Hz	Hz	Hz	Hz	NRFD (%)		NRFD (%)	
1 	9.2	0	0	5.5	5.3	5.0	2.9	2.9	16	12	12	42	41	28	28
2 	9.0	242	725	16.8	16.2	5.3	5.0	5.0	18	17	15	4	6	7	15
3 	8.5	726	725	18.2	18.0	5.4	5.3	5.2	19	19	18	1	2	-4	5

2

* Experimental apparent flexural stiffness EI_{app} from static bending test, see Table 3.3

3

Table 3.9. Comparison experimental-model results of CCC beam vibration studies

	Beam name	Source	Geom.	CLT			Concrete			Conn.	Experiment	Models		EI_{eff}	
			$L - w$	h_t	E_t	γ_t	h_c	E_c	γ_c	K_s	f_1	f_{1Wu}	f_{1FEM}	Static test	Wu <i>et al.</i>
			[m]	[mm]	[MPa]	[ton/m ³]	[mm]	[MPa]	[ton/m ³]	[kN/mm/m]	[Hz]	[Hz]	[Hz]	[$\times 10^{12}$ Nmm ²]	[$\times 10^{12}$ Nmm ²]
(1)	(2)	(3)	(4)	(5)	(6)	(7)	(8)	(9)	(10)	(11)	(12)	(13)	(14)	(15)	
(1)	UHPFRC	[46]	8.0 - 0.9	175	9.3	0.5	55	41.2	2.4	569	6.5	6.4	6.2	10.6	12.7
(2)	HPC#1		8.0 - 0.9	175	9.3	0.5	70	31.2	2.4	219	6.4	5.7	5.5	6.2	11.8
(3)	HPC#2		8.0 - 0.9	175	9.3	0.5	70	31.2	2.4	219	5.9	5.7	5.5	6.9	11.8
(4)	CCC S3	[107]	5.8 - 0.6	87	9.4	0.4	70	30.3	2.4	1.438	7.1	7.1	7.0	2.7	2.9
(5)	CCC S8		5.8 - 0.6	87	9.4	0.4	70	30.3	2.4	1.774	7.2	7.2	7.0	2.9	2.9
(6)	Bare CLT	[93]	5.8 - 0.9	150	10.7	0.6	-	-	-	-	8.8	8.8	-	2.7	2.7
(7)	B-45-s150		5.8 - 0.9	150	10.7	0.6	100	25.6	2.4	3.107	12.0	11.5	11.6	16.1	17.4
(8)	SFS-45-s150		5.8 - 0.9	150	10.7	0.6	100	25.6	2.4	2.378	12.0	11.4	11.5	16.4	17.1
(9)	SFS-45-s300		5.8 - 0.9	150	10.7	0.6	100	25.6	2.4	1.189	11.7	11.0	11.0	14.9	16.0
(10)	SFS-90-s150		5.8 - 0.9	150	10.7	0.6	100	25.6	2.4	175	11.5	8.8	8.9	13.8	10.2
(11)	Bare CLT 1	This study	8.7 - 1.0	175	9.2*	0.5	-	-	-	-	4.3	4.4	-	4.2	4.1
(12)	Bare CLT 2		8.7 - 1.0	175	9.0*	0.5	-	-	-	-	4.3	4.4	-	4.0	4.0
(13)	Bare CLT 3		8.7 - 1.0	175	8.5*	0.5	-	-	-	-	4.2	4.3	-	3.9	3.8
(14)	CCC 1		8.7 - 1.0	175	9.2*	0.5	80	27.9	2.3	0	5.0	2.9	2.9	5.5**	5.3
(15)	CCC 2		8.7 - 1.0	175	9.0*	0.5	80	27.9	2.3	334	5.3	5.0	5.0	16.8**	16.2
(16)	CCC 3		8.7 - 1.0	175	8.5*	0.5	80	27.9	2.3	1.001	5.4	5.3	5.2	18.2**	18.0

4

* Calibrated bending MOE, **Apparent flexural stiffness EI_{app}

3.6. CONCLUSION

CCC beams vibrational characteristics (fundamental frequency and damping) were investigated in this study regarding notched connectors. One could observe a reduction in terms of bending stiffness of the beams caused by the notched section. This aspect was assessed in this study through the analytical expression and experimental modulus calibration. In addition, the natural frequency and modal damping were reported and compared to the model results. The performance of non-composite beams was also presented in this study.

1. The composite beams have a fundamental frequency of about 5.3 to 5.4 Hz and damping of about 0.5% to 1.0%. Correspondingly, they are 5.0 Hz and 2.0% for the non-composite beam. Thus, the addition of the concrete layer increased the performance of CLT panels. Moreover, the damping ratio was highest in the case of the non-composite beam.

2. Both three beams could not meet the European or Canadian standard design requirements because of their substantial span. A span reduction would be an obvious obligatory to enhance vibrational performance. The change of the support condition, whether more rigid support or four-side supports, could be helpful, although this solution was not tested in this study.

3. The proposed simplified finite element model could be used as a quick implementation to evaluate natural frequencies, especially in complex structures. The application would not be limited to CCC beam structures but could be possible for the CCC floor systems. The drawback is that this model cannot describe the notched connector influence locally (depth, length, the distance between notches).

4. For the estimation of the fundamental frequency in engineering design, the Gamma method is adequate. However, Wu *et al.* [33] method could be an efficient candidate if the evaluation of higher-order mode frequency is involved since it was in closed-form and provided a more accurate mode-dependent result.

5. The presence of notches impacted the bending stiffness of the CLT panels. In general, the properties determination step in the design could be neglected, and theoretical expressions could evaluate the bending stiffness. However, careful assessment is recommended if the notched connector density is high (surface of notches occupied more than 5.0% of the CLT panel surface).

Based on these findings, the long-span CCC floor (design up to 8.0 m span using CLT 5-ply) with satisfied vibrational comfort is feasible. Future multi-objective optimization will be carried out using the presented analytical models.

ACKNOWLEDGEMENT

The authors are grateful to Natural Sciences and Engineering Research Council (NSERC) of Canada for the financial support through its IRC and CRD programs (IRCPJ 461745-18 and RDCPJ 524504-18), the Region Nouvelle Aquitaine for the financial support (ref. 2017-1R10223), and the industrial partners of the NSERC industrial chair on eco-responsible wood construction (CIRCERB).

4. OPTIMIZATION MULTI-OBJECTIVE OF CLT-CONCRETE COMPOSITE FLOORS USING NSGA-II

Résumé : Le bois lamellé collé croisé (cross laminated timber - CLT) est un produit en bois d'ingénierie composé de plusieurs couches collées sous la forme d'un panneau. Il est adapté particulièrement aux systèmes des planchers. Il pourrait être connecté mécaniquement à une couche de béton pour bénéficier des avantages des deux matériaux. Le composite CLT-béton (CCC) pourrait alors être une solution pour un système de plancher de longue portée pour les bâtiments à moyenne et grande hauteur. Néanmoins, la conception de ces plancher implique l'optimisation des éléments structuraux et non-structuraux. Cette étude s'est concentrée sur l'optimisation multi-objectifs du plancher CCC avec des connecteurs à l'entaille. Les objectifs étaient de minimiser l'épaisseur totale, le poids total et le coût total du matériau en tenant compte des contraintes structurelles, vibratoires et thermiques à l'aide de l'algorithme génétique. Les solutions sont présentées dans le sens du Front Pareto en fonction de différentes portées de plancher et de rapport coût bois/béton. Les influences des variables de décision et des contraintes dimensionnante sont démontrées. Toutefois, un seul type de plancher (CCC) est considéré et les aspects environnementaux (fonction objective et fonction contrainte) ne sont pas implémentée dans cette étude.

Abstract: Cross-laminated timber (CLT) is an engineered wood product made of multiple glued layers in the form of a panel suitable for flooring systems. CLT can also be mechanically connected to the concrete layer using the connector systems to create a CLT-concrete composite (CCC). This concept enhanced the structural performance of the floor and could be adopted for mid-and high-rise buildings. However, the design of the CCC floor involves the optimization of multiple structural and non-structural elements. In this study, we tackle the gap in the literature by carrying out a multi-objective optimization of the CCC floor with notched connectors by minimizing total thickness, total weight, and total material cost considering structural, vibration comfort, and especially, fire conditions constraints using the well-developed genetic algorithm (NSGA-II). The optimal solutions are presented in the Pareto fronts of multiple floor spans and cost ratio timber/concrete. The study also gives insight into the influence of design parameters and the governing design constraint. However, we only focus on one type of floor (CCC) and do not implement the environmental aspect of the structure.

4.1. INTRODUCTION

The timber-concrete composite (TCC) concept was first adopted to build bridge structures in the 1940s [60], [96], and the renovation of old timber structures [106]. Recently, this type of structure has been paid much more attention because of its many advantages on either concrete or timber flooring: environmental aspects, mechanical strength and stiffness, fire, seismic, acoustic, and thermal performance, suitability for prefabrication, and speed of construction on-site [96], [104]. Cross-laminated timber (CLT) is an engineered wood product made of multiple glued layers to form a panel. All or some CLT layers are oriented perpendiculars to their adjacent layer. Developed in '90, CLT is a relatively new engineered wood product, so does CLT-concrete composite (CCC). However, the latter inherited the mentioned advantages of former TCC structures, i.e., wooden beam-concrete slab.

Moreover, the gain for CCC floors over TCC floor in static height would make CCC more appealing for mid-and high-rise buildings [57]. CCC could be adapted for the long-span floor systems (more than 8 m), where the serviceability conditions usually control the design [144]. The CCC floor performance (i.e., stiffness, resistance, vibration, and acoustic performance) is generally enhanced compared to the bare CLT floor. The additional concrete layer with the shear connector systems could significantly increase the floor stiffness and resistance [44], [93], [122], [127]. Hence, the motivation for the investigation lies in the novelty and the mentioned potentials of this floor structure.

The CCC floor design comprises multiple elements such as component geometry or material grades to obtain the structurally and economically optimal solution. A robust optimization process, easy to implement during the structural design, is required. The design problem usually involves multiple objectives such as cost, structural and environmental performance [145], [146]. These objectives often conflict with each other, which means there is no unique best solution, but a set of compromise solutions identified on a Pareto front.

4.1.1. Structural multi-objective optimization

Many authors have addressed structural design optimization using various single-objective and multi-objective methods to optimize the conception and minimize the cost. Single-objective optimization (SOO) is the most straightforward approach to tackle one objective function at a time. The most popular objective is the construction/material cost. Klanšek and Kravanja [147], [148] developed a sophisticated cost model to compare the competitiveness of steel-concrete composite beams using the Nonlinear Programming method (NLP). Elachachi and Djellouli [149] used the

Sequential Quadratic Programming method (SQP) to optimize the element sizes of multi-story reinforced concrete structures. Poitras *et al.* [150] also optimized the cost of both composite and non-composite steel floors using Particle Swarm Optimization (PSO). A user-defined penalty factor was used when the constraints were violated. Jelusic and Kravanja [151] studied the optimal timber-concrete composite floor designs. The optimal solutions for a given vertical imposed load and structure span were found by minimizing the self-manufacturing cost using the Mixed Integer NLP method (MINLP). However, a practical optimization problem requires handling desirable but sometimes incompatible objectives that are usually multi-fields (i.e., structural, energetic, environmental).

Multi-objective optimization (MOO) is an eventual step to find a set of traded-off solutions that satisfy the required objectives. Leyva *et al.* [152] optimized the seismic design of reinforced concrete buildings by minimizing the inter-story drift and the total cost. Babaei and Mollayi [153] also optimized the structural design of the concrete frame by minimizing the total cost and the lateral roof displacement. Both studies utilized Non-dominated Sorting Genetic Algorithm II (NSGA-II). The number of research on the structural MOO of floor systems is limited. This is because of the problem-dependent nature of heuristic optimization and the novelty of TCC and CCC floor systems. The design of floor systems was recently studied by Decker [145] using Multi-objective PSO (MOPSO). The author investigated the optimal solutions for multi-story timber buildings by minimizing the heating needs, thermal discomfort, global warming potential, embodied energy and maximizing floor vibration comfort. Three structural design options were selected: concrete floor, CLT floor, and timber joist floor. The CLT floor with additional concrete screed was found to have close performances to concrete slabs in terms of vibration comfort, heating needs. The intervention of concrete helps reduce the heating needs with some environmental trade-off as compared to the floor without concrete. The difference between CLT floors with concrete screed and concrete floors lies in the embodied energy and the global warming potential.

4.1.2. Multi-objective optimization algorithm

In general, a multi-objective problem consisted of:

minimize/maximize M objectives: $f_m(\mathbf{x}), m = 1, 2, \dots, M$,

with solution vector of n decision variables: $\mathbf{x} = (x_1, x_2, \dots, x_n)$,

of n boundaries $x_i^{(Lower)} \leq x_i \leq x_i^{(Upper)}, i = 1, 2, \dots, n$

subjected to two types of constraints:

J inequalities $g_j(\mathbf{x}) \geq 0, j = 1, 2, \dots, J$;

K equalities $h_k(\mathbf{x}) = 0, k = 1, 2, \dots, K$;

There is no global and unique dominant solution in a MOO problem but a set of non-dominated solutions. The solution $x^{(1)}$ dominated $x^{(2)}$ ($x^{(1)} \preceq x^{(2)}$) when $x^{(1)}$ is “not worse” than $x^{(2)}$ in all objectives and $x^{(1)}$ is better than $x^{(2)}$ in at least one objective. The set of non-dominated solutions is called the Pareto front of the problem. In this investigation, NSGA-II was implemented using the package jMetalPy [154].

The present study aims to optimize notched CCC floor design by minimizing the thickness, weight, and cost of the floor components, such as CLT, concrete, connector, interlayer, fire protection while keeping the design in the range of structural constraints. The solutions found by the optimization would have to satisfy twelve constraint functions; hence the obtained results would be close to the actual structural design. The optimization results in a Pareto front that would allow designers to choose and develop their conception. The common design of the CCC floor was built and tested during the previous experimental study [130], [155]. The design was based on the Canadian standard for wood structures design CSA-O86:19 [9].

4.2. CLT-CONCRETE FLOOR DESIGN

4.2.1. CLT-concrete composite floor and the reference design

The design was performed for the 1m-strip CCC regarding the optimization variables (Table 4.3). Based on experimental results [130], a maximum of 3 rows of notched connectors can be set within a 1m-width. Figure 4.1 presents the maximum and minimum floor composition.

Regular concrete [156] was chosen for the design—the choice for concrete-related variable limited in six classes: from C20 to C45. The thickness of the concrete layer continuously varied from 60 mm to 180 mm, with a 5-mm step.

CLT from the local manufacturer (Chantiers Chibougamau, Québec, Canada) was chosen for the design. The CLT class varies from E1 to E3, defining its mechanical characteristics (elastic modulus, the strength of laminations, density, cost). CLT thickness varies from 89 mm to 244 mm, depending on the layup configuration (8-level variable). The floor bending stiffness depends on the CLT layup and the number and disposition of the connectors. The stiffness contribution of the transversal laminations was negligible (approximated as 1/30 of the parallel to grain modulus) and omitted while calculating the major axis bending stiffness [36]. This assumption was also adopted in the manufacturer’s product catalog [133].

The lower surface of the floor is made up of a fire-rated Type X gypsum board. Thus, there were four options at the disposal for the optimization. The thickness of interlayer h_i between the CLT and the concrete could enhance the effective bending stiffness while increasing the total thickness. Furthermore, the floor finish and other non-structural elements would add 1kN/m² additional permanent weight.

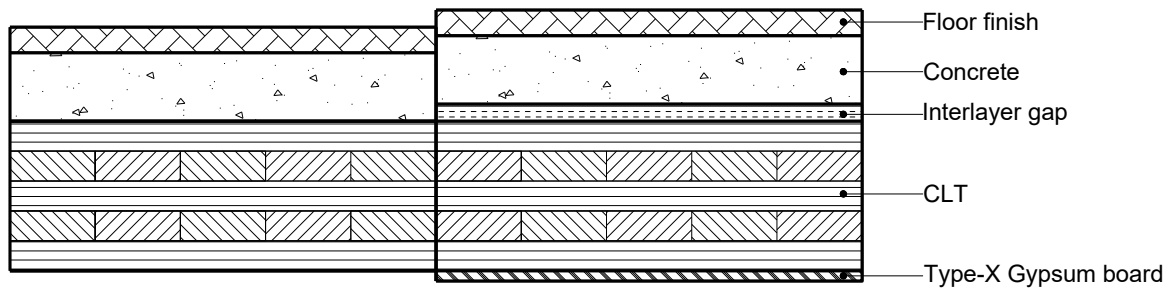


Figure 4.1. Minimum and maximum floor composition

This study exhibits a common CCC solution based on Canadian standards to demonstrate the usual local practices and optimization cases. An experimental CCC specimen [155] was fabricated and tested. It was a 9-m span per 1-m wide floor strip (Figure 4.2) using a 25-mm depth notched connector, 80 mm concrete C35, 175 mm CLT of class E1, and no interlayer. As pointed out in [155], the specimen span had to be reduced to satisfy the vibration constraint. However, we retained the 9-m span in this study and introduced a 19-mm gap between timber and concrete. This implementation was typical and could enhance structural and acoustic performance [57] and was commonly adopted by local constructors. The common solution had three rows of reinforced 25-mm-depth notched connectors with a 550-mm distance between connectors.

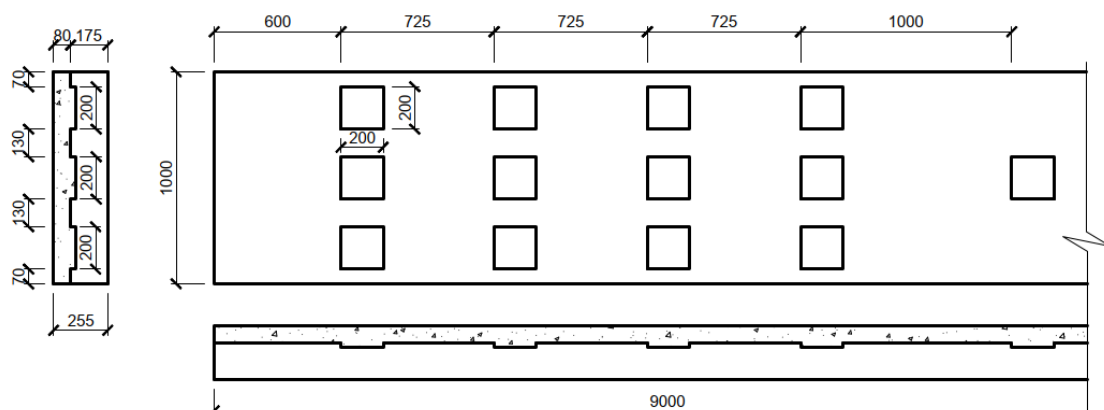


Figure 4.2. Connector layout of the tested CCC specimen [155]

4.2.2. Notch connector influence

The influence of notch depth t_n on the stiffness K_2 and the maximum resistance F_{max} was characterized by the previous experimental tests [130]. The mean stiffness K_2 was proposed in Equation (4.1). The relationship was described as a bilinear curve of the average response of K_2 . Mean value of K_2 was used directly in the constraint calculation.

$$K_2 = \begin{cases} 6.6t_n + 143 & (20 \leq t_n \leq 25) \\ -1.8t_n + 353 & (25 < t_n \leq 35) \end{cases} (kN/mm) \quad (4.1)$$

The mean maximum load F_{max} proposed in Equation (4.2) is a linear interpolation function of the average response of the tested specimens. It was then multiplied by the characteristic coefficient of 0.898 before introducing it into the optimization. The estimation of this value was discussed in Annex 2.

$$F_{max} = 5.19t_n + 42.7 (kN) \quad (4.2)$$

4.2.3. Design constraints

The structural, comfort vibration, and thermal constraints should validate each design found by the algorithm. The constraints adopted are presented and calculated according to Timber design standard CSA-O86:19 [9] and Concrete design standard CSA-A23:2014 [156].

- Serviceability limit state (SLS)
 - Deflection (Standard term and long-term)
 - Vibration requirement (Standard term)
- Ultimate limit state (ULS)
 - Bending moment resistance: Standard-term, Long-term, and Short-term (Fire conditions)
 - Connector shear resistance: Standard-term, Long-term, and Short-term (Fire conditions)
 - Shear resistance: Standard-term, Long-term, and Short-term (Fire conditions)

Table 4.1 presents the load combination used for each ULS and SLS constraint. The combination is composed of dead load (q_D), *i.e.*, floor self-weight and additional material, and live load ($q_L = 2.4 \text{ kN/m}^2$) for residential use and occupancy.

Table 4.1. Load combination, load duration factor, and bending stiffness of SLS and ULS constraints

State	Load q	Factor K_D	Bending stiffness $(EI)_{eff}$	Note
SLS	1.00L	-	$EI_{SLS,ST}$	Standard-term constraints
	1.00D + 0.30(1.00L) and 0.70L	-	$EI_{SLS,LT}$	Long-term constraints
		-	$EI_{SLS,ST}$	
ULS	1.00D + 0.50L	1.15	$EI_{ULS,ShT}$	Short-term constraints
	$\max\left(\frac{1.40D}{1.25D + 1.50L}\right)$	1.00	$EI_{ULS,ST}$	Standard-term constraints
	$\max\left(\frac{1.40D}{1.25D + 0.30(1.50L)}\right)$ and 0.70(1.50L)	0.65 1.00	$EI_{ULS,LT}$ $EI_{ULS,ST}$	Long-term constraints

The long-term coefficient in Table 4.2 conditions the material modulus and the shear connector stiffness in the long-term constraints. The creep coefficient of timber $K_{creep,t}$, concrete $K_{creep,c}$ and connector $K_{creep,cnt}$ are 2.0, 3.0, 4.0, respectively. The creep coefficient of timber $K_{creep,t}$ was taken following National Design Specification [17]. The creep coefficient of concrete $K_{creep,c}$ is calculated as (4.3) [156],

$$K_c = \left(1 + \frac{S}{1 + 50\rho'}\right) \quad (4.3)$$

The creep coefficient of the connector $K_{creep,cnt}$ is considered as twice the creep coefficient of timber $K_{creep,t}$ [157]. This conservative assumption was adopted in the absence of data from experimental tests or manufacturers [127].

Table 4.2. Creep coefficient for effective bending stiffness

Description	EI_{eff}	$K_{creep,t}$	$K_{creep,c}$	$K_{creep,cnt}$	Note
Standard-term, SLS	$EI_{SLS,ST}$	1.00	1.00	1.00	Full cross-section at time 0, SLS constraints
Long-term, SLS	$EI_{SLS,LT}$	2.00	3.00	4.00	Full cross-section at time ∞ , SLS constraints
Short-term, ULS	$EI_{ULS,ShT}$	1.00	1.00	1.00	Reduced cross-section at time 0, ULS constraints
Standard-term, ULS	$EI_{ULS,ST}$	1.00	1.00	1.00	Full cross-section at time 0, ULS constraints
Long-term, ULS	$EI_{ULS,LT}$	2.00	3.00	4.00	Full cross-section at time ∞ , ULS constraints

4.2.4. Optimization variables

Nine decision variables were divided into five related groups: geometry, concrete material, CLT, connector, and fire condition (Table 4.3). The chosen variables are the

principal ones in dimensioning a CLT-concrete floor. The material properties are chosen based on the catalog of the local providers (Chantiers Chibougamau for CLT panels, MyTiCon for screws, UniBeton for concrete, CANAC, or RONA for other supplies). The connector variables were chosen based on the experimental tests on the composite connector (notch) and the composite beams (CCC beams). Finally, the fire variables were prescribed in the Canadian standard CSA O86:19 [9].

Table 4.3. Optimization variables

Group	Name	Unit	Range	Type	Dependent variables
Geom.	Insulation thickness	mm	[0; 11; 19]	disc.	Density, Price
Concrete	Class		[C20; C25; C30; C35; C45]	disc.	Modulus, Compression strength, Density, Price
	Thickness	mm	[60 - 180, 5 mm]	disc.	
CLT	Class		[E1; E2; E3]	disc.	Modulus, Bending strength, Tension strength, Shear strength, Density, Price
	Thickness	mm	[89; 105; 143; 175; 197; 213; 244S; 244L]	disc.	
Connector	Connector rows	row	[1; 2; 3]	disc.	
	Connector distance	mm	[500 – 1000; 50mm]	disc.	
	Notch depth	mm	[20; 25; 30; 35]	disc.	
Fire	Thickness gypsum	mm	[0; 12.7; 15.9; 25.4]	disc.	Gypsum board time, Density, Price

The design parameters involved in the optimization process were fixed: floor span L (in mm) and fire resistance rating t_{fi} (in minutes). Fire resistance was characterized by the fire exposure rating time. The adopted extended exposure duration is 120 minutes in this study.

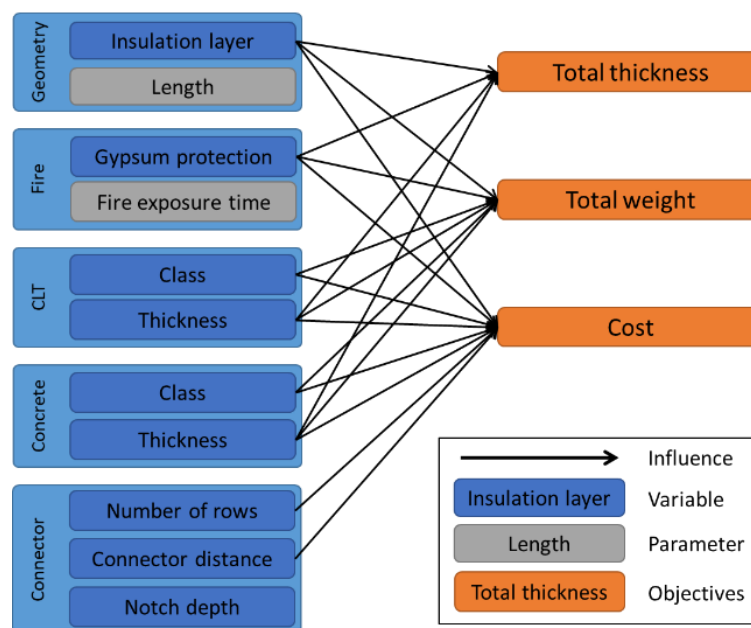


Figure 4.3. Design variable and objectives of the optimization

4.3. OPTIMIZATION PROBLEMS

4.3.1. Objectives functions

The optimization objectives are total weight, total thickness, and cost (Table 4.4). They are conflicting since using higher class material would reduce the weight and thickness and lead to a higher cost. These objectives were chosen to demonstrate that the application of CCC floor systems could provide economical solutions while satisfying the structural constraints. Thickness and weight are some of the most important aspects of a flooring system that would impact the design of other bearing structures and the total static height of the building.

Table 4.4. Optimization objectives

Name		Unit	Range
Thickness	h	mm	[149-464.4]
Weight	w	kg/m^2	-
Cost	C	Cost unit (CU/m^2)	-

The cost function was defined as the sum of constituent component costs, such as CLT, concrete, connector, interlayer, and fire protection element. This simplified expression includes the material, labor, transport, and eventual deconstruction cost of the floor. The sources of cost information were discussed in Annex 3.

The cost model was based on available data in the literature and was meant for this demonstration. A further undertaking should adopt a more elaborated and dedicated cost model for each application. The expressions for the cost function are the sum of material costs, Equation (4.4). The concrete cost expression was defined based on f_c , Equation (4.5) [151], [158]. The base price of concrete P_c was presented in Table 4.5.

The floor thickness is the sum thickness of CLT, concrete, interlayer, and fire protection element. The total weight is the weight of the floor per surface unit.

$$C = C_t + C_c + C_{cnt} + C_i + C_{gypts} \quad (4.4)$$

$$C_c = h_c P_c (-0.0003222 f_c^2 + 0.040571 f_c + 0.18829) \quad (4.5)$$

Table 4.5. Price and density of floor components

	Class	Price	Unit	Density	Unit
Timber	[E1; E2; E3]	[865; 821; 778]	CU/m ³	[515; 500; 490]	kg/m ³
Concrete	[C25]	[632]	CU/m ³	[2250]	kg/m ³
Connector	-	6	CU/cnt	-	-
Insulation	[11mm; 19mm]	[6.5; 8.25]	CU/m ²	[2.84; 4.27]	kg/m ²
Gypsum board	[12.7mm; 15.9mm; 25.4mm]	[9; 12; 15]	CU/m ²	[0.72; 0.72; 0.72]	kg/m ³

4.3.2. Constraints functions

The Gamma method [8] was adopted to calculate effective bending stiffness $(EI)_{eff}$ in the SLS and ULS constraints. The constraints functions derive mainly from regulatory requirements. For SLS constraints, the deflection of the floor strip under distributed standard-term and the long-term load was calculated. The CCC floor vibration aspect was considered an SLS constraint. The ULS constraints are bending moment resistance M_r , shear resistance of the composite section V_r , and horizontal shear resistance of the connectors $V_{r,\gamma,conn}$ [127].

The principal modeling assumption is to calculate the deflection d and d_{1kN} , fundamental frequency f_1 , internal force V_f and $V_{f,conn}$, moment M_f of a simply supported beam. The calculation of these quantities was explained in detail in the Canadian design guide for timber-concrete composite [127].

4.3.2.1. Deflection

The deflection d_{ins} and d_{LT} must not exceed the limit depends on the constraint of the corresponding load term. The maximum deflection d_{max} required by the Engineering wood design CSA O86-14 (updated 2017) [9] is $d_{max,ins} = L/360$ for instantaneous deflection due to live load, and $d_{max,LT} = L/180$ for total deflection due to long term load and the sustain part of live load (assumed at 30% of q_L) at the time $t = \infty$ as well as the non-sustain part of live load (70% of q_L) at the time $t = 0$.

$$d < d_{max} \quad (4.6)$$

where the deflection was calculated as

$$d = \frac{5}{384} \frac{qL^4}{(EI)_{eff}} \quad (4.7)$$

The contribution of shear deformation was negligible since the ratio L/h was higher than 30 [36]. Detailed calculations of the effective bending stiffness $(EI)_{eff}$ was presented in Annex 1.

4.3.2.2. Vibration

The vibration performance of the composite floor must comply with the empirical limit proposed in the Canadian design guide for timber concrete composite floors [127].

$$r > r_{min} = 5.75 \quad (4.8)$$

where:

$$r = \frac{f_1}{d_{1kN}^{0.14}} \quad (4.9)$$

$$d_{1kN} = \frac{PL^3}{48(EI)_{eff_{1m}}} \text{ at } P = 1kN \quad (4.10)$$

$$f_1 = \frac{\pi}{2L^2} \sqrt{\frac{(EI)_{eff_{1m}}}{m_L}} \quad (4.11)$$

4.3.2.3. Bending moment resistance

The factored bending moment must not exceed the bending moment resistance of the composite section, which is the weakest resistance between the concrete $M_{r,\gamma,c}$ and timber $M_{r,\gamma,t}$.

$$M_f \leq M_r \quad (4.12)$$

$$M_r = \min(M_{r,\gamma,c}, M_{r,\gamma,t}) \quad (4.13)$$

A bending moment M applied on the composite beam would induce a bending moment M_i and an axial force N_i on each layer; hence, bending stress and axial stress could be deduced. As per CSA O86-14 (2017) [9], the verification must combine axial force and bending moment. $M_{r,\gamma,c}$ and $M_{r,\gamma,t}$ are the equivalent moment that led to rupture of each material, *i.e.*, concrete and timber. Therefore, the resistance of timber in bending f_b and tension f_t and the compression resistance of concrete f_c were employed. Detailed developments could be found in the Canada TCC floors design guide [127]. When using the Gamma method to estimate ultimate resistance, the connectors are not allowed to yield. Therefore, the Elasto-Plastic model should be adopted to take into account the connector yielding [127]. However, we did not introduce these constraints into the optimization.

The calculation of $M_{r,\gamma,c}$ and $M_{r,\gamma,t}$ based on the Gamma method could be obtained as presented in Equations (4.14) and (4.15). Detailed calculations of timber resistance $M_{r,t}, T_{r,t}$ was presented in Annex 4.

$$M_{r,\gamma,t} = \frac{(EI)_{eff} T_{r,t} M_{r,t}}{\gamma_t (EA)_t a_t M_{r,t} + (EI)_t T_{r,t}} \quad (4.14)$$

$$M_{r,\gamma,c} = f_c \frac{(EI)_{eff}}{E_c (\gamma_c a_c + 0.5 h_c)} \quad (4.15)$$

Under fire conditions, the exposed side of the CLT cross-section was reduced by the effective char depth x_r . The nominal charring rate β_n of 0.8 mm/minute whether the char depth reached the first adhesive bond line or not.

$$x_r = x_{c,n} + x_t \quad (4.16)$$

$$x_{c,n} = \beta_n \cdot t \quad (4.17)$$

$$x_t = \begin{cases} 7t/20 & \text{if } t < 20 \\ 7 & \text{if } t > 20 \end{cases} \quad (4.18)$$

The strengths of timber (*i.e.*, F_b, F_v, F_t) in fire conditions are the mean strength. They were calculated by using the fire resistance factor $K_{fi} = 1.25$, with the resistance factor ϕ as unity ($\phi = 1.0$). The modifications factors ($K_{fi} = 1.25$, $\phi = 1.0$, $K_H = 1.0$) were multiplied using the appropriate equations. The short-term load was applicable during fire resistance conditions. The connector systems properties were not reduced since we assumed that the notch connector and reinforced screws were not yet exposed to fire. The theories of the Gamma method were applied for the reduced cross-section. The resistance in terms of bending moment $M_{r,t}$, tension $T_{r,t}$, and shear $V_{r,t}$ were recalculated based on the new CLT configuration. A calculation example for the bending moment resistance of CLT panel under 2-hour fire conditions was illustrated in Wood Design Manual [159, p. 857].

4.3.2.4. Connector shear resistance

The factored shear force applied at the position of the critical connectors $V_{f,conn}$ must not exceed the shear resistance due to the connector $V_{r,\gamma,conn}$.

$$V_{f,conn} \leq V_{r,\gamma,conn} \quad (4.19)$$

$V_{r,\gamma,conn}$ is the equivalent shear resistance of the composite section due to the resistance of the connector $F_{max,conn}$.

$$V_{r,\gamma,conn} = \frac{n(EI)_{eff}}{\gamma_t(EA)_t a_t S} F_{max,conn} \quad (4.20)$$

Note that Equation (4.20) is the shear flow calculation of built-up beams. The $F_{max,conn}$ is the maximum horizontal shear resistance of an individual connector. The estimation of $F_{max,conn}$ was discussed in Paragraph 4.2.2.

4.3.2.5. Cross-section shear resistance

The factored shear force V_f must not exceed the shear resistance V_r of the cross-section.

$$V_f \leq V_r \quad (4.21)$$

and the shear resistance of the composite section V_r is the least of the resistance due to concrete $V_{r,\gamma,c}$ and timber $V_{r,\gamma,t}$.

$$V_r = \min (V_{r,\gamma,c}, V_{r,\gamma,t}) \quad (4.22)$$

The shear resistance of the composite section obtained by using the Gamma method is $V_{r,\gamma,c}$ (concrete strength) and $V_{r,\gamma,t}$ (timber strength). Further developments are presented in [127]. Detailed calculations of concrete and timber resistance $V_{r,c}$, $V_{r,t}$ was presented in Annex 4.

$$V_{r,\gamma,c} = \frac{(EI)_{eff}}{(EI)_c + 0.5\gamma_c(EA)_c(2h_c - h_{c,eff} + h_i)a_c} V_{r,c} \quad (4.23)$$

$$V_{r,\gamma,t} = \frac{(EI)_{eff}}{(EI)_t + 0.5\gamma_t(EA)_t(h_t + h_i)a_t} V_{r,t} \quad (4.24)$$

4.4. OPTIMIZATION ALGORITHM

In this paper, we adopted the NSGA-II as the optimization algorithm. The genetic algorithm is a population-based metaheuristic [160] inspired by the process of natural selection and evolution. “Heuristic” describes a search/optimization method that provides an approximate solution within a reasonable computational cost. “A metaheuristic is a high-level problem-independent algorithmic framework that provides a set of guidelines or strategies to develop heuristic optimization algorithms,” according to Sörensen [161]. The genetic algorithm adopted the idea that each individual (i.e., design, solution) has their chromosome string constituted by many genes (variables) in an optimization population. The fittest individuals would be selected and produce offspring for the next generation using the operator such as mutation and crossover [162]. This algorithm was widely adopted for many optimization problems, such as construction scheduling managing site operations sustainability [163].

NSGA-II has the most robust and straightforward implementations with low time-computational complexity [164]–[168]. By ranking the whole population (parents and offspring) after every iteration, the non-dominated individuals are excluded before producing the next generation. NSGA-II was considered to outperform the MOPSO in practical study cases due to the mutation operator and the crowding distance, preventing the optimization from being trapped into the local optimum points and preserving the population diversity [169]. NSGA-II was popularly used for the MOO in the construction domain, such as structural, energy, and environmental design [152], [153], [170]–[173], site operation scheduling and logistic [174], [175], urban and infrastructure planning [176], [177]. Since our study concentrates on the floor structural performance, adopting NSGA-II would harness the vast literature base and permit further developments in multi-disciplinary applications.

The search parameters or hyperparameters for NSGA-II are population size, mutation rate, crossover rate, and generations. For this application, the number of generations is determined by multiple preliminary optimizations and observing the convergence rate of Fitness value and Hyper volume. Other parameters were determined by conducting test runs to determine the best fitness and time-optimal value. For example, one could observe in Figure 4.4 that the convergence could be obtained after 200 generations. The crossover rate, mutation probability, and population size were later set at 0.9, 0.3, and 400.

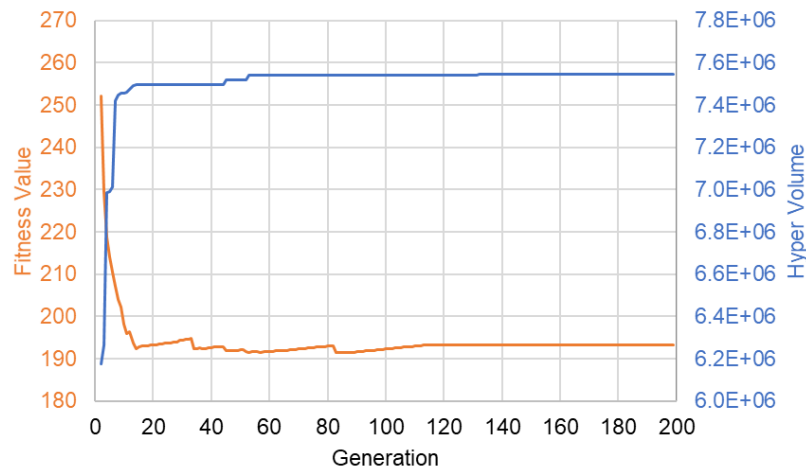


Figure 4.4. Fitness value and Hyper volume of the optimization

The time-complexity of the NSGA-II algorithm, developed by Deb et al., is $O(MN^2)$, with M being the number of objectives and N being the population size [164]. Using a computer with six physical cores clocked at 4.48 GHz and 16 Gb of RAM, the average calculation time of each optimization is about 10 minutes. Since the optimization utilizes the analytical model to estimate the performance of the configuration, the computational cost is reasonable.

4.5. ANALYSIS AND DISCUSSION

4.5.1. Pareto front of the optimal solutions and the reference solution

Figure 4.5 exhibits six solutions of the Pareto front in the objective coordinates (thickness, weight, and cost). Table 4.6 presents the choices of three optimized solutions and the common one. The optimization parameters of the floor span and the fire exposure duration were provided as 9.0 m and 2 hours, respectively. These optimal solutions are “equivalent.” The position of the common solution is also presented. One could see that it is dominated in all cases.

Table 4.6. Variables of some solutions

	Unit	Reference	Solution 1	Solution 2	Solution 3
Insulation thickness	mm	19	11	0	19
Timber class	-	E1	E1	E2	E3
Thickness	mm	175	197	213	213
Concrete class	-	C35	C35	C25	C20
Thickness	mm	80	60	60	60
Connector rows	rows	3	1	1	1
Connector distance	mm	600	500	650	700
Notch depth	mm	25	25	25	25
Thickness gypsum	mm	0	0	0	0
Total weight	kg/m ²	276,5	241,3	241,5	236,4
Total thickness	mm	274	268	273	292
Total cost	CU/m ²	253,2	236,0	222,8	216,7

Figure 4.6 exhibits the parallel coordinate plot of the Pareto front. Again, the long-term deflection, vibration, and short-term connector shear resistance constraints govern the designs, represented by the high ratio of load per resistance (*cf.* Annex 5).

In terms of timber choices, two distinct groups could be observed based on the CLT type (Figure 4.6). The solutions using a thinner CLT panel (197 mm) with the highest CLT class (E1) had the highest cost. The other went with lower CLT class (E2 and E3) had the most economical competitive solutions. A substantial timber panel would save costs in other aspects like lower concrete class and fewer connectors.

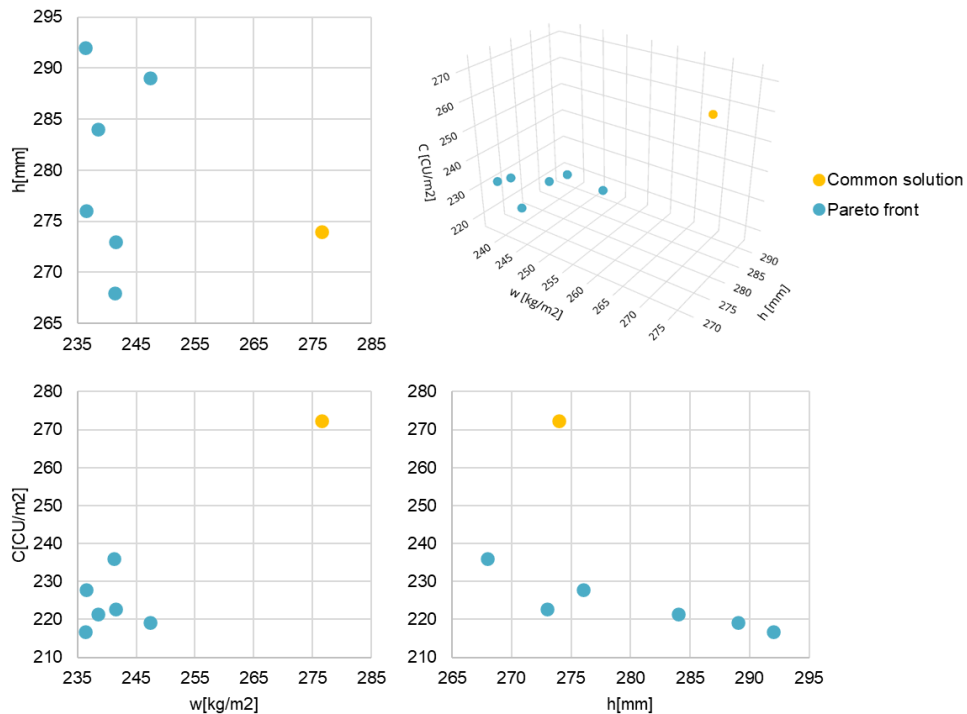


Figure 4.5. Pareto front of CLT-concrete solution for 9 m floor span

The thickest concrete layer was registered as 65 mm regarding the concrete choices. Therefore, increasing the concrete class was more advantageous than increasing the concrete thickness. A higher concrete class would only drive the cost up, while the thicker concrete layer would compromise overall thickness and the cost. Therefore, high-performance concrete could be less competitive in this specific case of the 9 m floor span.

In terms of the connectors, the notch depth of 20 and 25 mm was more advantaged than the two others, i.e., 30 and 35 mm, because the most profound notches were penalized in terms of stiffness while the two out of three governing constraints were serviceability one.

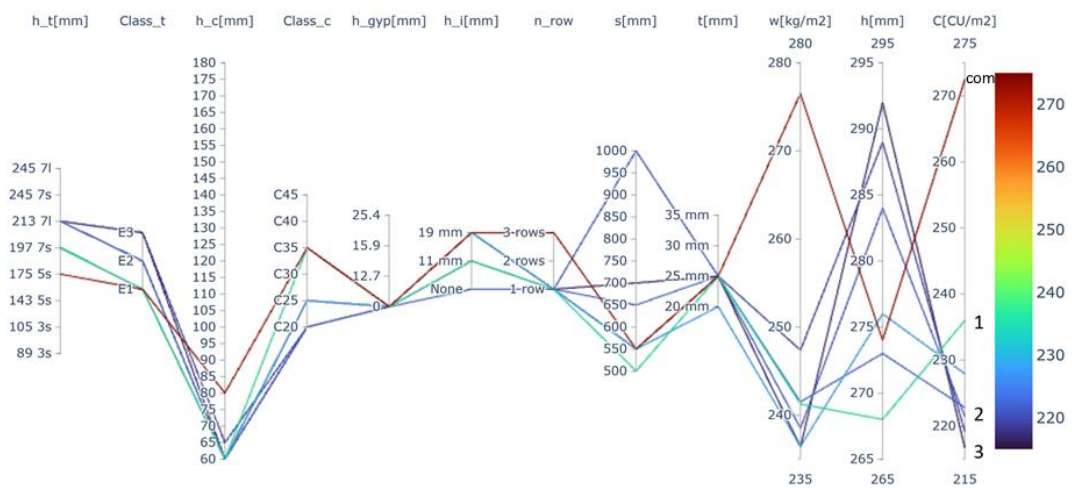


Figure 4.6. Parallel coordinate of the solutions for 9 m floor span. Detailed version is presented in Annex 5

For the 9 m floor span, timber proportion was more than 65% of the total cost. The reference solution was not economically optimized; hence, the connector took up to 11% of the cost while the corresponding number of the optimized one was about 4% (Table 4.7).

Table 4.7. Cost contribution

	Reference	Solution 1	Solution 2	Solution 3
Concrete	26%	19%	16%	14%
Timber	60%	67%	69%	65%
Gypsum board	0%	0%	0%	0%
Connector	11%	4%	3%	3%
Insulation	3%	3%	0%	3%

4.5.2. Parametric study

4.5.2.1. Variation of floor span

The span length is an essential parameter for the design of the CCC floor. A more demanding span would shift the Pareto front significantly, causing the increasing use of both timber and concrete (Figure 4.7).. The span was varied from 7m to 10m, representing the residential timber floor's medium to long span. The traditional timber-only solution would not be feasible without increasing the timber thickness substantially.

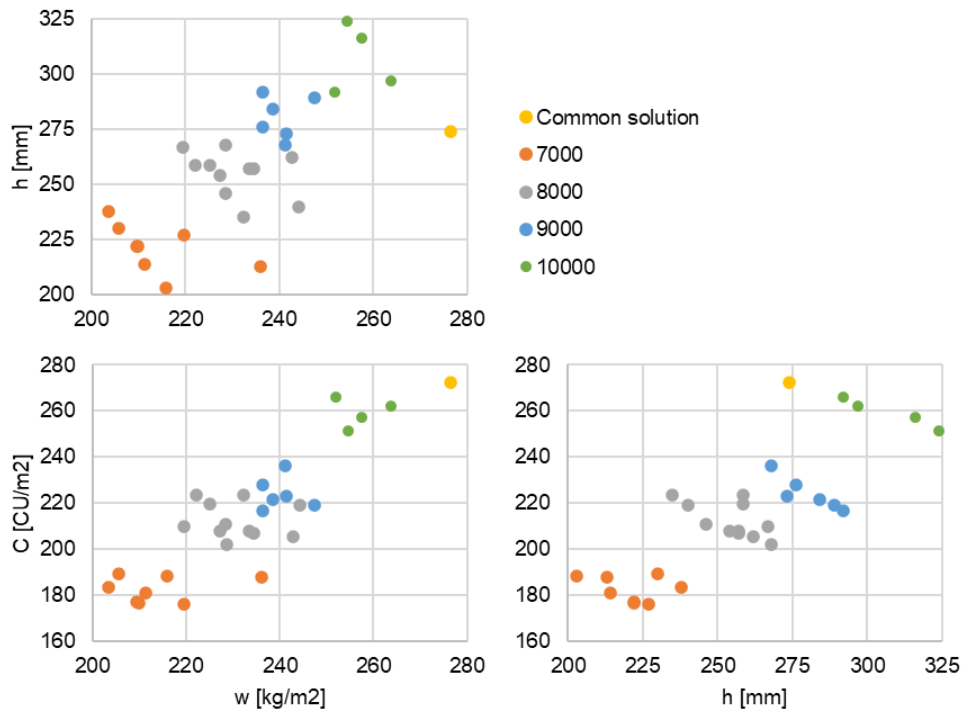


Figure 4.7. Pareto front of different floor span

4.5.2.2. Variation of cost ratio timber/concrete

The timber and concrete cost information would depend heavily on the timber manufacturer, the concrete provider, and project conditions. Hence, in this study, a range of cost ratios between timber and concrete was considered. The optimal solution would be balancing between the four variables of timber thickness, timber class, concrete thickness, and concrete class. The higher ratio of Timber/Concrete means that timber is more expensive than concrete (price per volume unit). In general, an expensive timber regarding cheap concrete would shift the optimal solutions toward “concrete” rather than “timber.”

For a 9 m or more floor span, the cheaper concrete cost would not significantly change the front Pareto. One could observe that the same set of timber-concrete

combinations (class and thickness) was obtained (Figure 4.8). The combination of thin timber - thick concrete could satisfy the structural constraints, but a 175 mm or 143 mm CLT panel would require at least 150 mm concrete or at least 80 mm concrete plus 20 mm interlayer (reference solution). These combinations would significantly increase the weight while the cost was still relatively high, as exhibited by the reference solution. In a less demanding floor span of 8 m or less, the reduced cost ratio T/C allowed the combination of thin timber - thick concrete (Figure 4.8).

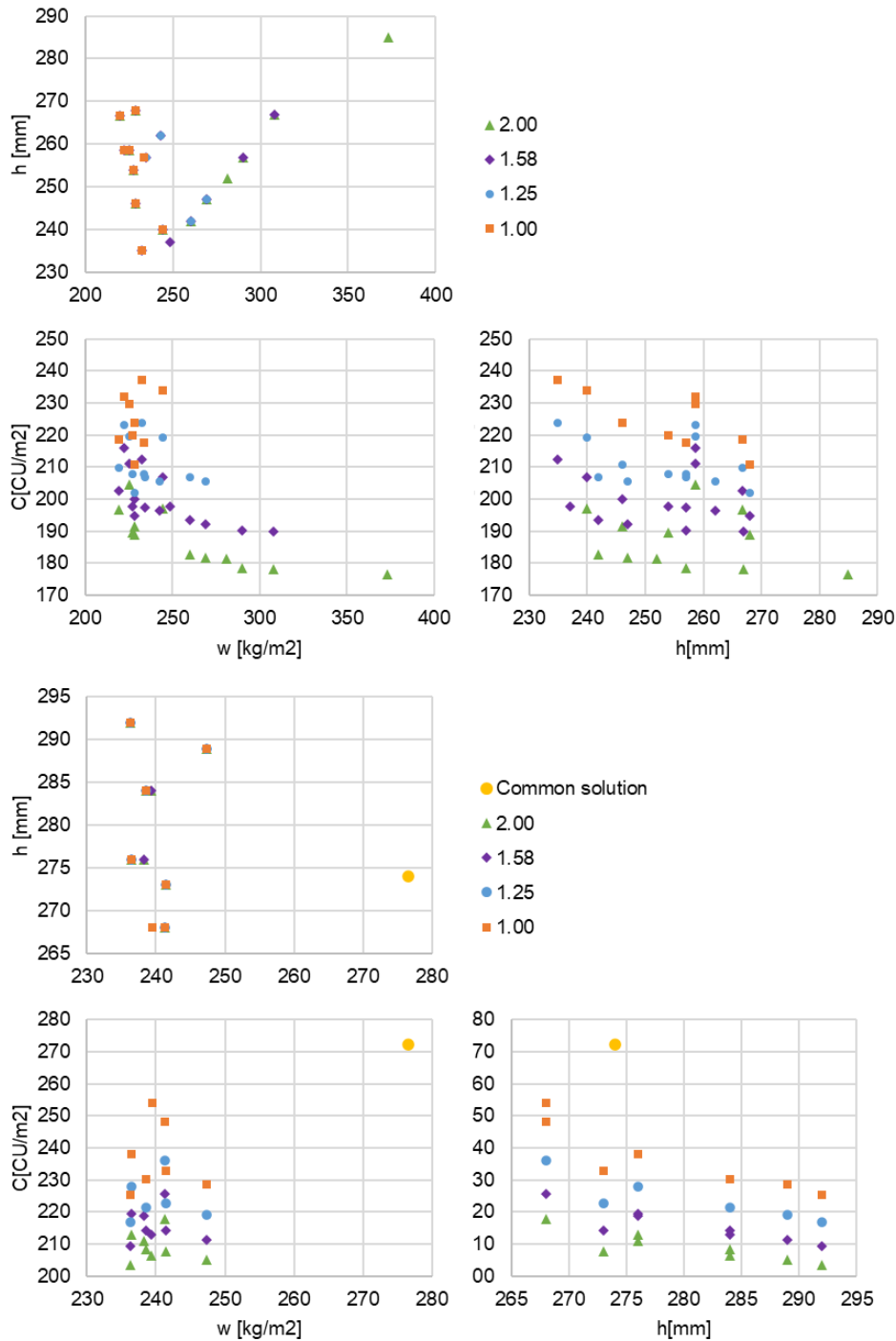


Figure 4.8. Pareto fronts of different ratio Timber/Concrete for 8 m (top) and 9 m (bottom) floor span

Since the information on the time penalty, hence cost penalty on delayed construction, was not available for implementation in this study, the parametric study on the cost ratio timber/concrete will not reflect a comprehensive view on the impact of this “solution shifting.” However, the different fronts Pareto provided that the solutions with less timber – more concrete were always existing in the feasible zone with very few environmental or construction time benefits while very cost competitive (in terms of raw materials).

4.6. CONCLUSION

The present study focused on a multi-objective optimization of the long-span CCC structure based on the structural and economic objectives, which is novel and has not been done before in the literature. The originality also lies in the constraint functions of fire conditions which are rarely seen in optimizing such structures. As a result, a set of compromised solutions for predefined floor span were found by minimizing the floor thickness, weight, and cost. In addition, the constraints imposed on the structural design were issued from regulatory design requirements, both SLS and ULS.

- Though marginally satisfied with the structural constraints, the common solution was not optimized for cost and weight. Nevertheless, the structural and economic improvements were demonstrated in this study.
- As expected, the SLS constraints (deflection and vibration) governed the designs of long-span CCC floors. In addition, the fire conditions introduced another governing ULS constraint. This conclusion was drawn based on structural assumptions adopted in the paper. However, some were conservative and could be changed when more experimental results were available.
- By decreasing the cost ratio of timber/concrete, the solution with more concrete and less timber could gain some competitiveness over the opposite one. However, the span condition caused the solutions to use more material to satisfy the structural constraints.

Our findings could provide the industry an insight into the dominance of the constraint functions and how design parameters, such as span length and cost, could impact the optimal solutions. Another critical aspect of these findings is that they made a case for the timber-concrete composite floor that uses CLT panels, promoting the utilization of these structures on future high-rise buildings. The optimization is simple for engineers to implement. It can determine economical and well-performed solutions while satisfying the construction standards.

Many aspects could be introduced into the optimization for future studies, such as comparing CCC with other floor solutions such as full-timber or full-concrete floors, implementing the environmental objective functions and constraint functions of the TCC and CCC, and the possibility of deconstructing the floor structures. In addition, the uncertainty (random and epistemic) in the data used and models could also substantially influence the optimal results and need to be addressed in future studies.

ACKNOWLEDGEMENT

The authors are grateful to Natural Sciences and Engineering Research Council (NSERC) of Canada for the financial support through its IRC and CRD programs (IRCPJ 461745-18 and RDCPJ 524504-18), the Region Nouvelle Aquitaine (France) for the financial support (ref. 2017-1R10223), and the industrial partners of the NSERC industrial chair on eco-responsible wood construction (CIRCERB).

CONCLUSION AND PERSPECTIVES

CONCLUSION

The presented research focused on the vibration performance of CCC structures and CCC design optimization regarding the structural constraints and objectives functions. The performance of CCC floors is principally conditioned by the connector systems and the constituent materials, in this case, timber and concrete. The literature review exhibited many connector solutions available for connecting a CLT panel to a concrete slab. However, most of them are patented and time-consuming to be implemented. The notched connector is a promising one when it could assure the stiffness and strength of the composite floor, allowing further achievement in terms of prefabrication and on-site safety while maintaining a reasonable construction cost and ease of deconstruction.

The design of long-span lightweight and semi-lightweight flooring such as CCC floors is governed by the serviceability limits of deflection and vibration. Nowadays, effective vibration criteria for timber floors are still in development regarding vibratory comfort. Although the correlations between human comfort, human annoyance, and dynamic responses were well documented, many vibration criteria are proposed in the literature. The difficulty lies in the complexity and multidimensionality of these criteria. A complicated vibration calculation prevents the engineers from using it, and a too simplified one often lacks precision. Therefore, this thesis aimed to evaluate the mentioned connection systems and their application for long-span CCC floors while concentrating on dynamic behaviors. The information acquired from the evaluation phase will be adopted to demonstrate a case for CCC flooring systems.

The connector geometry influenced the behavior of the notched composite connector used in CCC. The connector stiffness has peaked at a moderate notch depth, and cutting further toward the transversal lamination has caused a stiffness reduction. The impact of heel length on the connector stiffness is inconclusive because of the artificial eccentricity of the non-symmetry specimens. The connector resistance only depends on the notch depth and is insensitive to other geometrical parameters. The developed finite element model could accurately estimate the resistance of the notched connector.

Regarding the connector stiffness prediction, the model yielded an accurate trend in terms of notch depth. The proposed model used the Elasto-plastic behavior in parallel-to-grain compression for timber material and generalized it for other directions

through coefficients. However, the finite element model accuracy needs to be improved with a more advanced timber material model with different behavior depending on the grain direction. In the process of evaluating the notched connector, a connector with the ability to be deconstructed was proposed. This solution contributes to the design to deconstruction so that the timber and concrete material could be economically recovered and reused.

The presence of notched connectors impacts the performance of the bare CLT panel and the CCC beam. The bending stiffness of the CLT panel could be reduced when the upper surface of the panel is occupied by too many notches cut; careful stiffness assessment in these cases is recommended. Increasing the number of connectors could considerably enhance the bending stiffness of the CCC beam and hence, the fundamental frequency. However, the experimental results also indicated that the modal damping was reduced in stiffer CCC beams. The concrete layer increases the CCC beams stiffness, especially in the low and high composite beams. The dynamic behaviors of non-composite beams still need further investigation. The proposed models of composite beams could not successfully capture the fundamental frequency of this beam.

In the optimization phases, a set of optimized CCC floor designs could be obtained. The constraint functions of serviceability and ultimate limit states are mobilized to validate all the solutions found by the optimization algorithm. The serviceability constraints such as long-term deflection and vibration; and the constraints of bending under fire conditions governed the optimized designs. The specimen of CCC tested in the experimental campaign has been chosen as a usual CCC in Quebec, minus the acoustic interlayer. It appears not to be an optimized solution of the front Pareto. The competitiveness of the CCC floor depends on many input parameters, and one of the most important is the cost information.

PERSPECTIVES

The present study has demonstrated the use of a notched connector in the case of long-span CCC floors. This type of connector possesses many advantages and allows a widespread application of TCC structure. However, due to the particularities of CLT, long-term behaviors and rupture modes of CCC notched connectors still need to be thoroughly investigated. Furthermore, the stiffness of the connector is essential information for any dynamic assessment of CCC structures. This fact leads to the necessity of an accurate prediction of the connector shear stiffness through the numerical or analytical model.

Most builders widely adopt non-composite floor solutions, and it needs research attention and efforts to clarify the behavior of such solutions, especially in terms of vibration. It is worth mentioning that the present study only focused on the longitudinal responses of beam-like structures. Nevertheless, the transversal behavior of the connector systems and the impacts on the plate-like structures are relevant aspects for vibrational modeling.

The optimizations carried out in this study are pretty limited, and they could be improved by introducing the environmental parameters, other constraints functions, and objectives functions. All constraints are derived from the CSA building code. Therefore, such a study has to be carried out with Eurocode rules. Combining the structural and environmental performance, the TCC and CCC floors could gain further advantages over other solutions such as timber-only or concrete-only ones. However, such optimization would require a direct comparison with other floor types to be retained as the best building solution. The simplicity of constraints functions and objective functions, and advanced programming techniques are needed to assure the computational cost within the reasonable range.

Besides the shear test on the connector and the vibration tests on the composite beams, the long-term creep tests and the bending until rupture tests were also carried out on the three beams fabricated in the experimental campaign of this thesis. A detailed experimental report has been written and could provide enough information for another scientific publication. However, these works would be out of the scope of this study and would have required an extensive literature review. Therefore, the author decided not to present the mentioned work in this dissertation and published it elsewhere as a separate research project.

REFERENCES

- [1] E. Lukaszewska, H. Johnsson, and M. Fragiacom, "Performance of connections for prefabricated timber–concrete composite floors," *Mater Struct*, vol. 41, no. 9, pp. 1533–1550, Nov. 2008, doi: 10.1617/s11527-007-9346-6.
- [2] D. Yeoh, M. Fragiacom, P. Aldi, M. Mazzilli, and U. Kuhlmann, "Performance of notched coach screw connection for timber-concrete composite floor system," presented at the World Conference on Timber Engineering 2008, Miyazaki, Japan, Jun. 2008.
- [3] A. M. P. G. Dias, H. M. P. Cruz, S. M. R. Lopes, and J. W. van de Kuilen, "Stiffness of dowel-type fasteners in timber–concrete joints," *Proceedings of the Institution of Civil Engineers - Structures and Buildings*, vol. 163, no. 4, pp. 257–266, Aug. 2010, doi: 10.1680/stbu.2010.163.4.257.
- [4] K. Quang Mai, A. Park, and K. Lee, "Experimental and numerical performance of shear connections in CLT–concrete composite floor," *Materials and Structures*, vol. 51, no. 4, Aug. 2018, doi: 10.1617/s11527-018-1202-3.
- [5] C. Higgins, A. R. Barbosa, and C. Blank, "Structural Tests of Concrete Composite-Cross-Laminated Timber Floors," School of Civil and Construction Engineering, Corvallis, OR 97331, Final Report Report No. 17-01, Dec. 2017.
- [6] Y. Jiang and R. Crocetti, "CLT-concrete composite floors with notched shear connectors," *Construction and Building Materials*, vol. 195, pp. 127–139, Jan. 2019, doi: 10.1016/j.conbuildmat.2018.11.066.
- [7] WoodWorks, "Case study: Inspiration through Innovation At UMass Amherst, an Exposed Mass Timber Structure is a Teaching Tool," woodworks, <http://www.woodworks.org>, 2018. [Online]. Available: <http://www.woodworks.org/wp-content/uploads/UMass-Amherst-Olver-Design-Building-WoodWorks-Case-Study.pdf>
- [8] EN 1995-1-1, *Eurocode - Design of timber structures - Part 1-1. General - Common rules and rules for buildings*. European Committee for Standardization (CEN), 2002.
- [9] Canadian Standards Association, *CSA-O86:19. Engineering design in wood*. 2019.
- [10] P.-E. Gauthier, "Charpente en bois, notamment pour ossature de hangar agricole," FR1009171, May 26, 1952 [Online]. Available: <https://bases-brevets.inpi.fr/fr/document/FR1009171.html>
- [11] S. Gagnon and C. Pirvu, *CLT handbook: cross-laminated timber*. Québec: FPInnovations, 2011.
- [12] W. T. Architects, "Murray Grove | Waugh Thistleton Architects." <http://waughthistleton.com/murray-grove/> (accessed Jun. 25, 2021).
- [13] Canadian Wood Council and WoodWorks, "Brock Commons. A case study," WoodWorks, Canada, Mar. 2019.
- [14] Canadian Wood Council, WoodWorks, and Cecobois, "Origine. A case study," Canada, Mar. 2019.
- [15] J.-M. Jaeger, B. Ingrid, J. Cornudella, and R. Le Roy, "Quand les immeubles de grande hauteur sont en bois - When high rise buildings are made of wood," p. 2785426 Bytes, 2020, doi: 10.6084/M9.FIGSHARE.12034272.

- [16] “HoHo Vienna - Wooden tower - Woschitz Group.” <https://www.woschitzgroup.com/en/projekte/hoho-vienna-wooden-tower/> (accessed Jun. 26, 2021).
- [17] AWS, *National design specification for wood construction*. Leesburg, VA 20175: American Wood Council, 2015.
- [18] ICC, *International Building Code*. Washington, DC: International Code Council, 2015.
- [19] CSA, “Engineering design in wood. CSA Standard O86-14,” Ottawa, Ontario, Canada, 2014.
- [20] Service Bureau, “Timber concrete composite decks for bridges piers docks ramps buildings and other structures requiring heavy duty floors,” American Wood-Preserver Association, Apr. 1941.
- [21] D. Yeoh, M. Fragiacomò, M. De Franceschi, and K. Heng Boon, “State of the art on timber-concrete composite structures: literature review,” *J. Struct. Eng.*, vol. 137, no. 10, pp. 1085–1095, Oct. 2011, doi: 10.1061/(ASCE)ST.1943-541X.0000353.
- [22] J. N. Rodrigues, A. M. P. G. Dias, and P. Providência, “Timber-concrete composite bridges: State-of-the-art review,” *BioResources*, vol. 8, no. 4, pp. 6630–6649, Nov. 2013, doi: 10.15376/biores.8.4.6630-6649.
- [23] E. Karsh, “Building the Earth Sciences Building at the University of British Columbia,” *Equilibrium Consulting Inc*, Apr. 01, 2013. <https://www.eqcanada.com/selectedwork/ubc-earth-sciences-building> (accessed Apr. 27, 2021).
- [24] M. Van der Linden, “Timber-concrete composite floor systems,” University of Technology Delft, Delft, Netherlands, 1999.
- [25] A. M. P. G. Dias, “Mechanical behaviour of timber-concrete joints,” Delft University of Technology, Delft, 2005.
- [26] H. Werner, “Holz-Beton-Verbunddecke mit einer neuartigen Fugenausbildung,” *Bauen mit Holz 94 (1992) S. 312-324.*, 1992, [Online]. Available: <https://publikationen.bibliothek.kit.edu/77092>
- [27] N. M. Newmark, C. P. Siess, and I. M. Viest, “Test and analysis of composite beams with incomplete interaction,” *Proc. Soc. Exp. Stress Anal*, vol. 8, no. 1, pp. 75–92, 1951.
- [28] K. Möhler, “Über das Tragverhalten von Biegeträgern und Druckstäben mit zusammengesetzten Querschnitten und nachgiebigen Verbindungsmitteln,” Karlsruhe, 1956.
- [29] T.-T. Nguyen, L. Sorelli, and E. Brühwiler, “An analytical method to predict the structural behavior of timber-concrete structures with brittle-to-ductile shear connector laws,” *Engineering Structures*, vol. 221, p. 110826, Oct. 2020, doi: 10.1016/j.engstruct.2020.110826.
- [30] L. Zhang, S. Zhang, and Y. H. Chui, “Analytical evaluation to the timber-concrete composite beam connected with notched connections,” *Engineering Structures*, vol. 227, p. 111466, Jan. 2021, doi: 10.1016/j.engstruct.2020.111466.
- [31] Y.-F. Wu, R. Xu, and W. Chen, “Free vibrations of the partial-interaction composite members with axial force,” *Journal of Sound and Vibration*, vol. 299, no. 4–5, pp. 1074–1093, Feb. 2007, doi: 10.1016/j.jsv.2006.08.008.

- [32] M. V. Thai, S. Ménard, S. M. Elachachi, and P. Galimard, “Experimental report on the push-out test of CLT-concrete shear notched connector (Phase 1),” University of Quebec at Chicoutimi, University of Bordeaux, Internal laboratory report No. 01, 2019.
- [33] U. A. Girhammar, D. H. Pan, and A. Gustafsson, “Exact dynamic analysis of composite beams with partial interaction,” *International Journal of Mechanical Sciences*, vol. 51, no. 8, pp. 565–582, Aug. 2009, doi: 10.1016/j.ijmecsci.2009.06.004.
- [34] R. Xu and Y. Wu, “Static, dynamic, and buckling analysis of partial interaction composite members using Timoshenko’s beam theory,” *International Journal of Mechanical Sciences*, vol. 49, no. 10, pp. 1139–1155, Oct. 2007, doi: 10.1016/j.ijmecsci.2007.02.006.
- [35] S. C. Auclair, L. Sorelli, A. Salenikovitch, and M. Fafard, “The effect of rotatory inertia on the natural frequencies of composite beams,” *Journal of Sound and Vibration*, vol. 366, pp. 230–247, Mar. 2016, doi: 10.1016/j.jsv.2015.12.004.
- [36] V. Bajzecerová, “Bending stiffness of CLT-concrete composite members - comparison of simplified calculation methods,” *Procedia Engineering*, vol. 190, pp. 15–20, 2017, doi: 10.1016/j.proeng.2017.05.301.
- [37] ANSI/APA PRG-320-2019, *Standard for performance-rated cross-laminated timber*. APA - The Engineered Wood Association, 2019.
- [38] EN 16351:2021, *EN 16351:2021. Timber structures. Cross laminated timber. Requirements*. European Committee for Standardization (CEN), 2021.
- [39] E. Karacabeyli and S. Gagnon, Eds., *Canadian CLT Handbook, 2019 Edition*. Point-Claire, QC, Canada: FPIInnovations, 2019.
- [40] A. Sandoli and B. Calderoni, “The rolling shear influence on the out-of-plane behavior of CLT panels: a comparative analysis,” *Buildings*, vol. 10, no. 3, Art. no. 3, Mar. 2020, doi: 10.3390/buildings10030042.
- [41] H. Kreuzinger, “Scheiben und Schalen – ein Berechnungsmodell für gängige Statikprogramme (Plate and shell structures - A calculation model for common structural analysis programs),” *Bauen mit Holz 1*, pp. 34–39, 1999.
- [42] H. J. Blass, Ed., “Mechanically jointed beams and columns,” in *Timber Engineering – STEP 1*, Almere, The Netherlands, 1995. Accessed: Apr. 29, 2021. [Online]. Available: https://www.kstr.lth.se/fileadmin/kstr/pdf_files/Timber_Engineering_2017/Composite_paper_1.pdf
- [43] S. C. Auclair, “Développement d’un nouveau connecteur pour garantir la ductilité des structures composites en bois-béton,” University Laval, Quebec, 2016.
- [44] N. H. Abd. Ghafar, “Dynamic behaviour of LVL-concrete composite flooring systems,” Ph.D Thesis, University of Canterbury, 2015.
- [45] L. Zhang, Y. H. Chui, and D. Tomlinson, “Experimental investigation on the shear properties of notched connections in mass timber panel-concrete composite floors,” *Construction and Building Materials*, vol. 234, p. 117375, Feb. 2020, doi: 10.1016/j.conbuildmat.2019.117375.
- [46] S. Lamothe, “Développement d’un connecteur Rigide-Ductile-Économique pour dalles composites en bas lamellé-croisé et béton pour les bâtiments multiétages,” 2019, Accessed: Jul. 29, 2020. [Online]. Available: <https://corpus.ulaval.ca/jspui/handle/20.500.11794/34005>

- [47] Y.-J. Song, S.-Y. Baek, I.-H. Lee, and S.-I. Hong, "Variations of moisture content in manufacturing CLT-concrete composite slab using wet construction method," *BioResources*, vol. 16, no. 1, Art. no. 1, 2021.
- [48] T.-T. Nguyen, L. Sorelli, and X. (Alice) Wang, "Humidity exchange between CLT and UHPC slab in early age period," presented at the World Conference on Timber Engineering 2021, Santiago, Chile, Aug. 2021.
- [49] E. Steinberg, R. Selle, and T. Faust, "Connectors for timber–lightweight concrete composite structures," *Journal of Structural Engineering*, vol. 129, no. 11, pp. 1538–1545, Nov. 2003, doi: 10.1061/(ASCE)0733-9445(2003)129:11(1538).
- [50] H. B. Koh, A. B. Mohamad Diah, Y. L. Lee, and D. E. C. Yeoh, "Experimental study on shear behaviours of timber- lightweight concrete composite shear connectors," in *3rd Brunei Int Conf on Engineering and Technology*, Bandar Seri Begawan, Brunei, 2008, p. 10. [Online]. Available: <https://core.ac.uk/download/pdf/20558311.pdf>
- [51] K. Holschemacher, S. Klotz, and D. Weiße, "Application of steel fibre reinforced concrete for timber-concrete composite constructions," *LACER*, vol. 7, pp. 161–170, 2002.
- [52] S. Lamothe, L. Sorelli, P. Blanchet, and P. Galimard, "Engineering ductile notch connections for composite floors made of laminated timber and high or ultra-high performance fiber reinforced concrete," *Engineering Structures*, vol. 211, p. 110415, May 2020, doi: 10.1016/j.engstruct.2020.110415.
- [53] H. Kieslich and K. Holschemacher, "Composite constructions of timber and high-performance concrete," *AMR*, vol. 133–134, pp. 1171–1176, Oct. 2010, doi: 10.4028/www.scientific.net/AMR.133-134.1171.
- [54] D. E. C. Yeoh, M. Fragiaco, A. Buchanan, K. Crews, J. Haskell, and B. Deam, "Development of semi-prefabricated timber-concrete composite floors in Australasia," 2008, Accessed: Apr. 06, 2021. [Online]. Available: <https://ir.canterbury.ac.nz/handle/10092/2641>
- [55] L. Boccadoro, "Timber-concrete composite slabs made of beech laminated veneer lumber with notched connection," ETH Zurich, 2016. doi: 10.3929/ethz-a-010777925.
- [56] D. Djoubissie Denouwe, A. Messan, F. Eric, and A. Bouchair, "Influence of interlayer in timber-concrete composite structures with threaded rebar as shear connector-experimental study," *American Journal of Civil Engineering and Architecture*, vol. 6, pp. 38–45, Jan. 2018, doi: 10.12691/ajcea-6-1-5.
- [57] M. A. H. Mirdad and Y. H. Chui, "Load-slip performance of Mass Timber Panel-Concrete (MTPC) composite connection with Self-tapping screws and insulation layer," *Construction and Building Materials*, vol. 213, pp. 696–708, Jul. 2019, doi: 10.1016/j.conbuildmat.2019.04.117.
- [58] B. L. Deam, M. Fragiaco, and A. H. Buchanan, "Connections for composite concrete slab and LVL flooring systems," *Mater Struct*, vol. 41, no. 3, pp. 495–507, Apr. 2008, doi: 10.1617/s11527-007-9261-x.
- [59] A. Gerber, "Full scale testing of timber-concrete composite floor systems," University of British Columbia, Vancouver, Canada, 2015.
- [60] D. Yeoh, "Behavior and design of timber-concrete composite floor system," University of Canterbury, Christchurch, New Zealand 8140, 2010.
- [61] R. Rijal, "Dynamic performance of timber and timber-concrete composite flooring systems," University of Technology, Sydney, Sydney, 2013.

- [62] R. M. Gutkowski, K. Brown, A. Shigidi, and J. Natterer, "Investigation of notched composite wood–concrete connections," *J. Struct. Eng.*, vol. 130, no. 10, pp. 1553–1561, Oct. 2004, doi: 10.1061/(ASCE)0733-9445(2004)130:10(1553).
- [63] S. C. Auclair, L. Sorelli, and A. Salenikovich, "A new composite connector for timber-concrete composite structures," *Construction and Building Materials*, vol. 112, pp. 84–92, Jun. 2016, doi: 10.1016/j.conbuildmat.2016.02.025.
- [64] D. J. Inman, *Engineering vibration*, Fourth edition. Boston: Pearson, 2014.
- [65] D. E. Allen and G. Pernica, "Control of floor vibration," *Construction Technology Update*, vol. 22, 1998.
- [66] S. Ohlsson, "Serviceability criteria - especially floor vibration criteria," in *1991 International Timber Engineering Conference*, London, Sep. 1991, vol. 1.
- [67] L. J. Hu, Y. H. Chui, and D. M. Onysko, "Vibration serviceability of timber floors in residential construction," *Progress in Structural Engineering and Materials*, vol. 3, no. 3, pp. 228–237, 2001, doi: <https://doi.org/10.1002/pse.69>.
- [68] K. Jarnerö, "Vibrations in timber floors - Dynamic properties and human perception," Linnaeus University, Växjö, 2014.
- [69] E. Ussher, K. Arjomandi, J. Weckendorf, and I. Smith, "Predicting effects of design variables on modal responses of CLT floors," *Structures*, vol. 11, pp. 40–48, Aug. 2017, doi: 10.1016/j.istruc.2017.04.006.
- [70] J. Negreira, A. Trollé, K. Jarnerö, L.-G. Sjökvist, and D. Bard, "Psycho-vibratory evaluation of timber floors – Towards the determination of design indicators of vibration acceptability and vibration annoyance," *Journal of Sound and Vibration*, vol. 340, pp. 383–408, Mar. 2015, doi: 10.1016/j.jsv.2014.12.001.
- [71] L. Hu and Y. H. Chui, "Development of a design method to control vibrations induced by normal walking action in wood-based Floors," presented at the World Conference on Timber Engineering 2004, Lahti, Finland, Jun. 2004.
- [72] I. S. ISO 2631-1, "Mechanical vibration and shock - Evaluation of human exposure to whole-body vibration - Part 1: General requirements," International Organization for Standardization, 2003. [Online]. Available: <https://www.iso.org/standard/23012.html>
- [73] D. Onysko, L. J. Hu, E. D. Jones, and B. Di Lenardo, "Serviceability design of residential wood framed floors in Canada," Canada Wood Products Research Institute, NRCC-38501, 2000.
- [74] L. Hu, Y. Chui, and D. Onysko, "Vibration serviceability of timber floors in residential construction," *Progress in Structural Engineering and Materials*, vol. 3, pp. 228–237, Jul. 2001, doi: 10.1002/pse.69.
- [75] D. M. Onysko, "Serviceability criteria for residential floors based on a field study of consumer response," Forintek Canada Corp, Ottawa, Canada, Project Report 03-50-10-008, 1985.
- [76] National Research Council of Canada, *National Building Code of Canada. Commentary A: Serviceability criterion for deflections and vibrations*. Ottawa: National Research Council of Canada, 1985.
- [77] J. D. Dolan, "Designing to reduce floor vibrations in wood floors," *Virginia Polytechnic Institute and State University*.
- [78] J. D. Dolan, T. M. Murray, J. R. Johnson, D. Runte, and B. C. Shue, "Preventing annoying wood floor vibrations," p. 6, 1999.

- [79] J. R. Johnson, "Vibration acceptability in wood floor systems," Thesis, Virginia Tech, 1994. Accessed: Mar. 29, 2021. [Online]. Available: <https://vtechworks.lib.vt.edu/handle/10919/41946>
- [80] L. J. Hu, "Serviceability design criteria for commercial and multi-family floors," Forintek Canada Corporation, Sainte-Foy, Quebec, Canada, Canadian Forest Service Report No. 4, 2000.
- [81] F. Ljunggren, "Floor vibration - Dynamic properties and subjective perception," Ph.D. Thesis, Luleå University of Technology, 2006.
- [82] S. Ohlsson, *Springiness and human-induced floor vibrations: a design guide*. Stockholm, Sweden: Swedish Council for Building Research, 1988.
- [83] S. Ohlsson, *Floor vibrations and human discomfort*. Göteborg: Div. of Steel and Timber Structures, Chalmers Univ. of Technology, 1982.
- [84] A. Ebrahimpour and R. L. Sack, "A review of vibration serviceability criteria for floor structures," *Computers & Structures*, vol. 83, no. 28, pp. 2488–2494, Nov. 2005, doi: 10.1016/j.compstruc.2005.03.023.
- [85] I. Smith and Y. H. Chui, "Design of lightweight wooden floors to avoid human discomfort," *Can. J. Civ. Eng.*, vol. 15, no. 2, pp. 254–262, Apr. 1988, doi: 10.1139/l88-033.
- [86] Y. H. Chui and I. Smith, "A serviceability criterion to avoid human discomfort for light-weight wooden floors," in *Symposium/Workshop on Serviceability of Buildings*, Ottawa, Ontario, Canada, 1988, pp. 512–525.
- [87] L. Hu *et al.*, "Design method for controlling vibrations of wood-concrete composite floors systems," presented at the World Conference on Timber Engineering 2016, Vienna, Austria, Aug. 2016.
- [88] Project team SC5.T3, "EN 1995-1-1. Project team SC5.T3. Sub-task 7. Vibrations. Milestone 2," CEN European Committee for Standardization, SC5.T3, milestone 2 draft October 2018, Apr. 2019.
- [89] W. Schirén and T. Swahn, *Vibrations in residential timber floors: A comparison between the current and the revised Eurocode 5*. 2019. Accessed: Mar. 29, 2021. [Online]. Available: <http://urn.kb.se/resolve?urn=urn:nbn:se:lnu:diva-89293>
- [90] L. Hu, "Development of a performance criterion for controlling vibrations in wood-based floors," presented at the World Conference on Timber Engineering 2002, Shah Alam, Malaysia, Aug. 2002.
- [91] P. Hamm, A. Richter, and S. Winter, "Floor vibrations – new results," presented at the World Conference on Timber Engineering 2010, Trentino, Italy, Jun. 2010.
- [92] L. Hu and S. Gagnon, "Controlling cross-laminated timber (CLT) floor vibration: Fundamentals and method," presented at the World Conference on Timber Engineering 2012, Auckland, New Zealand, Jul. 2012.
- [93] K. Quang Mai, A. Park, K. T. Nguyen, and K. Lee, "Full-scale static and dynamic experiments of hybrid CLT–concrete composite floor," *Construction and Building Materials*, vol. 170, pp. 55–65, May 2018, doi: 10.1016/j.conbuildmat.2018.03.042.
- [94] L. Zhang and Y. H. Chui, "Numerical study of the geometry effect of notched connections in mass timber panel-concrete composite floors," *mocs*, pp. 587–596, May 2019, doi: 10.29173/mocs142.
- [95] EN 26891: 1991, *Timber structures. Joints made with mechanical fasteners. General principles for the determination of strength and deformation characteristics*. European Committee for Standardization (CEN), 1991.

- [96] E. Lukaszewska, "Development of prefabricated timber-concrete composite floors," Ph.D. Thesis, Luleå University of Technology, 2009.
- [97] E. P. Carvalho and E. V. M. Carrasco, "Influence of test specimen on experimental characterization of timber–concrete composite joints," *Construction and Building Materials*, vol. 24, no. 8, pp. 1313–1322, Aug. 2010, doi: 10.1016/j.conbuildmat.2009.12.036.
- [98] D. J. Ewins, *Modal testing: theory, practice, and application*, 2nd ed. Baldock, Hertfordshire, England; Philadelphia, PA: Research Studies Press, 2000.
- [99] W. Heylen, S. Lammens, and P. Sas, "Modal analysis: theory and testing," 1999.
- [100] J. He and Z.-F. Fu, *Modal analysis*. Oxford; Boston: Butterworth-Heinemann, 2001.
- [101] A. M. P. G. Dias and L. F. C. Jorge, "The effect of ductile connectors on the behaviour of timber–concrete composite beams," *Engineering Structures*, vol. 33, no. 11, pp. 3033–3042, Nov. 2011, doi: 10.1016/j.engstruct.2011.05.014.
- [102] M. Fragiaco and E. Lukaszewska, "Time-dependent behaviour of timber–concrete composite floors with prefabricated concrete slabs," *Engineering Structures*, vol. 52, pp. 687–696, Jul. 2013, doi: 10.1016/j.engstruct.2013.03.031.
- [103] M. Fragiaco, C. Amadio, and L. Macorini, "Short- and long-term performance of the 'Tecnaria' stud connector for timber-concrete composite beams," *Mater Struct*, vol. 40, no. 10, pp. 1013–1026, Oct. 2007, doi: 10.1617/s11527-006-9200-2.
- [104] A. Frangi, M. Knobloch, and M. Fontana, "Fire design of timber-concrete composite slabs with screwed connections," *J. Struct. Eng.*, vol. 136, no. 2, pp. 219–228, Feb. 2010, doi: 10.1061/(ASCE)ST.1943-541X.0000101.
- [105] D. Yeoh, M. Fragiaco, A. Buchanan, and C. Gerber, "Preliminary research towards a semi-prefabricated LVL–concrete composite floor system for the australasian market," *Australian Journal of Structural Engineering*, vol. 9, no. 3, pp. 225–240, Jan. 2009, doi: 10.1080/13287982.2009.11465025.
- [106] A. Ceccotti, "Composite concrete-timber structures," *Prog. Struct. Engng Mater.*, vol. 4, no. 3, pp. 264–275, Jul. 2002, doi: 10.1002/pse.126.
- [107] A. R. Gerber, "Timber-concrete composite connectors in flat-plate engineered wood products," University of British Columbia, 2016.
- [108] Khorsandnia Nima, Valipour Hamid, Schänzlin Jörg, and Crews Keith, "Experimental Investigations of Deconstructable Timber–Concrete Composite Beams," *Journal of Structural Engineering*, vol. 142, no. 12, p. 04016130, Dec. 2016, doi: 10.1061/(ASCE)ST.1943-541X.0001607.
- [109] NRC - CNRC, *Evaluation Listing CCMC 13654-L Nordic X-Lam*. National Research Council of Canada, 2013. [Online]. Available: https://www.nordic.ca/data/files/datasheet/file/13654_e.pdf
- [110] ASTM C39/C39M - 18, *Test Method for Compressive Strength of Cylindrical Concrete Specimens*. ASTM International, 2018. doi: 10.1520/C0039_C0039M-18.
- [111] MyTiCon, "Structural screw design guide," MyTiCon Timber Connectors, Feb. 2020. Accessed: May 22, 2020. [Online]. Available: <https://mtcsolutions.com/wp-content/uploads/2019/04/Screws-Design-Guide-VC-1.1.pdf>
- [112] TiComTec, "Technical dossier - HBV systems. English version," TiComTec, TiComTec GmbH, Goethestr. 60, D-63808 Haibach, May 2014. [Online]. Available: www.ticomtec.de

- [113]A. M. P. G. Dias, J. W. Van de Kuilen, S. Lopes, and H. Cruz, "A non-linear 3D FEM model to simulate timber–concrete joints," *Advances in Engineering Software*, vol. 38, no. 8–9, pp. 522–530, Aug. 2007, doi: 10.1016/j.advengsoft.2006.08.024.
- [114]C. Sandhaas and J. W. G. van de Kuilen, "Material model for wood," *HERON*, vol. 58, no. 2/3, pp. 179–199, 2013.
- [115]S. Hollenbeck, "Numerical Modeling of Mass Timber Connections," Oregon State University, 2018.
- [116]B. Franke and P. Quenneville, "Numerical modeling of the failure behavior of dowel connections in wood," *J. Eng. Mech.*, vol. 137, no. 3, pp. 186–195, Mar. 2011, doi: 10.1061/(ASCE)EM.1943-7889.0000217.
- [117]F. P. Laboratory, "Wood handbook: wood as an engineering material.," *General technical report FPL ; GTR-113. Madison, WI: U.S. Department of Agriculture, Forest Service, Forest Products Laboratory: xi, [463] pages : ill. ; 28 cm.*, vol. 113, p. 509, 1999, doi: 10.2737/FPL-GTR-113.
- [118]ASTM D143 - 14, *Test Methods for Small Clear Specimens of Timber*. ASTM International, 2014. doi: 10.1520/D0143-14.
- [119]EN 338 - 2009, *Structural timber - Strength classes*. European Committee for Standardization (CEN), 2009.
- [120]*Abaqus 6.14 Online Documentation*. 78140 Velizy-Villacoublay, France: Dassault Systèmes, 2014. Accessed: Jul. 07, 2020. [Online]. Available: <http://ivt-abaqusdoc.ivt.ntnu.no:2080/v6.14/books/usb/default.htm>
- [121]A. Dias, J. Schänzlin, P. Dietsch, and Shaker Verlag GmbH, *Design of timber-concrete composite structures. A state-of-the-art report by COST Action FP1402/WG 4*. 2018.
- [122]C. Mertens, Y. Martin, and F. Dobbels, "Investigation of the vibration behaviour of timber-concrete composite floors as part of a performance evaluation for the belgian building industry," *Building Acoustics*, vol. 14, no. 1, pp. 25–36, Jan. 2007, doi: 10.1260/135101007780661383.
- [123]P. G. G. dos Santos, C. E. de J. Martins, J. Skinner, R. Harris, A. M. P. G. Dias, and L. M. C. Godinho, "Modal frequencies of a reinforced timber-concrete composite floor: Testing and modeling," *Journal of Structural Engineering*, vol. 141, no. 11, p. 04015029, Nov. 2015, doi: 10.1061/(ASCE)ST.1943-541X.0001275.
- [124]N. H. A. Ghafar, B. Deam, M. Fragiaco, and A. Buchanan, "Vibration Performance of LVL- Concrete Composite Floor Systems," p. 7.
- [125]E. Lukaszewska and M. Fragiaco, "Static and dynamic (vibration) performance of composite beams with prefabricated concrete slab," in *World Conference on Timber Engineering 2010*, Trentino, Italy, Jun. 2010, p. 10.
- [126]Z. Xie, X. Hu, H. Du, and X. Zhang, "Vibration behavior of timber-concrete composite floor under human-induced excitation," *Journal of Building Engineering*, p. 101744, Aug. 2020, doi: 10.1016/j.job.2020.101744.
- [127]S. C. Auclair, "Design guide for timber-concrete composite floors in Canada," FPIInnovation, Point-Claire, QC, Canada, Special Publication SP-540E, 2020.
- [128]International Organization for Standardization, *ISO/TR 21136:2017 - Timber structures — Vibration performance criteria for timber floors*. 2017. Accessed: Oct. 22, 2020. [Online]. Available: <https://www.iso.org/cms/render/live/en/sites/isoorg/contents/data/standard/06/99/69963.html>

- [129]O. Døssing, "Structural testing. Part 2: Modal analysis and simulation," Mar. 1988.
- [130]M. V. Thai, S. Ménard, S. M. Elachachi, and P. Galimard, "Performance of notched connectors for CLT-concrete composite floors," *Buildings*, vol. 10, no. 7, Art. no. 7, Jul. 2020, doi: 10.3390/buildings10070122.
- [131]EN 408:2010 - A1:2012, *Timber structures - Structural timber and glued laminated timber - Determination of some physical and mechanical properties*. European Committee for Standardization (CEN), 2012.
- [132]American Wood Council, *ANSI/AWC NDS-2015 National Design Specification (NDS) for Wood Construction*. 215AD. Accessed: Jul. 01, 2021. [Online]. Available: <https://awc.org/codes-standards/publications/nds-2015>
- [133]Nordic Structures, "Nordic X-Lam: Design properties," Nordic Structures, May 2018.
- [134]W. Pawlowski, L. Kaczmarek, and P. Louda, "Theoretical and experimental modal analysis of the cylinder unit filled with PUR foam," *EiN*, vol. 18, no. 03, pp. 428–435, Jun. 2016, doi: 10.17531/ein.2016.3.15.
- [135]B. Peeters and H. Van der Auweraer, "PolyMax: a revolution in operational modal analysis," presented at the 1st International Operational Modal Analysis Conference, Copenhagen, Denmark, Apr. 2005.
- [136]J. Zhou, "Chapter 6: Effective bending and shear stiffness of cross laminated timber by modal testing: method development and application," in *Simultaneous measurement of elastic constants of engineered wood-based panels by modal testing*, 2018.
- [137]I. Glisovic and B. Stevanovic, "Vibrational behaviour of timber floors," presented at the World Conference on Timber Engineering 2010, Trentino, Italy, 2010.
- [138]J. Turmo, J. A. Lozano-Galant, E. Mirambell, and D. Xu, "Modeling composite beams with partial interaction," *Journal of Constructional Steel Research*, vol. 114, pp. 380–393, Nov. 2015, doi: 10.1016/j.jcsr.2015.07.007.
- [139]J. Zhou, "Simultaneous measurement of elastic constants of engineered wood-based panels by modal testing," University of New Brunswick., 2018. Accessed: May 26, 2021. [Online]. Available: <https://unbscholar.lib.unb.ca/islandora/object/unbscholar%3A9312/>
- [140]J. Zhou, Y. H. Chui, J. Niederwestberg, and M. Gong, "Effective bending and shear stiffness of cross-laminated timber by modal testing: Method development and application," *Composites Part B: Engineering*, vol. 198, p. 108225, Oct. 2020, doi: 10.1016/j.compositesb.2020.108225.
- [141]R. Rijal, B. Samali, R. Shrestha, and K. Crews, "Experimental and analytical study on dynamic performance of timber-concrete composite beams," *Construction and Building Materials*, vol. 75, pp. 46–53, Jan. 2015, doi: 10.1016/j.conbuildmat.2014.10.020.
- [142]E. Ussher, K. Arjomandi, J. Weckendorf, and I. Smith, "Prediction of motion responses of cross-laminated-timber slabs," *Structures*, vol. 11, pp. 49–61, Aug. 2017, doi: 10.1016/j.istruc.2017.04.007.
- [143]A. Ebrahimpour, A. Hamam, R. L. Sack, and W. N. Patten, "Measuring and Modeling Dynamic Loads Imposed by Moving Crowds," *Journal of Structural Engineering*, vol. 122, no. 12, pp. 1468–1474, Dec. 1996, doi: 10.1061/(ASCE)0733-9445(1996)122:12(1468).
- [144]M.-V. Thai, S. M. Elachachi, S. Ménard, and P. Galimard, "Vibrational behavior of cross-laminated timber-concrete composite beams using notched connectors,"

- Engineering Structures*, vol. 249, p. 113309, Dec. 2021, doi: 10.1016/j.engstruct.2021.113309.
- [145] S. A. Decker, "Développement d'une méthode d'optimisation multiobjectif pour la construction bois: prise en compte du confort des usagers, de l'impact environnemental et de la sécurité de l'ouvrage," p. 261, 2015.
- [146] S. A. Decker *et al.*, "Optimisation multi-objectif de planchers intermédiaires bois tenant compte d'objectifs mécaniques et environnementaux," May 2015.
- [147] U. Klanšek and S. Kravanja, "Cost estimation, optimization and competitiveness of different composite floor systems—Part 1: Self-manufacturing cost estimation of composite and steel structures," *Journal of Constructional Steel Research*, vol. 62, no. 5, pp. 434–448, May 2006, doi: 10.1016/j.jcsr.2005.08.005.
- [148] U. Klanšek and S. Kravanja, "Cost estimation, optimization and competitiveness of different composite floor systems—Part 2: Optimization based competitiveness between the composite I beams, channel-section and hollow-section trusses," *Journal of Constructional Steel Research*, vol. 62, no. 5, pp. 449–462, May 2006, doi: 10.1016/j.jcsr.2005.08.006.
- [149] S. M. Elachachi and F. Djellouli, "Optimized dimensional design of standard reinforced concrete structures," presented at the 22nd National Conference of the A.U.G.C., Marne la Vallée, France, Jun. 2004.
- [150] G. Poitras, G. Lefrançois, and G. Cormier, "Optimization of steel floor systems using particle swarm optimization," *Journal of Constructional Steel Research*, vol. 67, no. 8, pp. 1225–1231, Aug. 2011, doi: 10.1016/j.jcsr.2011.02.016.
- [151] P. Jelusic and S. Kravanja, "Optimal design of timber-concrete composite floors based on the multi-parametric MINLP optimization," *Composite Structures*, vol. 179, pp. 285–293, Nov. 2017, doi: 10.1016/j.compstruct.2017.07.062.
- [152] H. Leyva *et al.*, "Earthquake design of reinforced concrete buildings using NSGA-II," *Advances in Civil Engineering*, vol. 2018, pp. 1–11, Nov. 2018, doi: 10.1155/2018/5906279.
- [153] M. Babaei and M. Mollayi, "Multi-objective optimization of reinforced concrete frames using NSGA-II algorithm," *Engineering Structures and Technologies*, vol. 8, no. 4, pp. 157–164, Dec. 2016, doi: 10.3846/2029882X.2016.1250230.
- [154] A. Benítez-Hidalgo, A. J. Nebro, J. García-Nieto, I. Oregi, and J. Del Ser, "jMetalPy: A Python framework for multi-objective optimization with metaheuristics," *Swarm and Evolutionary Computation*, vol. 51, p. 100598, Dec. 2019, doi: 10.1016/j.swevo.2019.100598.
- [155] M. V. Thai, S. M. Elachachi, S. Ménard, and P. Galimard, "Vibrational behavior of CLT-concrete composite beams using notched connectors," *Engineering Structures*, 2021.
- [156] Canadian Standards Association, *CSA-A23.3-14. Design of concrete structures*. 2014.
- [157] M. Fragiaco and A. Ceccotti, "A Simplified Approach for Long-Term Evaluation of Timber-Concrete Composite Beams," p. 6, Jun. 2004.
- [158] S. Kravanja, T. Žula, and U. Klanšek, "Multi-parametric MINLP optimization study of a composite I beam floor system," *Engineering Structures*, vol. 130, pp. 316–335, Jan. 2017, doi: 10.1016/j.engstruct.2016.09.012.
- [159] Conseil canadien du bois, *Wood design manual, 2017: the complete reference for wood design in Canada*. 2017.

- [160]E.-G. Talbi, *Metaheuristics: from design to implementation*. John Wiley & Sons, 2009.
- [161]K. Sörensen, “Metaheuristics-the metaphor exposed,” *Intl. Trans. in Op. Res.*, vol. 22, no. 1, pp. 3–18, Jan. 2015, doi: 10.1111/itor.12001.
- [162]M. Mitchell, *An introduction to genetic algorithms*. Cambridge, Mass.: MIT Press, 1996.
- [163]I. Alothaimen and D. Arditi, “Overview of multi-objective optimization approaches in construction project management,” *Multicriteria optimization - Pareto-optimality and Threshold-optimality*, Jul. 2019, doi: 10.5772/intechopen.88185.
- [164]K. Deb, A. Pratap, S. Agarwal, and T. Meyarivan, “A fast and elitist multi-objective genetic algorithm: NSGA-II,” *IEEE Trans. Evol. Computat.*, vol. 6, no. 2, pp. 182–197, Apr. 2002, doi: 10.1109/4235.996017.
- [165]K. Deb, S. Agrawal, A. Pratap, and T. Meyarivan, “A fast elitist non-dominated sorting genetic algorithm for multi-objective optimization: NSGA-II,” in *Parallel Problem Solving from Nature PPSN VI*, Berlin, Heidelberg, 2000, pp. 849–858. doi: 10.1007/3-540-45356-3_83.
- [166]K. Deb and R. B. Agrawal, “Simulated binary crossover for continuous search space,” 1994.
- [167]K. Deb and D. Deb, “Analysing mutation schemes for real-parameter genetic algorithms,” *Int. J. Artif. Intell. Soft Comput.*, vol. 4, no. 1, pp. 1–28, Feb. 2014, doi: 10.1504/IJAISC.2014.059280.
- [168]N. Srinivas and K. Deb, “Multiobjective optimization using nondominated sorting in genetic algorithms,” *Evolutionary Computation*, vol. 2, no. 3, pp. 221–248, Sep. 1994, doi: 10.1162/evco.1994.2.3.221.
- [169]A. Hojjati, M. Monadi, A. Faridhosseini, and M. Mohammadi, “Application and comparison of NSGA-II and MOPSO in multi-objective optimization of water resources systems,” *Journal of Hydrology and Hydromechanics*, vol. 66, no. 3, pp. 323–329, Sep. 2018, doi: 10.2478/johh-2018-0006.
- [170]D. G. Eliades, M. P. Michaelides, C. G. Panayiotou, and M. M. Polycarpou, “Security-oriented sensor placement in intelligent buildings,” *Building and Environment*, vol. 63, pp. 114–121, May 2013, doi: 10.1016/j.buildenv.2013.02.006.
- [171]M. Hamdy, A. Hasan, and K. Siren, “A multi-stage optimization method for cost-optimal and nearly-zero-energy building solutions in line with the EPBD-recast 2010,” *Energy and Buildings*, vol. 56, pp. 189–203, Jan. 2013, doi: 10.1016/j.enbuild.2012.08.023.
- [172]J. Carreras, D. Boer, G. Guillén-Gosálbez, L. F. Cabeza, M. Medrano, and L. Jiménez, “Multi-objective optimization of thermal modelled cubicles considering the total cost and life cycle environmental impact,” *Energy and Buildings*, vol. 88, pp. 335–346, Feb. 2015, doi: 10.1016/j.enbuild.2014.12.007.
- [173]C. Kasinalis, R. C. G. M. Loonen, D. Cóstola, and J. L. M. Hensen, “Framework for assessing the performance potential of seasonally adaptable facades using multi-objective optimization,” *Energy and Buildings*, vol. 79, pp. 106–113, Aug. 2014, doi: 10.1016/j.enbuild.2014.04.045.
- [174]M. Parente, P. Cortez, and A. Gomes Correia, “An evolutionary multi-objective optimization system for earthworks,” *Expert Systems with Applications*, vol. 42, no. 19, pp. 6674–6685, Nov. 2015, doi: 10.1016/j.eswa.2015.04.051.

- [175]E. Fallah-Mehdipour, O. Bozorg Haddad, M. M. Rezapour Tabari, and M. A. Mariño, "Extraction of decision alternatives in construction management projects: Application and adaptation of NSGA-II and MOPSO," *Expert Systems with Applications*, vol. 39, no. 3, pp. 2794–2803, Feb. 2012, doi: 10.1016/j.eswa.2011.08.139.
- [176]"Network Design through the Phasing of Construction Approach," *Procedia Engineering*, vol. 89, pp. 823–830, Jan. 2014, doi: 10.1016/j.proeng.2014.11.513.
- [177]O. El-Anwar and T. A. Aziz, "Integrated Urban-Construction Planning Framework for Slum Upgrading Projects," *Journal of Construction Engineering and Management*, vol. 140, no. 4, p. B4014003, Apr. 2014, doi: 10.1061/(ASCE)CO.1943-7862.0000672.
- [178]A. M. P. G. Dias, A. R. D. Martins, L. M. C. Simões, P. M. Providência, and A. A. M. Andrade, "Statistical analysis of timber–concrete connections – Mechanical properties," *Computers & Structures*, vol. 155, pp. 67–84, Jul. 2015, doi: 10.1016/j.compstruc.2015.02.036.
- [179]M. L. Delignette-Muller and C. Dutang, "fitdistrplus: An R Package for Fitting Distributions," *J. Stat. Soft.*, vol. 64, no. 4, 2015, doi: 10.18637/jss.v064.i04.
- [180]E. Graber, "Feasibility of cross laminated timber panels in construction: a case study of Carbon12," *Construction Management*, Jun. 2020, [Online]. Available: <https://digitalcommons.calpoly.edu/cmisp/394>
- [181]A. Hyams, S. Watts, J. Sweet, and D. K. S. 30 July 2020, "Cost model: CLT frame buildings," *Building*. <https://www.building.co.uk/cost-model-clt-frame-buildings/5107248.article> (accessed Feb. 02, 2021).

ANNEX

ANNEX 1. Effective bending stiffness of composite section using Gamma method

The longitudinal effective bending stiffness of composite beam EI_{eff} was as:

$$(EI)_{eff} = (EI)_0 + \gamma_c(EA)_c a_c^2 + \gamma_t(EA)_t a_t^2 \quad (A1.1)$$

$$a_c = \frac{\gamma_t(EA)_t}{\gamma_c(EA)_c + \gamma_t(EA)_t} h_d \quad (A1.2) \quad a_t = \frac{\gamma_c(EA)_c}{\gamma_c(EA)_c + \gamma_t(EA)_t} h_d \quad (A1.3)$$

The stiffness of the non-composite section $(EI)_0$ is the sum of longitudinal stiffness of timber and concrete:

$$(EI)_0 = (EI)_c + (EI)_t \quad (A1.4)$$

$$h_d = \frac{h_t}{2} + h_{ieff} + \frac{h_{ceff}}{2} \quad (A1.5)$$

$$h_{ieff} = h_i + h_c - h_{ceff} \quad (A1.6)$$

$$h_{ceff} = \min\left(\sqrt{\alpha^2 + \alpha(h_t + 2h_c + 2h_i)} - \alpha, h_c\right) \quad (A1.7)$$

$$\alpha = \frac{\gamma_t}{\gamma_c} \cdot \frac{(EA)_t}{E_c b_c} \quad (A1.8)$$

$$\gamma_c = 1; \quad \gamma_t = \frac{1}{1 + \frac{\pi^2 (EA)_t}{L^2 K}} \quad (A1.9)$$

ANNEX 2. Characteristic value of slip modulus and maximum load

There are 13 different configurations, with 60 specimens tested in the previous experimental test on the notch connector [130]. This means that these configurations have their distribution. To create a random distribution from all experimental data, a method of mixing these configurations was adopted. The idea is to create a dimensionless distribution x^{adim} associated with the mean value \bar{x} of each distribution [178]. Given a random distribution x , then $x = \bar{x}.x^{adim}$, so $x^{adim} = x/\bar{x}$. These dimensionless distributions always have a mean value $\mu_{x^{adim}}$ of 1.00 and the standard deviation $\sigma_{x^{adim}}$ of σ_x/\bar{x} . The goodness-of-fit (GOF) test is used to compare the fit of different distributions on an experimental data set. Many GOF tests were reported in the literature. Here, we used the Kolmogorov-Smirnov, Anderson-Darling, and Cramer von Mises test, which are suitable for continuous distribution [179].

Table A2.1. Goodness-of-fit statistics summary

	Normal	Lognormal	Weibull	Gamma	Logistic
Goodness-of-fit statistics of slip modulus K1 distribution					
Kolmogorov-Smirnov	0,0693	0,0803	0,0986	0,0768	0,0703
Cramer-von Mises	0,0434	0,0443	0,0746	0,0434	0,0623
Anderson-Darling	0,2833	0,3160	0,4542	0,3010	0,3850
Goodness-of-fit statistics of slip modulus K2 distribution					
Kolmogorov-Smirnov	0,0916	0,1084	0,0646	0,1030	0,0732
Cramer-von Mises	0,0955	0,1395	0,0316	0,1234	0,0705
Anderson-Darling	0,6030	0,8869	0,2041	0,7832	0,5468
Goodness-of-fit statistic of maximum load Fmax distribution					
Kolmogorov-Smirnov	0,0693	0,0803	0,0986	0,0768	0,0703
Cramer-von Mises	0,0434	0,0443	0,0746	0,0434	0,0623
Anderson-Darling	0,2833	0,3160	0,4542	0,3010	0,3850

Table A2.2. Distribution parameters of slip modulus K1, K2, and maximum load Fmax distribution

	Slip modulus K1	Slip modulus K2	Maximum load Fmax
Distribution type	Normal	Weibull	Normal
Mean value	1,000	13,762*	1,000
StD of Mean value	0,013	1,431	0,008
Standard deviation	0,099	1,039*	0,062
StD of Standard deviation	0,0091	0,010	0,006
Characteristic value	0,838	0,837	0,898

*Weibull law uses shape (a) and scale (b) as its parameters.

The experiment statistics were calculated by a package in R language [179] and reported in Table A2.1. The smaller those statistics are, the better. The distributions for fitting in this analysis are normal, log-normal, gamma, Weibull, and logistic distribution. These are continuous probability density functions.

The parameters of the fitted distribution were then determined by the maximum likelihood method. Furthermore, the same statistical analysis of the timber-concrete connection was carried out by Dias *et al.* [178].

Characteristic values (0,838 for K1 and 0,898 for Fmax) , reported in Table A2.2, are defined at the 5% fractile of the considered distribution. The corresponding characteristic values in the study of Dias *et al.* [178] are 0,639 and 0,856 for slip modulus K1 and maximum load Fmax, respectively, in the case of notches reinforced with steel fasteners. The result was much higher (0,838 for K1) due to the consistency of the test setup and the fact that only one connector type was tested. Dias *et al.* reported a lower value based on many studies on a variety of connector types.

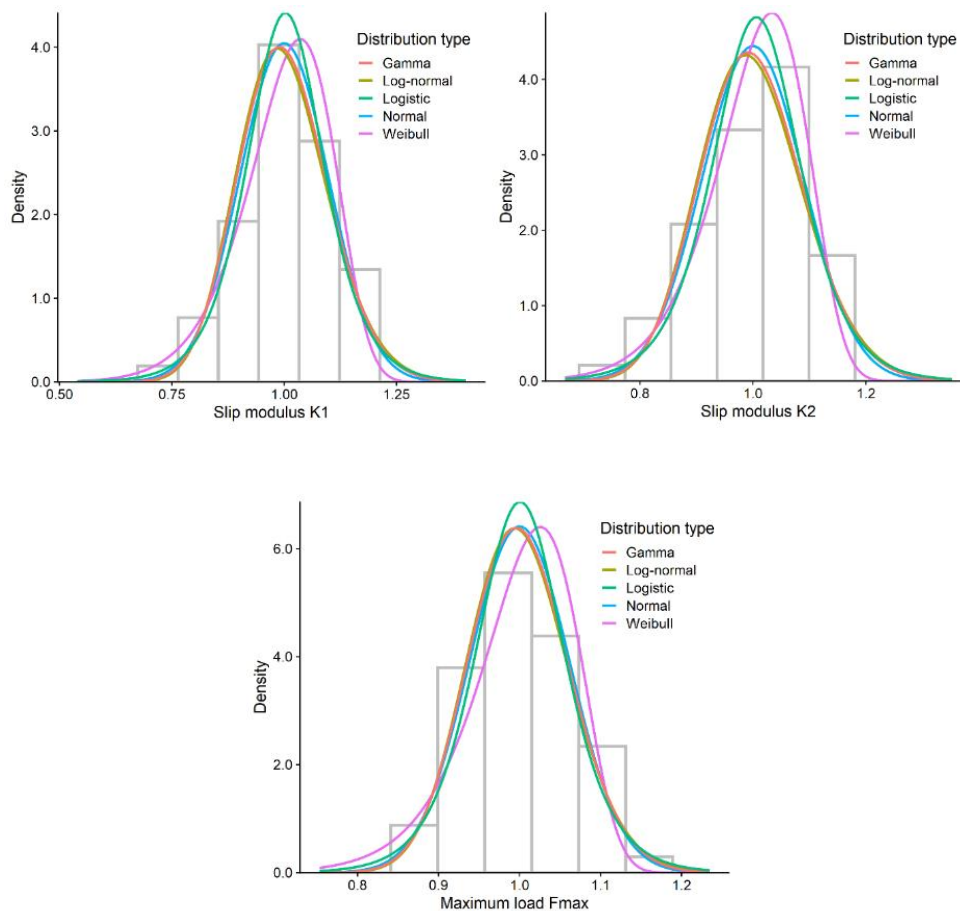


Figure A2.1. Dimensionless distribution of slip modulus K1, K2, and maximum load Fmax

ANNEX 3. Timber and concrete cost

Table A3.1 presents a summary of available information on the cost of timber and concrete. The information of the Carbon12 project [180] was not disclosed as cost per volume unit; hence, the comparison of cost ratio timber per concrete (T/C) was carried out. The ratio T/C of material cost could range from 2.46 to 2.94 based on available sources [151], [180]. The advantage of timber is enhanced by including labor cost, and the ratio T/C reduces to about 1.13 to 1.25. An undisclosed source (in France) provided that the average cost of a TCC composite floor system (timber beam – concrete deck) was about 200 to 250 €/m², depending on the span, thickness, surface, fire protection, and acoustic requirements. By applying the cost presented by Hyams *et al.* [181], the cost per floor surface arrived at a comparable cost of about 215 to 240 €/m² for a 9-m floor (Figure 4.6).

Table A3.1. Available information on timber – concrete cost

Study	Timber	Concrete	T/C	Description
Jelusic and Kravanja [151] 2017	250 €/m ³	85 €/m ³	2.94	Material cost. Additional expressions are available for execution cost. GLT beam C24 and concrete C25/30
Graber [180] 2020	17 \$/sf	6.9 \$/sf	2.46	Material cost of Carbon12 project (Oregon, USA)
	2.8 \$/sf	10.6 \$/sf	-	Labor cost of Carbon12 project
	19.8 \$/sf	17.5 \$/sf	1.13	Material and labor cost of Carbon12 project
Hyams <i>et al.</i> [181] 2020	150 £/m ² 714 £/m ³	160 £/m ² 571 £/m ³	1.25	Material and labor cost. CLT thickness 210 mm. Concrete slab 280 mm

ANNEX 4. Resistance of timber and concrete

Moment resistance of timber [9]

$$M_{r,t} = \phi F_b S_{eff} K_{rb} \quad (A4.1)$$

$$S_{eff} = \frac{(EI)_{eff}}{E_t} \cdot \frac{2}{h} \quad (A4.2)$$

$$F_b = f_b K_D K_H K_{Sb} K_T \quad (A4.3)$$

Tensile resistance of timber [9]

$$T_{r,t} = \phi F_t A_{t,net} \quad (A4.4)$$

$$A_{t,net} = b_t h_{t,long} \quad (A4.5)$$

$$F_t = f_t K_D K_H K_{St} K_T \quad (A4.6)$$

Shear resistance of timber [9]

$$V_{r,t} = \phi F_v \cdot \frac{2A_t}{3} \quad (A4.7)$$

$$F_v = f_v K_D K_H K_{Sv} K_T \quad (A4.8)$$

$$A_t = b_t h_t \quad (A4.9)$$

Shear resistance of concrete [156]

$$V_{r,c} = 0.21 \phi_c \lambda \sqrt{f_c} b_c h_c \quad (A4.10)$$

ANNEX 5. Detailed parallel plot of Figure 4.6

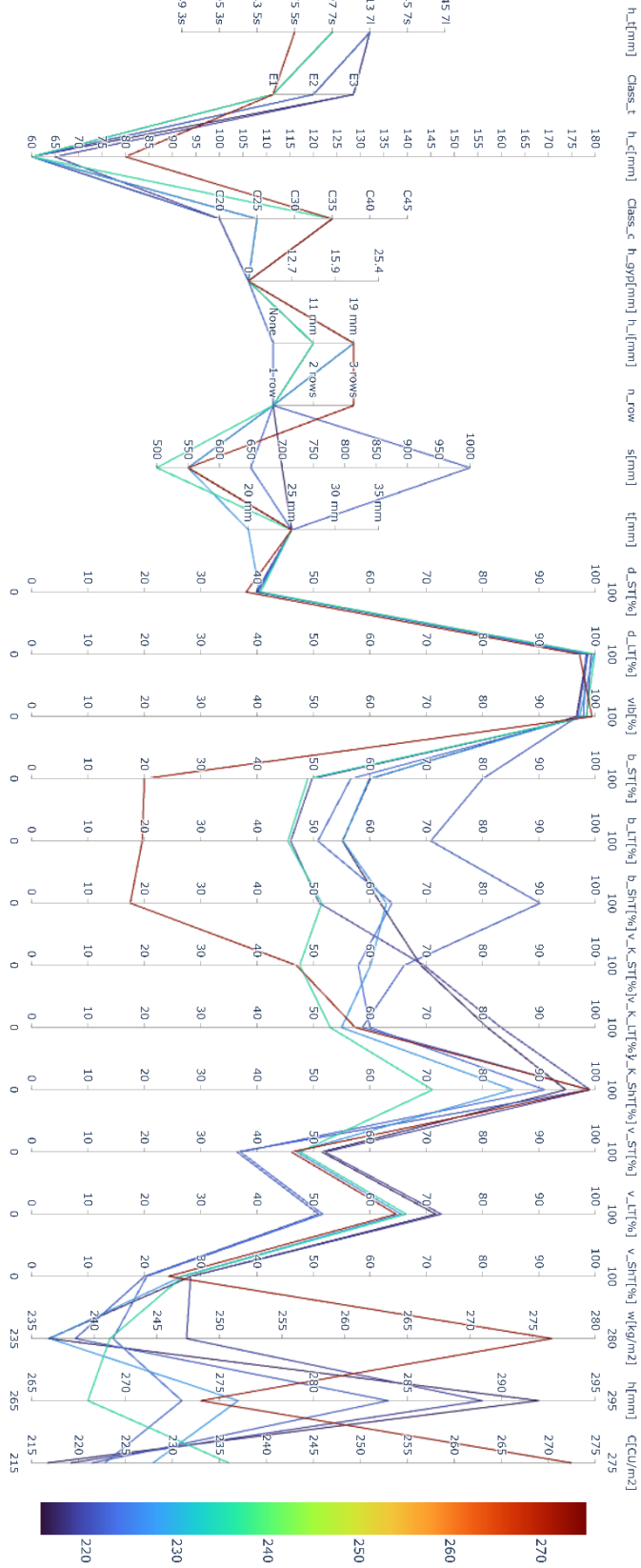
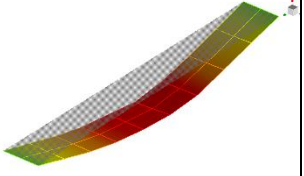
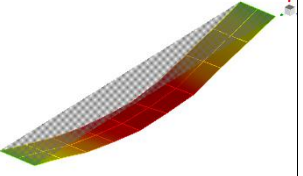
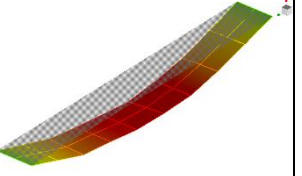
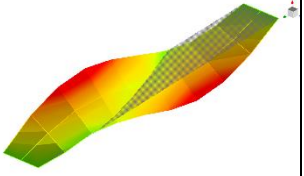
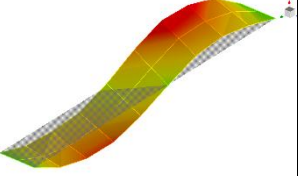
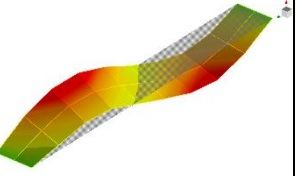
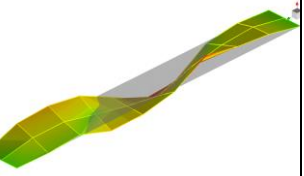
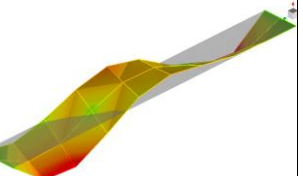
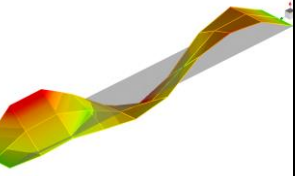
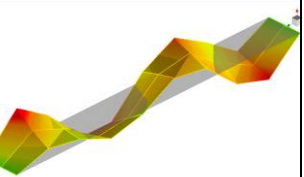
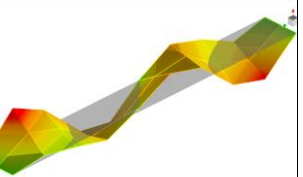
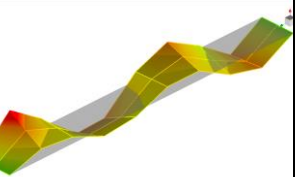
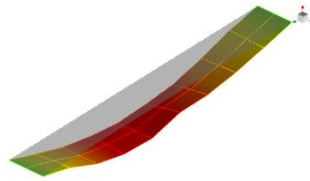
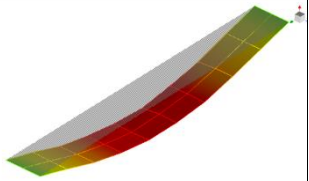
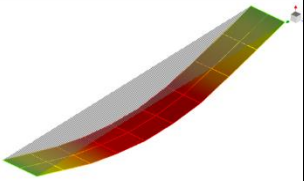
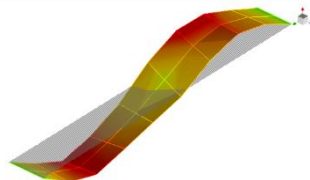
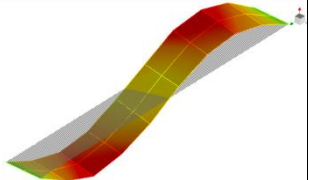
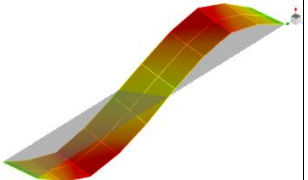
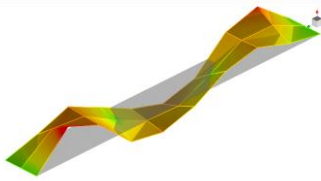
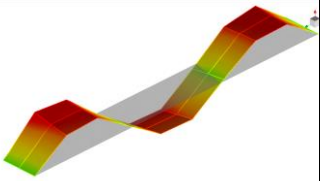
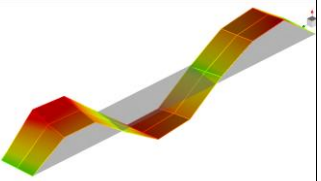
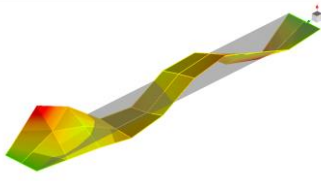
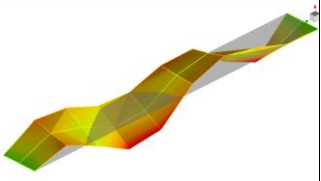
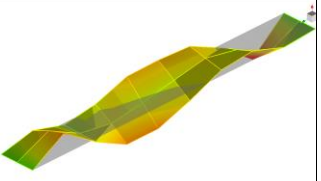


Figure A5.1. Parallel coordinate of the solutions for 9 m floor span

ANNEX 6. Mode shape of bending modes of CLT and CCC beams

Mode	Beam 1 Bare CLT panel	Beam 2 Bare CLT panel	Beam 3 Bare CLT panel
1	 4.30 Hz	 4.26 Hz	 4.17 Hz
2	 16.49 Hz	 15.70 Hz	 15.50 Hz
3	 34.62 Hz	 32.29 Hz	 32.68 Hz
4	 58.75 Hz	 59.08 Hz	 56.93 Hz

Mode	Beam 1 CCC 28 days	Beam 2 CCC 28 days	Beam 3 CCC 28 days
1	 4.95 Hz	 5.27 Hz	 5.35
2	 16.02 Hz	 18.11 Hz	 18.52
3	 28.77 Hz	 33.53 Hz	 35.62 Hz
4	 44.63 Hz	 49.70 Hz	 52.09 Hz